

*Doctoral thesis submitted for the degree of Doctor
of Philosophy in Telecommunication Engineering
Postgraduate Program: TECOMBER*

Wireless Channel Characterization and MIMO Performance Analysis in Complex Indoor Scenarios at Sub-6 GHz Bands

Presented by:

Luis Lenin Trigueros Chavarria

Supervised by:

Dr. Francisco Falcone Lanas and Dr. Carlos Del Rio

Pamplona, March 2023

“A winner is just a loser who never gave up.”

Winston Churchill

Contents

| | |
|---|-------------|
| Abstract | x |
| Acknowledgements | xiii |
| Chapter 1: Introduction | 1 |
| 1.1 Motivation | 2 |
| 1.2 Objectives | 5 |
| 1.3 Structure of the Thesis | 7 |
| Chapter 2: Wireless Communications | 11 |
| 2.1 Evolution of Wireless Communications | 12 |
| 2.2 Wireless Technologies | 16 |
| 2.2.1 Wireless Personal Area Network (WPAN) | 17 |
| 2.2.1.1 Bluetooth | 17 |
| 2.2.1.2 Zigbee | 18 |
| 2.2.1.3 RFID | 20 |
| 2.2.1.4 NFC | 21 |
| 2.2.2 Wireless Local Area Network (WLAN) | 22 |
| 2.2.2.1 WiFi | 23 |
| 2.2.3 Wireless Metropolitan Area Network (WMAN) | 25 |
| 2.2.3.1 WiMAX | 25 |
| 2.2.4 Wireless Wide Area Network (WWAN) | 26 |
| 2.2.4.1 Mobile Networks | 26 |
| 2.2.4.2 5G Technology | 29 |

| | |
|--|-----------|
| 2.3 RF Signals Propagation Mechanism | 32 |
| 2.3.1 Free-Space Propagation | 33 |
| 2.3.2 Reflection | 33 |
| 2.3.3 Diffraction | 34 |
| 2.3.4 Scattering | 35 |
| 2.4 Propagation Models in Wireless Channel | 36 |
| 2.4.1 Theoretical Models | 36 |
| 2.4.2 Empirical Models | 37 |
| 2.4.3 Deterministic Models | 38 |
| Chapter 3: MIMO Systems Theory | 40 |
| 3.1 Historical Outlook to MIMO | 41 |
| 3.2 MIMO Communications | 43 |
| 3.2.1 MIMO Channel Models | 44 |
| 3.2.1.1 Cluster Models | 45 |
| 3.2.1.1 Correlative Models | 45 |
| 3.3 The MIMO Channel | 46 |
| 3.4 Space-Time Coding | 49 |
| 3.4.1 The Alamouti Scheme | 50 |
| 3.4.1.1 The Encoding and Transmission Sequence | 52 |
| 3.4.1.2 The Combining Scheme | 54 |
| 3.4.1.3 Maximum Likelihood Decision Rule | 54 |
| 3.4.2 Space-Time Block Codes (STBC) | 56 |
| 3.4.2.1 The Coding Scheme | 56 |
| 3.4.2.2 The Decoding Algorithm | 60 |
| 3.4.3 Space-Time Trellis Code (STTC) | 61 |
| 3.4.3.1 Encoder Structure for STTC | 62 |
| 3.4.3.2 Generator Description | 63 |
| 3.4.3.2 Generator Polynomial Description | 65 |

| | |
|--|------------|
| 5.3.2.2 Phase Evolution Analysis | 127 |
| 5.3.2.3 Spatial Receive Diversity Evaluation | 131 |
| 5.3.3 Results and Application | 132 |
| Chapter 6: Conclusions and Future Work | 133 |
| 6.1 Conclusions | 134 |
| 6.2 Future Work | 139 |
| Bibliography | 140 |
| Appendix A: Measurement Equipment Specification | 147 |
| Appendix B: STLC Encoding and Decoding Structures | 151 |
| List of Publications | 153 |

Abstract

The continue evolution in wireless communication systems aims to provide adequate parameters in terms of higher transmission bit rates, capacity and increased spectral efficiency. All these deriving from the context of IoT, IIoT and the 5G applications such as Enhanced Mobile Broadband (eMBB), Ultra-Reliable Low-Latency Communications (uRLLC) and Massive Machine-Type Communications (mMTC). Physical layer functionalities such as MIMO can increase throughput and provide higher coverage/capacity relations. However, its performance is directly affected by radio channel characteristics defined in the radio channel matrix and other conditions such as employed antenna spacing, human scattering influence or phase evolution effect.

In this research work, three particular and useful study cases have been performed. Firstly, the performance of a MIMO system operating within a 5G NR FR1 capable band is analyzed, by considering volumetric channel analysis in frequency/power as well as in time domain and the impact of variable antenna spacing. The results show a clear benefit in received power level as antenna spacing is increased from 1λ to 3λ in the case of a complex indoor scenario.

Secondly, we analyzed the influence of human scattering in a complex indoor environment consisting in a conference room in a plenary layout. For this study, 5G NR FR1 frequency band was also considered. Results show that 0% of human occupancy has 3 dB enhancement over 100% occupancy when analyzing BER values. Besides, it was also observed an important decrease in total power levels received: there is a loss of around 10 dBm when 50% occupancy, another 6 dBm loss when premise is complete compering with 50% and a total of 16 dBm of loss between 100% occupancy over empty place.

In the context of IoT and IIoT, aiming to enable context aware environments, distributed transceiver systems capable of providing low cost, low latency capabilities are required. Single Input Multiple Output systems provide an adequate solution by enabling non-coherent energy-based detection. Phase distributions play a key role in transceiver location and hence overall system operation.

Finally, in this thesis, SIMO operation based on volumetric phase analysis is performed on indoor scenarios, employing deterministic 3D Ray Launching channel estimation. The proposed methodology enables the estimation of system performance as a function of distributed transceiver location, aiding in network planning and deployment tasks.

Acknowledgments

First of all, I would like to thank God, for never letting me alone in all the difficulties that I have been through the development of this thesis. The road was long, difficult, and rough and I would not have come this far without his strength.

I want to give a huge thanks to Dr. Francisco Falcone and Dr. Carlos Del Rio, for the unconditional support and advices I received from Them. They have done a great job and their help was even beyond their responsibilities as supervisors.

Finally, thanks to my family, and especially to my daughters, for all the patient and understanding for the time that I had to stole them and for the support. To my mother of course, for always be there for me.

Chapter 1

Introduction

HUMAN beings are permanently hungry for knowledge, and by this innate nature we always reach the frontier of the known and we are also always interested in the unknown. Technology in general is an exciting field of knowledge, and it can be said that it is one of the most important engines of many aspects of human life such as the economy, industry, states, and communication between people. In relation to technology and communication, there is the development of avant-garde wireless networks, which are very necessary today and a source of motivation to undertake research activities and the development of doctoral thesis such as the one presented in this document. This chapter is devoted to present the motivation for the realization of this thesis in section 1.1. The main objectives of this work are described in section 1.2 as well, which were the guidelines to conduct the research tasks. Finally, the complete structure of this thesis is explained in section 1.3, helpful for readers interested in specific sections of this work and then they can find out what chapter to address directly.

1.1 Motivation

The present world has greater communication requirements every day, communications that at the same time allow mobility. It is for this reason that mobile network technologies are constantly evolving to meet this global demand. In current times, the ancient "voice call" has taken a backseat due to the dynamics of modern and everyday life. The many digital communication applications such as social networks, video conferences, instant messaging, business communication platforms, etc., in addition to being largely free, are better suited to the digital lifestyle.

This wide variety of communication platforms and their inherent need for mobile data networks to function, are the driving forces behind the technology industry to develop such networks. Additionally, it is not only about communicating people, with the era of IoT (Internet of Things) where a network of physical devices such as vehicles, appliances, watches, cameras, pet collars, home sensors, software, etc. they interconnect with each other and grow exponentially every second. The number of IoT devices is growing 22% year-on-year, and it is estimated that by 2023 there will be up to 17.2 billion of connected IoT devices.

Moreover, With the boom of the fourth industrial revolution, also known as Industry 4.0, which is characterized by a fusion of technologies that is disintegrating the borders between the physical, digital, and biological spheres, all this communication requirements are more demanding. Industry 4.0 is also known as the Industrial Internet of Things or IIoT

The Industrial Internet of Things (IIoT) is the use of smart sensors and actuators to enhance manufacturing and industrial processes. IIoT uses the power of smart machines and real-time analytics to take advantage of the data that "dumb machines" have produced in industrial settings for years. The driving philosophy behind IIoT is that smart machines are not only better than humans at capturing and analysing data in real time, but they are also better at communicating important information that can be used to drive business decisions faster and more accurately.

In the next Figure 1.1 we can see the applications of IoT, which is focused on consumer solutions, and IIoT.

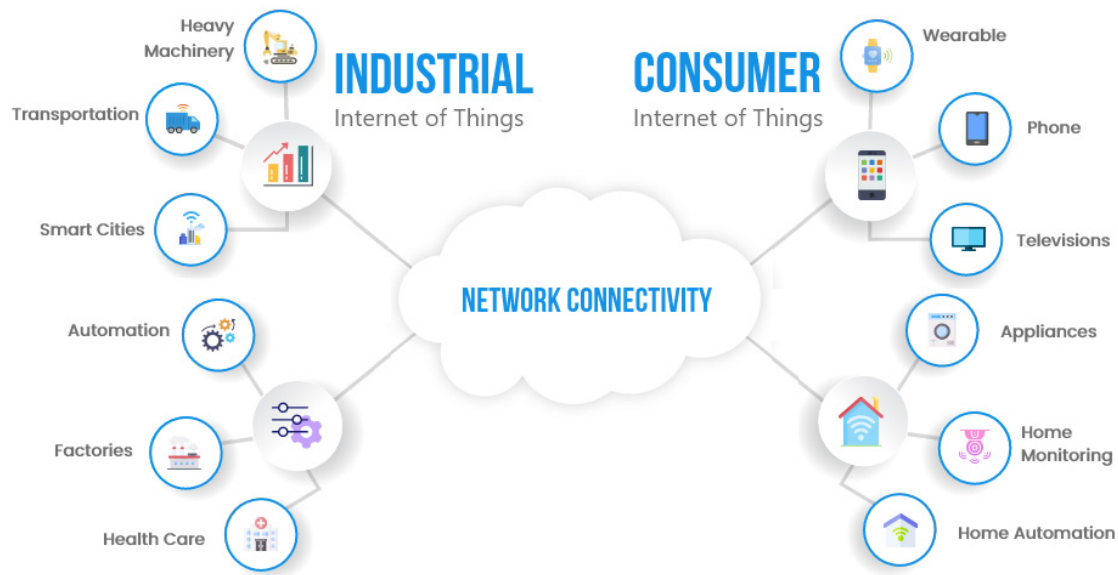


Figure 1.1 IIoT and IoT applications.

This growing demand for data transmission will largely be supplied by mobile data networks between other technologies. As we may know, these networks are made up of elements in which one or both ends of the connection are in constant movement, given this operating condition the radio channel is used (wireless communications) to establish and maintain the link. Motivated by this, the work developed in this thesis focuses fundamentally on the study and characterization of wireless channel and other aspects related to these networks, for instance 5G, more specifically on MIMO systems.

In order to accomplish the technical requirements for implementing IoT and IIoT, 5G Networks is one of most likely technologies to be deployed in these scenarios. 5G Networks is the marketing term for technologies that meet the requirements of ITU IMT-2020 and 3GPP R15. Some of the most important features of 5G include high transfer rates, low latency, high mobility, and high connection density. 5G requirements can be found in Figures 1.2.

As other mobile network standards, 5G make use of MIMO systems, and one of the most prominent versions is Massive MIMO, that will be implemented to significantly increase network capacity. Massive MIMO is the most compelling sub-6 GHz physical layer technology for future wireless access. The main concept is the use of large antenna arrays at base stations to simultaneously serve many terminals.

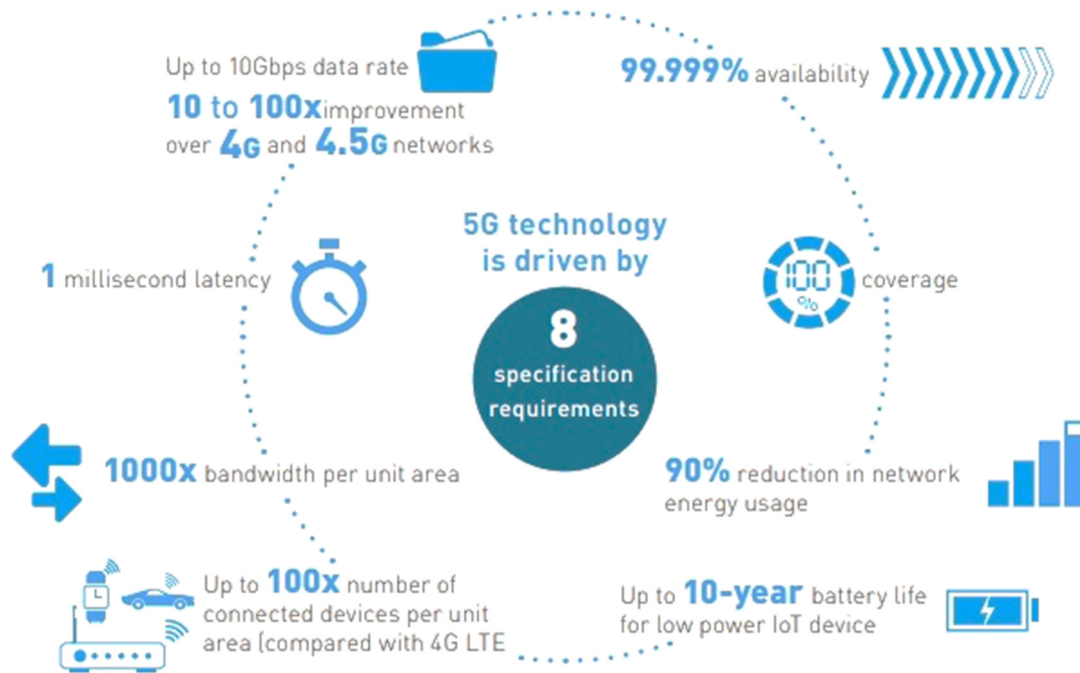


Figure 1.2 Technical requirements for 5G.

To understand the challenges of the new networks, and more specifically of the MIMO technology, it is necessary to emphasize the implications of the use of the radio channel; Many of the wireless communication channels consist of *multiple paths* for the signal from the transmitter to the receiver. This multiplicity of paths leads to a phenomenon known as *multipath attenuation*. Multipath is caused by the presence of objects in the physical environment that, through the propagation mechanisms, alter the path of the radiated energy. These objects are known as *Scatterers*.

Figure 1.3 depicts schematically a multipath channel.

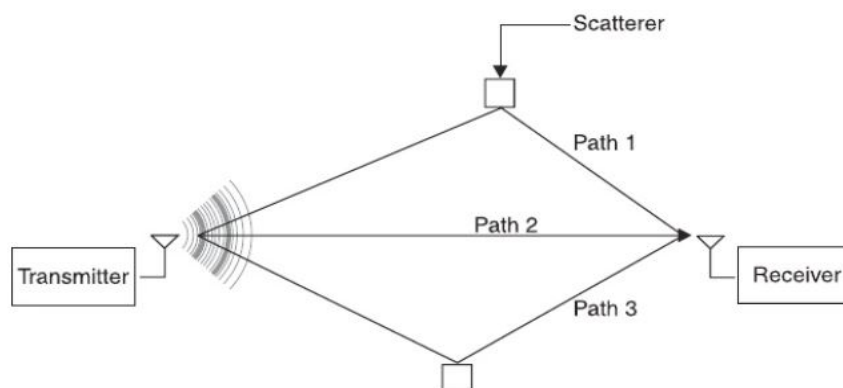


Figure 1.3 Multipath channel physical scheme.

The paths are of different lengths, and hence the signal arrives at the receiver with different amplitude and phase. In some cases, the multiple signals combine destructively at the receiver creating what is known as *multipath interference*. To combat this effect and take advantage of multipath, we use *space-time coding*, which is the basis of MIMO.

MIMO (Multiple-Input Multiple-Output) is a technology that uses multiple antennas for transmission and reception. MIMO sends multiple data streams (depending on the number of transmit antennas) over multiple antennas and each transmitted data stream travels through different paths in the channel until it reaches the receiver antenna. See Figure 1.4.

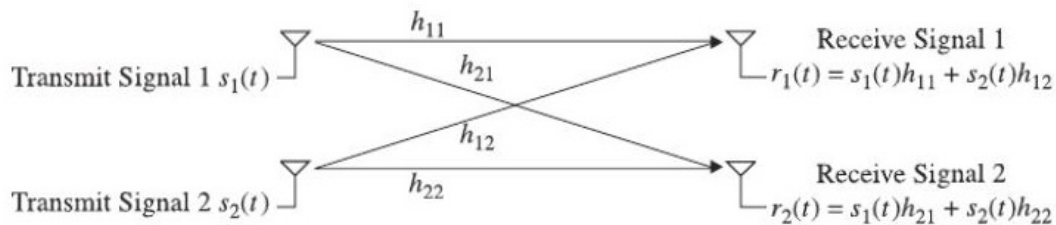


Figure 1.4 MIMO: Space-Time coding technique

Considering everything that has been said about the importance of wireless networks, such as 5G, for IoT applications, IIoT and communication requirements in general; It is required to deepen the study of the systems and the MIMO channel, their performance in different environments, as well as the wireless channel characterization to ease the building of more efficient network planning and designing tools.

1.2 Objectives

After previously explained the relevance of wireless networks and MIMO systems, the general purpose of this thesis is to develop a complete study in a number of different environments where wireless channel characterization and MIMO performance analysis will be accomplished in complex indoor scenarios. In a more specific way, the objectives of this work are the following:

- The more basic and first objective will be to do a deep review of currently in use wireless technology, looking to understand how this work can be applied. In this line, to present a study of state of the art about MIMO and space-time coding is another objective, representing the most important technical feature employed in this thesis.
- The second objective is to implicitly validate the in-house developed 3D Ray Launching algorithm, by using it for simulating different complex indoor scenarios and RF parameters applicable to potentially 5G deployments.
- To analyse and present the effect of variable antenna spacing considering complex indoor scenarios, in which all the scattering elements will be considered. In this way, wireless channel characterization in terms of received power levels and time domain parameters for the complete volume of the scenario under analysis will be obtained, for 5G NR FR1 frequency band at 3.7 GHz.
- Making use of the simulation result and analysis accomplished with varying antenna spacing, another objective is to assess the validity of this data and to evidence possible differences between the simulated scenario and real values, by means of a measurement campaign to be carried out with a VCO and a portable spectrum analyser.
- To evaluate the effect of human body scattering considering complex indoor scenarios at 5G NR FR1 frequency band of 3,7 GHz. Making use of wireless channel characterization, another objective is to analyse MIMO performance in this environment.
- To study the phase evolution impact in receive diversity applications, by means of the analysis of SIMO system operation in high node density indoor scenarios where rich multipath effects are given. To obtain the received phase distributions as a function of cuboid distributions, which are then employed to analyse impact on $1 \times N$ SIMO channel performance.

This thesis pursues to fulfil all these objectives, in that way, this work is intended to contribute with engineering tools by providing these different study cases where wireless channel characterization, MIMO performance analysis and phase evolution impact analysis will be achieved.

These tools are in form of the complete analysis to be developed and the results to be obtained in this work with aid of the 3D RL algorithms, that will be useful for wireless coverage planification, throughput and capacity forecast in complex indoor environments.

1.3 Structure of the Thesis

This thesis is structured in six key chapters, covering each of them important subjects of the research work done during the thesis development. Following these main sections, we present the bibliography employed in this work. We also include two appendixes, Appendix A with a list of measurement equipment specification used during the RF estimation campaign, and Appendix B with a table of STLC structures. Finally we enumerate the publications derived from this work.

The present introductory chapter, Chapter 1, is focused on describing the motivation, structure, and the objectives of the thesis. Figure 1.4 depicts in a general and schematic way the process summary followed up during carrying out the thesis.

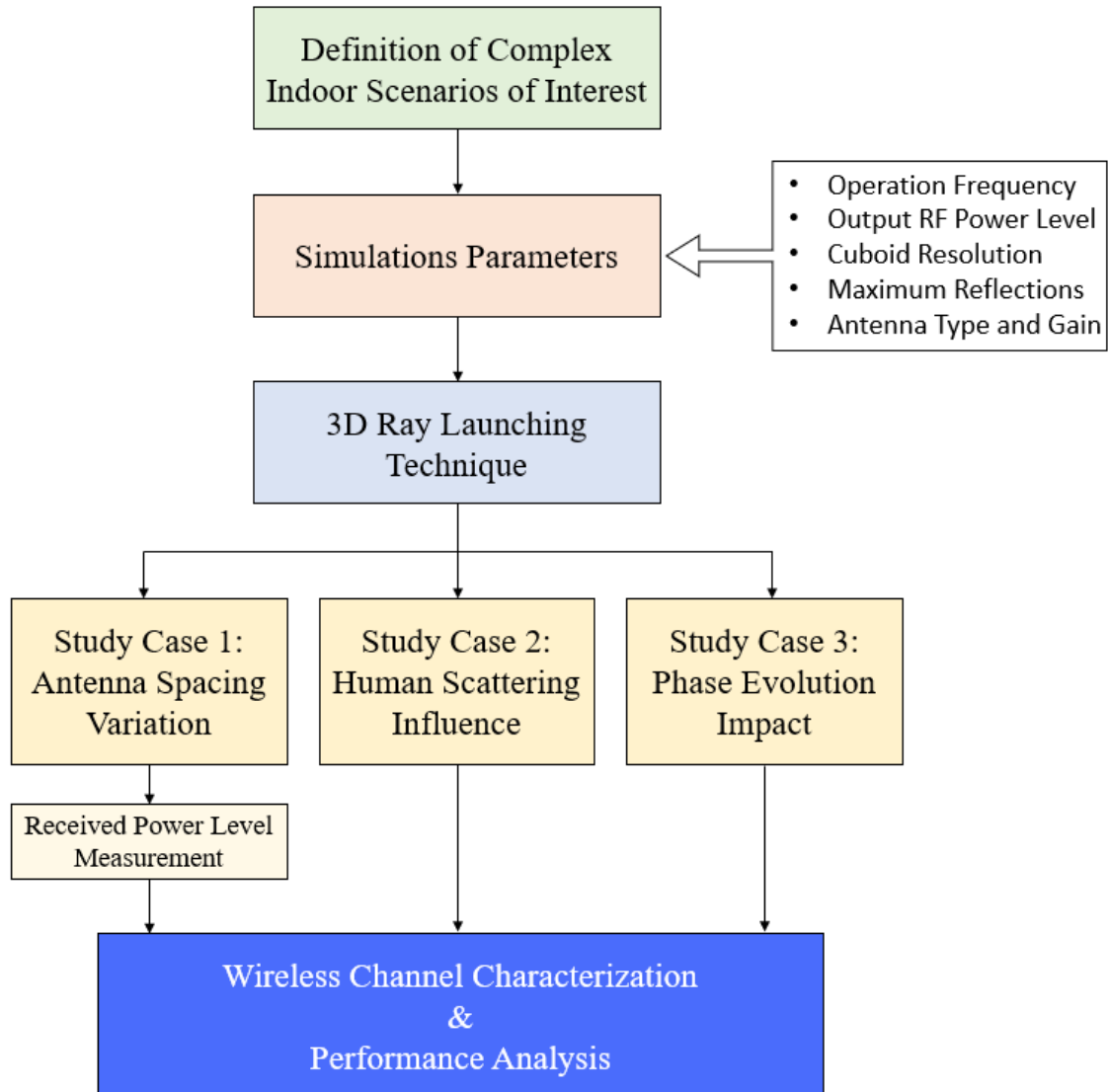


Figure 1.4 Description of methodology to develop this thesis.

Chapter 2 presents a complete review of wireless communications. We firstly show a brief outlook in the evolution of these technologies along the history. A description of current wireless technologies is presented, making special emphasis on those who are relevant to this work, 5G for instance. Then, this chapter also explains how wireless signals propagate over the space by means of the propagation mechanism, being these phenomena a highly important aspect for understanding the MIMO technique. Finally, a review of wireless path loss prediction models is covered, including theoretical, empirical and deterministic models.

Chapter 3 is a section totally dedicated to address the MIMO system theory, which is the most important part of wireless communication field, in the physical layer and digital signal processing applied to this thesis. We start by covering a historical review of the origin of MIMO and its evolution. We present the MIMO communications basis and available MIMO channel models. Then, a complete description of MIMO channel and multipath implications is also explained, see Figure 1.5. The key space-time coding methods such as Space-Time Block Codes (STBC), Space-Time Trellis Code (STTC) and Space-Time Line Code (STLC) are widely described as well. Finally, we explain how this technique are used in this thesis.

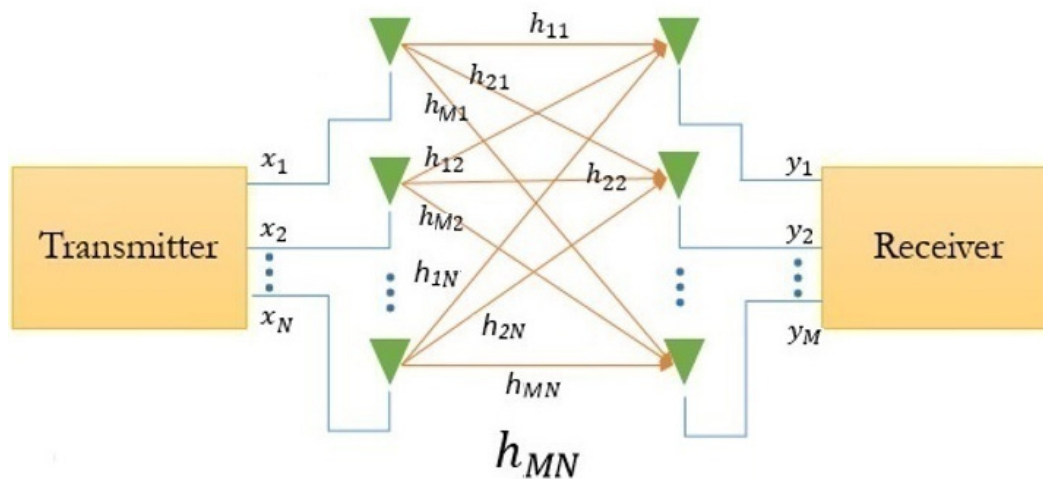


Figure 1.5 The MIMO channel model.

Chapter 4 is devoted to depicting the methodology employed to characterize the complex indoor scenarios selected. This includes a detailed explanation of ray launching and ray tracing theory, which is implemented in the simulation algorithm, and the way of geometrical optics and geometrical theory of diffraction are used to improve the accuracy and reduce complexity of these techniques. In this chapter, we thoroughly explain how the in-house developed 3D ray launching algorithm works, encompassing the manner the scenarios are built by means of matlab functions and how logically the simulations are performed. Finally, we describe the form the results from simulations are used to achieve the MIMO performance analysis with the aid of separated developed matlab scripts.

Chapter 5 is the most important section of this document, here we present the core of the thesis. We firstly defined three study cases that were relevant for planification and designing of wireless systems implementing MIMO, such as 4G, 5G, WiFi 6, and so on. In the first case we analyse the effect of antenna spacing in the performance of MIMO, we accomplished this by simulating different settings of radiating elements withing the same complex indoor scenarios. Second study was the analysis of influence of human presence as scatterers withing an indoor environment, by varying the quantity of people inside the area in different simulation iterations, we could establish the effect over the performance of a determined system. We finally implemented a third scenario with operation frequency and characteristic of importance for IIoT applications and uRLLC functionalities, where the phase evolution impact was analysed. For all these three study cases, the scenario characteristic was perfectly described, and the results and possible application were also commented.

Finally, Chapter 6 is dedicated to do a compilation of the results obtained during the thesis was developed. We also summarize the most important conclusion for the entire work. Additionally, we also proposed and commented future work and research activities that could complement this thesis.

The list of measurement equipment utilized in the research activities are attached in the Appendix A. In the end, Appendix B presents a table with STLC encoding and decoding structures.

Chapter 2

Wireless Communications

WIRELESS networks, since decades, have been gaining great popularity because the mobility it offers. This mobility is crucial in the society to keep the digital lifestyle going by doing many activities at the same time, for example, working in tablets while being in the metro in the way to office. In this chapter, due to the high importance of this, a brief overview of wireless communications is presented in order to understand how this networks work. In section 2.1, we firstly outline a small historical review in the evolution of wireless communications. Next, we present a summary of current wireless technologies and its classification in section 2.2, doing a deep exploration in technologies relevant for this thesis. Then, in section 2.3, we study the way these wireless signals are propagated in the medium so the information can travel from transmitter to receiver. Finally, section 2.4 is dedicated to analysing the different propagation models used to characterizing the wireless channel, which is also highly relevant in this thesis.

2.1 Evolution of Wireless Communications

The wireless communications can be defined as telecommunications made through radioelectric waves [1]. This occurs basically when the energy from an oscillating current is radiated off a conductor into space as radio waves, this oscillation rate is known as Radio Frequency (RF). The radioelectric waves are defined by the ITU (International Telecommunication Union) as the electromagnetic waves that are propagated in the space without artificial guide [2]. The radiocommunication is based on the overlaying of the information we need to transmit over an electromagnetic wave called carrier, the process of placing this information on the carrier is denoted as modulation. As a result of this process, a modulated wave is generated, then, this one is sent to the propagation medium through a coupling device with the medium called antenna. But prior to we could know all this theory described before, a lot of work was done by many people along the years.

Looking back to history, wireless communications as we know it presently is the result of many contributions of people over the last two centuries. The electromagnetism is fundamental to understand the way this communication was developed; let's say that everything began when in eighteenth century the electricity was discovered, such invention is commonly credited to Benjamin Franklin. Also in 1800, the battery was invented by Alessandro Volta. After these remarkable inventions, scientists began to reckon that a relation between electricity and magnetism might be possible. It was in 1820, when Hans Christian Ørsted observed for the first time, that he could force a compass needle to deflect at right angles to a current-carrying wire [3]. Figure 2.1 depicts the Ørsted experiment.

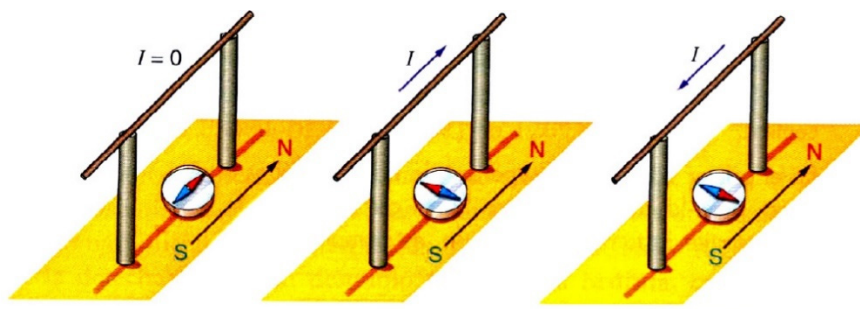


Figure 2.1. Ørsted experiment with needles.

The experiment was pretty simple, he could divert a magnetized needle when placing close to a conductor where current electricity was circulating, demonstrating the presence of magnetic field generated by the electric current. This discovery was highly important as showed the relation between magnetism and electricity. After this event, other physicists like Michael Faraday, André Ampère and Joseph Henry worked in the task of defining the mathematical relations between electricity and magnetism, finding out it was a hard task. It is James Cleck Maxwell who is largely credited with discovering the laws of electromagnetism, these laws were presented in his publication in 1861, today known as the four laws of electromagnetism:

1. *Gauss's Law*: Depicts the electric field produced by electric charges
2. *Gauss's Law of Magnetism*: States that individual magnetic charges cannot exist.
3. *Faraday's Law of Induction*: Shows the electric field produced by a changing magnetic field.
4. *Ampère's Circuital Law*: Shows the magnetic field produced by an electric current.

In 1864, Maxwell published his work “A Dynamical Theory of the Electromagnetic Field” where he presented his well-known Maxwell's Equations. He also predicted that light was an electromagnetic wave and followed the same laws as electromagnetic fields. Additional, Maxell described a wave equation explaining how propagation of electromagnetic (EM) waves through a medium occurs [3]. Maxwell supposed that, using a time-varying current, it was possible to generate electromagnetic waves that travelled at the speed of light.

The work done by Maxell inspired the German physicist Heinrich Hertz, who during the late nineteenth century was trying to find proof of EM waves depicted by Maxwell. Hertz is often credited with building the world's first wireless transmitter using a Ruhmkorff-type induction coil connected to a center-fed dipole equipped with a spark gap. In the experiment, the receiver was a simple loop antenna with similar spark gap. When the system was transmitting, sparks appeared at the receive-antenna gap when transmitter and receiver where placed close enough [3]. Figure 2.2 shows the setup of Hertz's experiment.

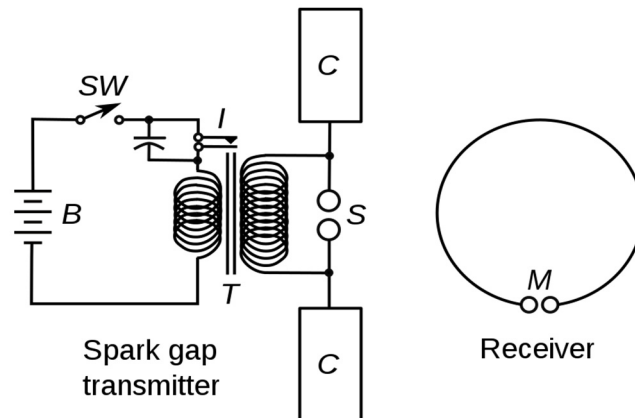


Figure 2.2. Experimental spark-gap transmitter-receiver of Hertz.

Hertz's experiment demonstrated that the EM waves travelled at the speed of light, despite having a much larger wavelength than light. By that time, Hertz didn't realize the huge importance that his discovery will mean for future works in wireless transmissions, inspiring an entirely new field of research.

Another milestone in the fascinating evolution of wireless communications, is the research done by Nicola Tesla who firstly demonstrated the wireless propagation of power to vacuum tubes. Tesla stated that this technology could be used to transmit information between to different location, and then, after continuing his research, in 1896, Tesla could transmit a continuous-wave signal over a distance of approximately 48Km from New York to West Point.

In twentieth century, the wired telegraph was a broadly accepted communication way between locations. Even though the Trans-Atlantic cable for telegraph was already in operation to communicate North America and Europe, the huge handicap of needing to have both terminals linked by a wire made impossible to use this technology for example on ships, moreover, the difficulty and high cost of maintenance tasks, all these gave rise to Guglielmo Marconi the interest to develop a telegraph device to operate in a wireless way. The ideas from visionaries such as Hertz and Tesla were taken by Marconi who polished these works to extend the range between transmitter and receiver.

It was in 1901, after some years of working in different designs, when Marconi made his celebrated Trans-Atlantic transmission from England to Canada reaching a distance of approximately 3.500 km [3]. Even tough, both works from Tesla and Marconi were remarkable and of high importance for developing the wireless communications, in 1943, few time after Tesla’s death, the US Supreme Court revoked one of Marconi’s patents and named Tesla “the inventor of the radio”. Figure 3.3 describes the evolution of wireless communications chronologically.

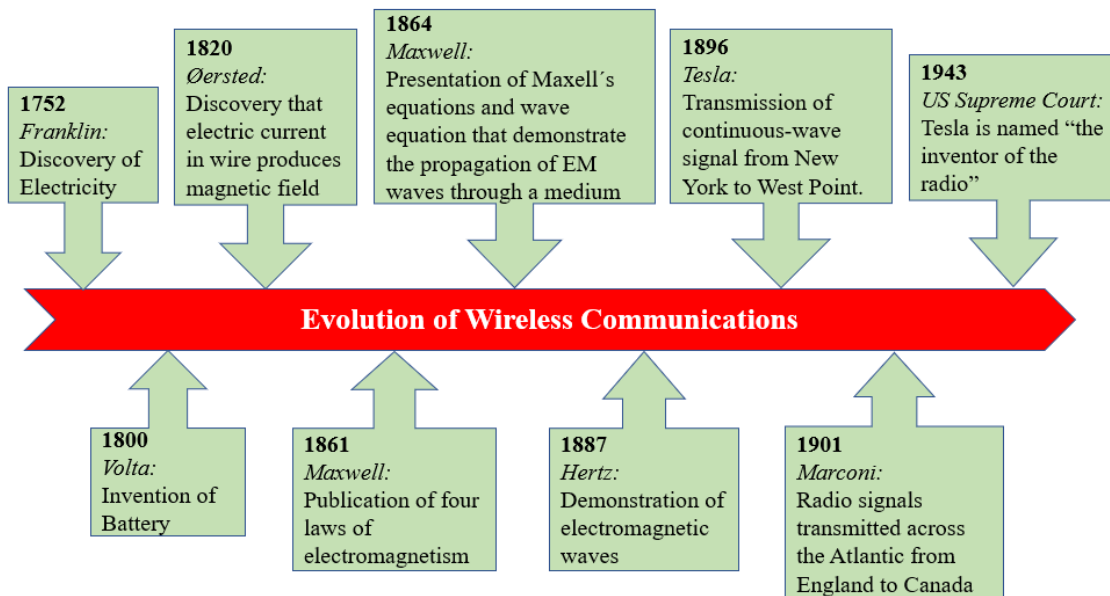


Figure 2.3. Evolution of wireless communication over the time.

All these geniuses and their works have inspired hundreds of other scientists over the time and from all over the world, and new research and advances are being presented and in progress today. Wireless communication continues to be a study field of great interest for engineers, this is obviously because electromagnetic waves propagation is the base for technologies such as 5G mobile networks, which is nowadays a key component for civilization in many manners.

2.2 Wireless Technologies

Since the wireless communications have advanced enough to be capable of transmitting information from one device to another, engineers have been focusing their efforts to improve aspects of this communication as transmission capacity or bit rate, delay, coverage, reliability, etc. Perhaps, wireless networks began to penetrate the market in the 1990s or at least started to be fundamental for enterprises, science research, governments, and society.

With the tremendous growth of humanity, the development of new and demanding application for social interaction, the implementation of avant-garde tools for health care industry, robotic implementations in manufacturing and so on, the goal is to send as much data as far as possible and as fast as possible. Pursuing this goal, network technologies can face numerous challenges inherent in wireless channel. For this reason, wireless technologies can be classified according to application, range, capacity, environment, device dimension and other aspects. Next, we have a commonly used wireless technology classification:

- Wireless Personal Area Network (WPAN)
- Wireless Local Area Network (WLAN)
- Wireless Metropolitan Area Network (WMAN)
- Wireless Wide Area Network (WWAN)

In the next part of this chapter, a brief description of the most important and more commonly used wireless technologies will be presented, and especially a deeper description of 5G will be found. 5G networks is a mobile standard included in the WWAN technology type. This technology is currently being implemented in some developed countries and is perceived to be able to fulfill all the communications requirements of modern society.

Below Figure 2.4 depicts the wireless communication technologies and how are related between them in the classification scheme.

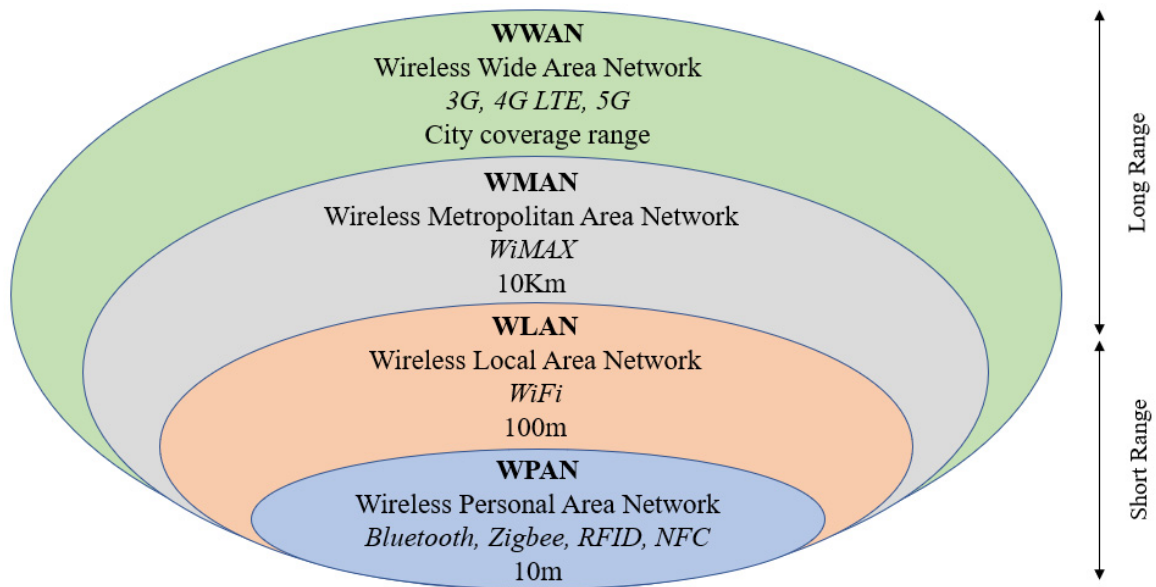


Figure 2.4. Wireless technology classification.

2.2.1 Wireless Personal Area Network (WPAN)

WPAN includes the wireless networks of short-range, reaching few of meters of coverage. This technology is usually used for interconnecting small and peripheral devices such as printers, mobile phones, headphones, appliances and so on without using cables.

Following a brief description of standards of WPAN will be presented.

2.2.1.1 Bluetooth

The Bluetooth connection is one of the most used technologies along WiFi. It is an industrial specification created by Bluetooth Special Interest Group, Inc. that allow the transmission of voice and data between wireless devices over the ISM band of 2,4 GHz. The communication protocols of Bluetooth are designed especially for devices of low power consumption, requiring short-range coverage, and based on transceivers of low cost.

The Bluetooth devices can be classified in two ways; referring to their transmission power and to channel capacity. The following two tables shows these classifications.

Table 2.1. Bluetooth classes and transmissions power.

| Class | Max Power Allowed (mW) | Max Power Allowed (dBm) | Coverage (Approx.) |
|---------|------------------------|-------------------------|--------------------|
| Class 1 | 100 mW | 20 dBm | ~100m |
| Class 2 | 2.5 mW | 4 dBm | ~5-10m |
| Class 3 | 1 mW | 0 dBm | ~1m |
| Class 4 | 0.5 mW | -3 dBm | ~0.5m |

Table 2.2. Bluetooth versions and channel capacity.

| Version | Bandwidth |
|-------------------|-----------|
| Version 1.2 | 1 Mbit/s |
| Version 2.0 + EDR | 3 Mbit/s |
| Version 3.0 + HS | 24 Mbit/s |
| Version 4.0 | 32 Mbit/s |
| Version 5 | 50 Mbit/s |

2.2.1.2 Zigbee

Zigbee is a set of communication protocols between devices especially designed for IoT application. Zigbee has a lower power consumption within the rest of WPAN standards and the hardware is pretty simple, allowing a low cost of manufacturing. It is focused on applications that require secure communications with low data rate and maximizing the service life of its batteries. The domotic, home automation applications, medical sensors, and toys, are the areas in which this technology is stronger.

This standard is now very popular because various of its characteristics that differentiate it from other technologies: low power consumption, mesh network topology capability, easy integration.

Zigbee is implemented on the ISM band for use cases like industrial, scientific, and medical applications; specifically in the frequency of 868 MHz in Europe, 915 MHz in United States and 2,4 GHz in all over the world.

The most common way to define the type of Zigbee devices is according to its role in the network.

- Zigbee Coordinator (ZC). It is in charge of controlling the network, and is the most complete type of device, only one must exist in the network.
- Zigbee Router (ZR). It interconnects separate devices in the network topology, as well as providing an application layer for executing user code.
- Zigbee End Device (ZED). It is not capable to transmit information intended for other devices. For ZED is mandatory to communicate with its parent node (ZR). This Zigbee type can be asleep most of the time, increasing the average life of its batteries. A ZED has minimal memory requirements and is therefore significantly cheaper.

In the following Figure 2.5 a list of practical applications of Zigbee networks is presented.

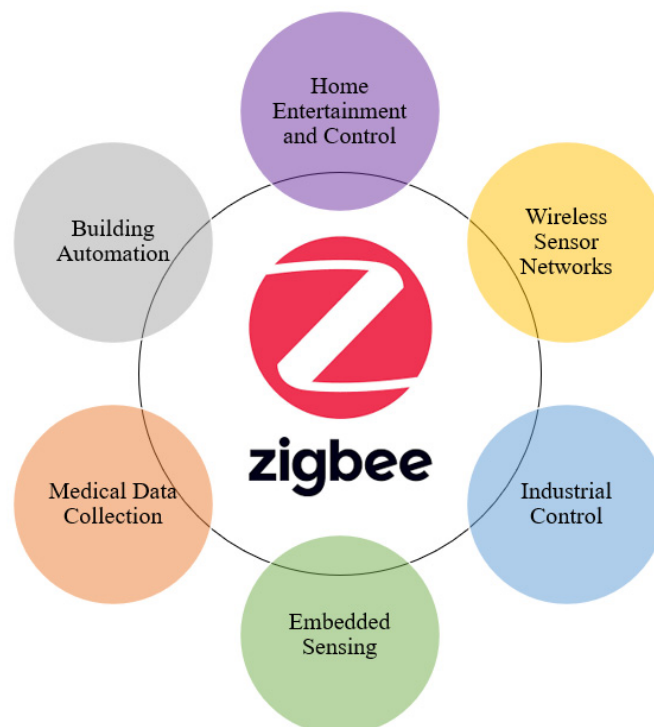


Figure 2.5. Zigbee technology applications.

2.2.1.3 RFID

The RFID technology or Radio Frequency Identification is basically a system for storing and retrieving specific data that implies the use of devices referred to tags, cards or transponders RFID. The main goal of RFID is to identify the identity of an object (for example its serial number, item id, etc.) using electromagnetic waves.

RFID tags are small devices, similar to a sticker, that can be attached or incorporated into a product, an animal or a person. Following Figure 2.6 shows a RFID tag internally.

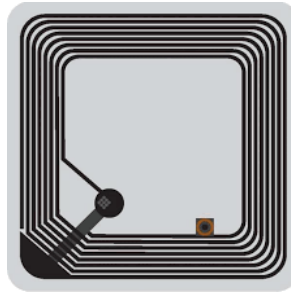


Figure 2.6. RFID tag sample.

An RFID system is based on a Transponder or RFID tag and a RFID Reader or Transceiver, and additionally, a computer software that connects the digital information to a database and serves as interface with the User.

RFID system architecture and operating:

- **Transponder:** It consists of an integrated circuit (chip) and an antenna. The RFID Reader, which is also equipped with an antenna, emits an electromagnetic field, when the Transponder enters the action field of the Reader, it absorbs its electromagnetic energy and converts it into electrical energy that charges a capacitor and uses it to transmit its identification code to the Reader itself.

There are two types of Transponders: *read only* (the code is unique and is personalized during production) and *read and write* (the RFID Reader can modify the information contained in the Transponder).

- **RFID Reader:** It is formed by the circuit that emits electromagnetic field through an antenna and electronics that receive and decode the information received from the Transponder. Then, this information is sent to the computer software.

One of the main characteristic and advantage of RFID is the use of radio frequency, instead of using infrared waves for instance, this implies that not direct vision is required between transmitter and receiver.

RFID systems can be classified according to the radio frequency used. The next table describes this classification.

Table 2.3. RFID frequency and use.

| Frequency | Band | Use case |
|-------------|------|--|
| 13,53 MHz | HF | Worldwide for passive RFID tags. |
| 433 MHz | UHF | Used by many active tags. |
| 902-928 MHz | UHF | RFID readers used in USA. |
| 865-868 MHz | UHF | Passive RFID readers used in Europe. |
| 2.4 GHz | UHF | WiFi frequency band used in USA with some active tags. |

2.2.1.4 NFC

NFC (Near Field Communication) is a wireless communication technology for short-range and high frequency that enables the exchange of data between devices. NFC communicates by induction in a magnetic field, where two spiral antennas are placed within their respective near fields. It works in the 13,56 MHz band; this means that no restrictions are applied, and it does not require any license for its use.

One of the most important advantages of NFC is the communication speed, which is almost instantaneous without previous pairing. Its use is transparent to users and NFC technology equipments are able to send and receive information at the same time. Its main disadvantage is the very small range, which is an action field at most in a range of 20 cm.

The NFC technology supports two modes of operation, all devices of the NFCIP-1 standard must support both modes:

- Active: Both devices generate their own electromagnetic field.
- Passive: Only one device generates the electromagnetic field and the other takes advantage of modulation of the load to be able to transfer the data.

The NFCIP-1 protocol can work at various speeds such as 106, 212, 424 or 848 Kbit/s.

Finally, in the next table we can find a comparison between the four technologies of WPAN described before.

Table 2.4. WPAN technologies comparison.

| Type | Maximum Coverage | Frequency | Maximum Bit Rate | Communication |
|------------------|------------------|-----------------------------------|-------------------------|----------------|
| Bluetooth | 100m | 2,4 GHz | 50 Mbps | Bidirectional |
| ZigBee | 100m | 868 MHz / 915 MHz / 2,4 GHz | 250 Kbps | Bidirectional |
| RFID | 3m | Variable | Variable | Unidirectional |
| NFC | 20cm | 13,56 MHz | 106/212/242/848 kbps | Bidirectional |

2.2.2 Wireless Local Area Network (WLAN)

The wireless technology more widely used is for sure the WLANs. These networks are very flexible and versatile allowing deployments at indoor and outdoor environments. The WLANs gained popularity as an alternative to wired local area networks or as an extension of these.

This technology has grown a lot because it allows to provide connectivity in situations where, for example, no cables can be deployed, such as buildings already built or where the density of users is so great that wired networks are not viable, such as stadiums and university campuses.

WLAN systems use radio frequency at 2,4 GHz or 5 GHz, these allow greater mobility to users by minimizing wired connections. These networks are very popular in homes and businesses to share Internet access wirelessly among multiple computers and other devices. Figure 2.7 shows a schematic view of the WLAN to share Internet access.

The most common implementation is via an Access Point. Each AP can provide connectivity to multiple devices. The AP have coverage range of approximately 150 m in open areas, so in large areas such as a university campus or a building, more than one AP is probably needed.

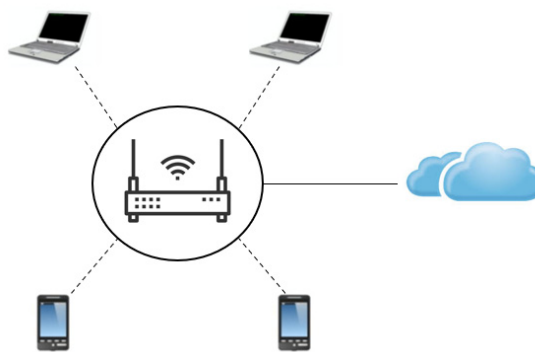


Figure 2.7. Schematic view of the WLAN to share Internet access.

The practical implementation of WLAN is the WiFi technology, both terms are synonyms or are interchangeable. Following a description of WiFi is provided.

2.2.2.1 WiFi

WiFi is a brand of the Wi-Fi Alliance, the trade organization that complies with the 802.11 standards related to wireless local area networks. WiFi is normally accepted as the acronym of Wireless Fidelity, denoting a high-performance wireless system.

The IEEE 802.11 standard was designed to replace the equivalent physical and MAC layers of the 802.3 (Ethernet) standard. This means that the only thing that differentiates a WiFi network from an Ethernet network is how the data frames or packets are transmitted, the rest is identical. Therefore, an 802.11 wireless local area network is fully compatible with all the services of 802.3 wired (Ethernet) local area networks (LANs).

The key components of the WiFi network are:

- **Station:** Devices manufactured with an IEEE 802.11 network adapter (laptop computers, smartphones, tablets, etc.) allowing them to connect to the WiFi network. Another station could be a desktop computer when equipped with IEEE 802.11 network adapter.
- **Access Point (AP):** The core component allowing the connection of many devices simultaneously. Another role is bridging connection between the wireless medium and the wired infrastructure.
- **Distribution System:** Important since they provide mobility between APs, for frames between different access points or with the terminals, they are relevant since it is the mechanism that controls where the station is to send the frames.

The WiFi standards are classified as *Generations* and every new version includes different improvements in relation to the predecessor. Next table show the characteristics and comparison between generations.

Table 2.5. WiFi generations characteristics

| WiFi Generations | | | | |
|----------------------|-------------|----------------------|---------------------|---------|
| | WiFi 4 | WiFi 5 | WiFi 6 | WiFi 6E |
| Launch Year | 2007 | 2013 | 2019 | 2021 |
| IEEE standard | 802.11n | 802.11ac | 802.11ax | |
| Max data rate | 600 Mbps | 3,2 Gbps | Up to 7 Gbps | |
| Frequency | 2,4 / 5 GHz | 5 GHz | 2,4 / 5 GHz | 6 GHz |
| Security | WPA 2 | WPA 2 | WPA 3 | |
| Channel size | 20, 40 MHz | 20, 40, 80, 160 MHz | 20, 40, 80, 160 MHz | |
| Modulation | 64-QAM OFDM | 256-QAM OFDM | 1024-QAM OFDMA | |
| MIMO | 4x4 MIMO | 4x4 MIMO, DL MU-MIMO | 8x8 UL/DL MU-MIMO | |

2.2.3 Wireless Metropolitan Area Network (WMAN)

The idea of wireless metropolitan area network represents an evolution of the concept of wireless local area network to a broader scope, covering larger areas in a metropolitan environment. A WMAN could be depicted as the sum of many wireless local area networks interconnected. This kind of networks may extend up to 50 km.

The main WMAN technology today is WiMAX (Worldwide Interoperability for Microwave Access). Its use is becoming more widespread, especially in rural or hard-to-reach areas. WiMAX can reach a bit rate of about 70 Mbps in a radius of several kilometres.

2.2.3.1 WiMAX

This technology is based on the IEEE 802.16 standard and is focused on the air interface between the transceiver station of the subscriber and base station transceiver. This standard use frequencies from 2,5 to 5,8 GHz and can have a coverage of up to 70 km. The standard 802.16 is divided into two groups according to the type of mobility it provides: Fixed WiMAX. 802.16-2004 (802.16d) and Mobile WiMAX. 802.16-2005 (802.16e).

- Fixed Access (802.16d): In this type, a radio link is established between the base station and a user equipment located in the user's home. For the fixed environment, the maximum theoretical speeds that can be obtained are 70 Mbps with a channel size of 20 MHz.
- Mobility (802.16e): This type allows the user to move in a similar way to that which can occur in others mobile network technologies.

In 2011 was approved the IEEE 802.16m or WirelessMAN-Advanced. This one was a candidate for the 4G network, in competition for the LTE Advanced standard. The interface defined by 802.16m is the base of the second-generation WiMAX, sometimes it referred to as WiMAX 2. It is based on OFDMA (Orthogonal Frequency Division Multiple Access) and it is backward compatible with 802.16e.

WiMAX 2 offers greater system capacity with peak rates of more than 300 Mbit/s. However, at this time, it seems that this technology is at great disadvantage against the new other technologies being deployed like 4G-LTE or even 5G.

2.2.4 Wireless Wide Area Network (WWAN)

A Wireless Wide Area Network (WWAN) is also named as Wireless Broadband. WWANs is deployed in the way of cell towers to transmit a radio signal within a range of several kilometres to a moving or stationary device. The main difference in relation to WMAN is that this last one has a range of only a few kilometres delivering connectivity to stationary or very slow-moving devices. This type of technology is commonly known as mobile networks. The reason of this is that the network topology is focused on delivering connectivity to devices with high capacity of motion while keeping a high performance.

2.2.4.1 Mobile Networks

The mobile network (also known as cellular network) is a network built based on radio cells (or simply cells) each with its own transmitter, known as a base station. These cells are used in order to cover different areas to provide radio coverage over an area larger than one cell, and also to obtain the more spectrum efficiency possible by reusing frequency channels in base stations enough separated to avoid interference.

In a very general way, a mobile network topology is composed by the next three elements:

- **Base Stations (BS):** These are fixed stations that communicate with mobile units in a cell and that are controlled by a control station (MTSO).
- **Mobile Units or User Equipment (UE):** These are the station with mobility. The mobile terminals itself or any other device such as tablets, PDAs, and laptops.

- Mobile Telephone Switching Office (MTSO): These are the control stations. They are fixed stations that connect the BS with the fixed telephone network or transfer calls from BS to UE. In mobile networks with data services, the MTSO also provide data connectivity between the UE and other networks like Internet.

The Figure 2.7 depicts a mobile network topology in a very basic way.

Since its invention, the mobile networks have experienced a tremendous development due to the new demanding services and the huge evolution of mobile terminals industry. At present day, the mobile networks not only provide conventional telephony services but high-speed data services including real-time connections, rich multimedia contents, and so on.

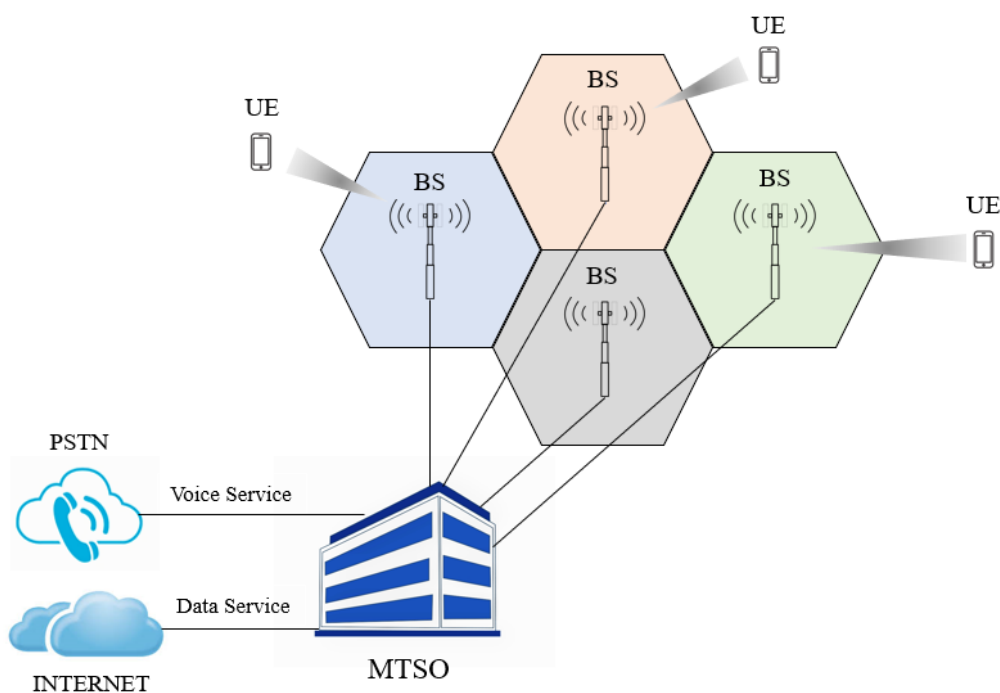


Figure 2.7. Basic mobile network topology.

The first mobile cellular communications systems emerged in the world by the beginning of the 80s, later named as 1G. When mobile networks began to be developed, each country created its own network architecture and mobile terminals, there was not any collaboration or compatibility between these systems causing that mobile terminals only worked in the country of origin.

In 1982, a consortium of European countries created the GSM (Groupe Spéciale Mobile) to develop the cellular technology that would provide a common European mobile phone service. GSM technology revolutionized cellular communications in the early 90s.

By 1987, The GSM consortium made the basic design for the GSM system, this implemented a narrowband TDMA system (Time Division Multiple Access) and GMSK (Gaussian Minimum Shift Keying) modulation scheme, reaching all major European cities by 1991 [4]. A second stage of this design was released in 1995, this time including sending data, fax, and video at a rate of 9,6 Kbps. Additionally, this version was enriched with Short Message Service (SMS) having a greater reception than expected. This design, including all these features, was known as 2G.

The great success of GSM system caused that many countries in the world adopted this technology, reaching territories outside Europe becoming GSM a global and not only a European technology. That was how the acronym GSM was transformed to “Global System for Mobile Communication”. Currently the GSM system is operational in most countries of the world [4].

Later in 2001, GSM evolved into GPRS (General Packet Radio Service), known as 2.5G. GPRS technology main improvement was to send the voice signal in digital format (packets), rather than sending it through the usual telephone circuits. GPRS was designed to make use of Internet in the mobile phones, reaching a maximum bit rate of 171,2 Kbps. Improvements continued and GPRS evolved to EDGE (Enhanced Data Rates for GSM Evolution) technology, this time implementing the 8PSK (8 Phase Shift Keying) modulation. EDGE uses the same bandwidth as GSM but increasing in speed to 384 Kbps.

The 3G system was developed and UMTS (Universal Mobile Telecommunications System) appeared in the mid-2000s. It is also called W-CDMA (Wideband Code Division Multiple Access) because this is the access technology implemented. The maximum bit rate of UMTS was 2 Mbps, allowing the implementation of features such as multimedia capabilities, Internet access, audio and video streaming in real time or video conference calls. In the next years, 3G systems continued evolving and some other standards appeared in this category. One of the most important was

HSPA+ (High Speed Packet Access), where MIMO (Multiple Input Multiple Output) technology was introduced for the first time, and with 64-QAM modulation scheme reaching a bit rate of 21 Mbps.

Eventually around 2010, 3G evolved to 4G systems, also known as LTE (Long Term Evolution). The idea with LTE was to comply with all the requirements of IMT-A (International Mobile Telecommunications - Advanced), involving the use of IP protocol in all the services provided. In LTE standard, an advanced radio interface is implemented, it uses OFDMA (Orthogonal Frequency Division Multiple Access) for the DownLink and SC-FDMA (Single Carrier - Frequency Division Multiple Access) for the UpLink. MIMO was included because its successful performance in the previous standard.

4G LTE and its improved version, LTE-Advanced, are the network standards more implemented in world and under exploitation mostly. These networks raise peak capabilities of 100 Mbps in downlink and 50 Mbps in uplink operating at channel bandwidth of 20 MHz. LTE provides latency of 10 ms, leading to the development and use of high demanding application like video streaming, high-definition multimedia content, real-time services, IoT applications, etc.

2.2.4.2 5G Technology

The progressive implementation of applications that make use of more demanding transmission bit rates, better latency, and the capability of serving as much device as possible at the same time, has led to new network technology called 5G. This technology is still under development and is implemented in few countries and cities.

The most notable advantage of this technology is that it will support greater bandwidth, which will translate into higher download speeds, that can exceed 10 Gbps. Additional to this huge improvement in bit rate, the latency accomplished is 1 ms. These characteristics implies that applications that currently 4G cannot support, are possible with 5G. The most important three applications for 5G are eMBB (Enhanced Mobile Broadband), uRLLC (Ultra-Reliable Low-Latency Communications), and mMTC (Massive Machine-Type Communications):

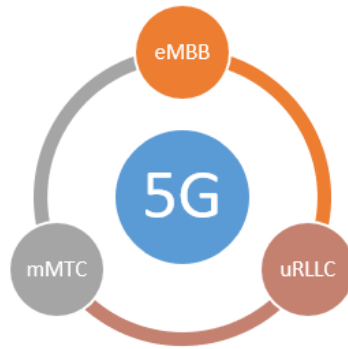


Figure 2.8. Three main applications of 5G networks.

In order of facilitating the transition from 4G to 5G, two phases of the new standard have been established by the 3GPP (entity in charge of establishing mobile telephony standards). An initial phase, Release 15 3GPP or better known as 5G NSA (Non-Standalone), which offers greater use of the 4G infrastructure; and the second phase, Release 17 or 5G SA (Standalone / full 5G), which requires a large amount of new hardware.

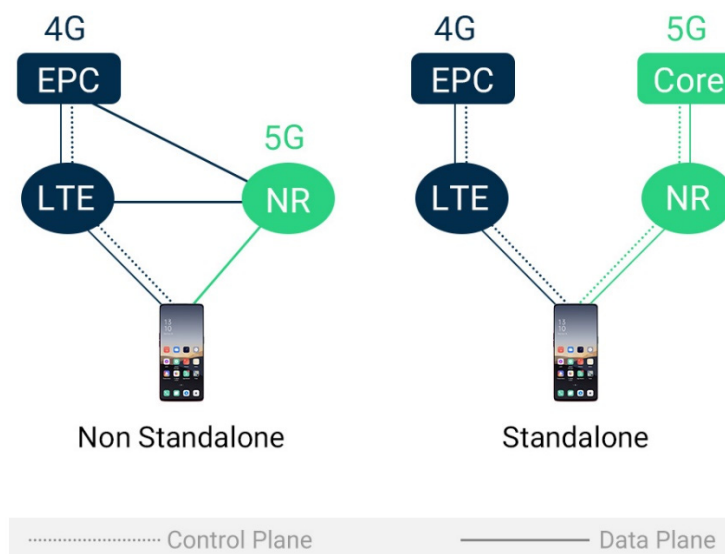


Figure 2.9. 5G networks in two phases (5G NSA, 5G SA).

While the 5G NSA infrastructure is implemented keeping the 4G Evolved Packet network Core (EPC) and the air Interface evolves from LTE to New Radio (NR), with the 5G SA, both the air interface and the core part are New Radio (NR) and Next Generation Core (NGCN). The 5G NSA is also 5G, but it does not have all the advantages.

With the 5G NSA, which is already beginning to be available, users of compatible smartphones will be able to benefit from a higher speed that will increase up to 2 Gbps, a latency that drops to 10 ms and greater stability and reliability in the connection, even in mobility or in crowds, thanks to technologies such as Massive MIMO.

Finally, the next table shows the main characteristics and comparison of all mobile network generations.

Table 2.6. Mobile network standard generations

| Generation | | | | |
|----------------------|------------|-----------|--------------------|--------------------|
| | 2G | 3G | 4G | 5G |
| Launch Year | 1991 | 2001 | 2010 | 2018 |
| Technology | GSM | CDMA | LTE | NR, Massive MIMO |
| Access system | TDMA | W-CDMA | OFDMA / SC-FDMA | NOMA |
| Bit rate | 171,2 Kbps | 21 Mbps | 100 Mbps | Higher than 1 Gbps |
| Latency | 600 ms | 120 ms | 10 ms | 1 ms |

With aim of providing high speed data services to the users and supply the increasing demand of connectivity; many operators and enterprises choose to employ a mix of different wireless technologies to reach the most users as possible, taking advantage of the fact that these users can operate different devices with different connectivity capabilities.

For example, many operators deploy WiFi network (WLANs) to supply connectivity in locations where a great percentage of users can utilize tablets and mobile phone at same time, a university campus for instance, then these users can choose to connect their tablet devices to WiFi while their mobile phones are connected to 4G network (WWAN).

In Table 2.7, a brief resume of wireless technologies is presented.

This chapter is important in the sense that understanding the different wireless technologies is crucial for this thesis. In this work, three use cases have been accomplished and analyzed, and the results can be applied in the development of technologies such as WPAN, WLAN and/or WWAN.

Table 2.7. Type of wireless technologies

| | WPAN | WLAN | WMAN | WWAN |
|------------------------|--|---|--|---|
| Type of Network | Personal Area Network | Local Area Network | Metropolitan Area Network | Wide Area Network |
| Goal | Transmit signals between devices in limited areas, typically few meters. | Provide Internet access within a house, building or limited outdoor area. | Provide access outside office and home networks. | Provide access outside the range of WLANs and WMAN. |
| Connectivity | Bluetooth, ZigBee, RFID, NFC | WiFi | WiMAX | 4G LTE / 5G |

2.3 RF Signals Propagation Mechanism

The principle of the telecommunications is the transmission of information between two or more points by means of a medium like wire, optical fiber, or electromagnetic waves. When the transmission medium is the electromagnetic waves, this is commonly known as wireless communication. The EM waves accomplish this transmission through the propagation mechanisms, which in turn, are directly determined or affected by the transmission channel, in this case the space, so called wireless channel.

The wireless channel is affected by many factors such as interference produced by other transmitters, changes in the environment, the presence of scatterers like human bodies, metal objects, tables, chair and so on. These factors impact directly in the signal being transmitted by the response of the propagation mechanism and possibly causing a failure in the data transmission.

In order of ensuring the proper performance, every telecommunication system must be designed so that in the receiver a minimum Signal to Noise Ratio (SNR) is obtained to guarantee operation. In the case of wireless channel, EM waves are exposed to different phenomena that can alter its propagation, influencing the received power, and therefore the SNR.

The way to ensure the appropriate SNR needed for a successful transmission, is understanding the propagation characteristics of an environment to make a correct implementation and deployment of the network.

Next, a brief description of the main propagation mechanisms will be presented.

2.3.1 Free-Space Propagation

The free space propagation model is used to predict received signal strength when the transmitter and receiver have a clear, unobstructed line-of-sight path between them [1]. This is an ideal condition mostly present with microwave line-of-sight radio links.

The free space model predicts that received power decays as a function of the distance between transmitter and receiver, this is known as free space path loss. The free space power received by a receiver antenna which is separated from a radiating transmitter antenna by a distance r , is given by the Friis free space equation:

$$\frac{P_R}{P_T} = \frac{1}{4 \cdot \pi \cdot r^2} \cdot D_T \cdot A_{efR} = \left(\frac{\lambda}{4 \cdot \pi \cdot r} \right)^2 \cdot D_T \cdot D_R = \left(\frac{1}{\lambda \cdot r} \right)^2 \cdot A_{efT} \cdot A_{efR}$$

Free space path loss increases with the square of distance between the antennas because the radio waves spread out by the inverse square law and decreases with the square of the wavelength of the EM waves. Observing the above formula, the distance and frequency of operation are key parameters to estimate the received power level in free space propagation.

2.3.2 Reflection

The EM waves when travelling from transmit antenna to receive antenna can face many obstacles in the way. The material parameters of these elements (dielectric permittivity and loss tangent at frequency of operation) influence the propagation of these EM waves. When an EM wave impacts on an obstacle, a reflection is observed.

The percentage of the reflected energy will depend on the material of the object hit by the propagating wave. Figure 2.10 shows a representation of reflection phenomenon, where the incident angle (θ_i) and the reflected angle (θ_r) are equal.

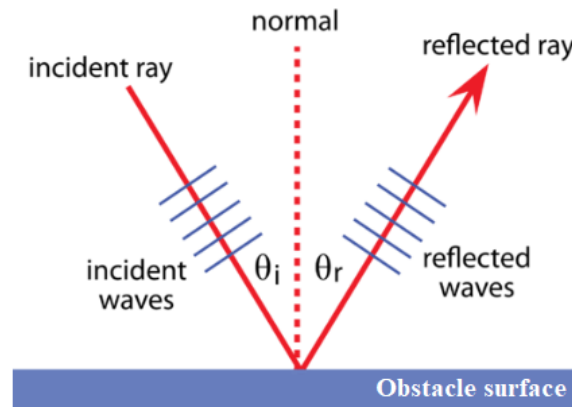


Figure 2.10. Reflection phenomenon representation.

The superposition of the direct and reflected wave gives rise to the so-called space wave. The space wave creation can be constructive or destructive depending on the phases of the direct and the reflected waves [5].

2.3.3 Diffraction

Another phenomenon that can occur when EM waves impact objects is the diffraction. This mechanism is completely related to the shape and size of the area impacted and shows up when it reaches an edge or very narrow object.

When diffraction takes place, the obstacle re-radiates part of the intercepted energy. The diffraction makes possible the reception of the radiated waves even in the case that there is no direct visibility between transmit antenna and receive antenna [5].

After the diffraction phenomenon, the diffracted energy could have different behaviors according to the characteristics of the impacted area. Even though there will be a shadow zone immediately behind the obstacle, the signal will diffract around the obstacle and start to fill the void. It is found that diffraction is more pronounced when the obstacle becomes sharper and more like a "knife edge" (see Figure 2.11).

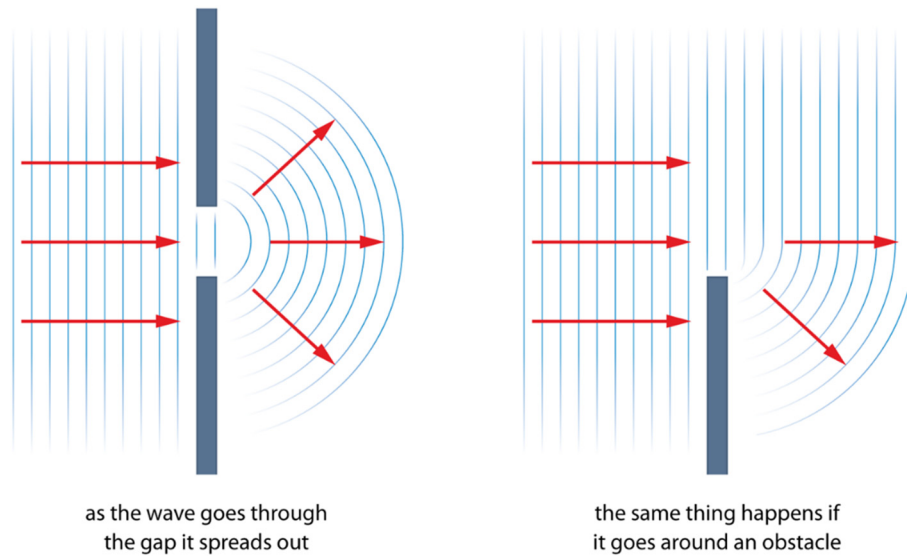


Figure 2.11. Diffraction phenomenon representation.

2.3.4 Scattering

Scattering is the process by which an extremely small obstacle (or point in the space) in the path of an EM wave, continuously removes energy from the incident wave and re-radiates the energy into the total solid angle centered at the point impacted.

This extremely small obstacle is usually a rough surface or irregularities in the area. The dimensions of this “obstacle” impacted should be in the order of the wavelength (λ) of the incident wave for the scattering to arise (see Figure 2.12).

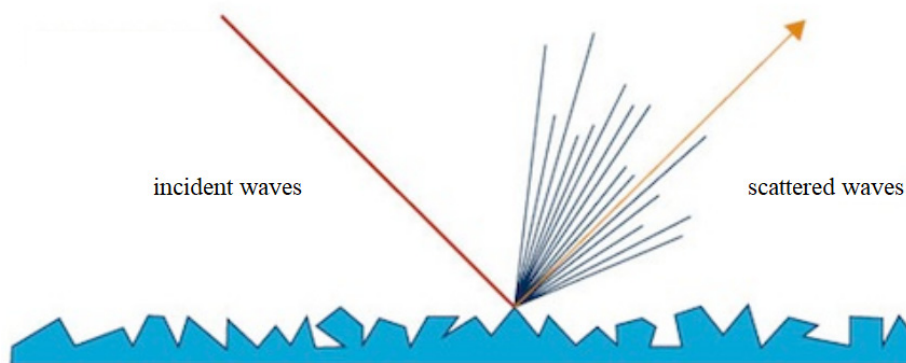


Figure 2.12. Scattering phenomenon representation.

2.4 Propagation Models in Wireless Channel

As mentioned before, the continue increase of devices connected with the appearance of IoT, the high and growing demand of connection capacity in terms of bit rate and coverage; have led to the designing of wireless systems became a very challenging task. One of the key factors in the process of designing a system is the estimation of received power level within the scenarios where the wireless communication systems are going to be deployed.

With the aim to do an accurate prediction of wireless characteristics of the environment, including the power estimation; the propagation models play a key role in this purpose.

The radio propagation models are mathematical formulation for the characterization of radio wave propagation as a function of environments characteristic, distances, frequency, and other conditions. A model is usually developed to anticipate the behaviour of propagation for all identical links under identical constraints. These models could predict the path loss along a link or the effective coverage area of a transmitter, for instance.

Propagation models can be classified as theoretical, empirical, and deterministic. Following, a brief description of these models will be presented.

2.4.1 Theoretical Models

Employing theoretical approach to estimate radio propagation within complex environments such as urban, suburban, or indoor areas is basically an unmanageable electromagnetic problem because there is no enough detailed geometric description of the coverage area and the several boundary conditions within the scenarios.

One of these models is Free Space model, based on the Friis formula. In this technique, the radiated energy by an omnidirectional antenna spreads as the surface of a sphere centered on the antenna. This model of propagation is used to predict the power of the signal between the transmitter and receiver when there is a clear line of sight.

Another example of theoretical model is the Diffracting Screens. This model is derived using physical optics assuming uniform spacing and heights of buildings. This model is based on a geometrical generalization of Walfisch and Bertoni model [6].

In this technique is considered the impact of the rooftops and building height by using diffraction to predict average signal strength at street level. A general description of the of model is depicted in Figure 2.13.

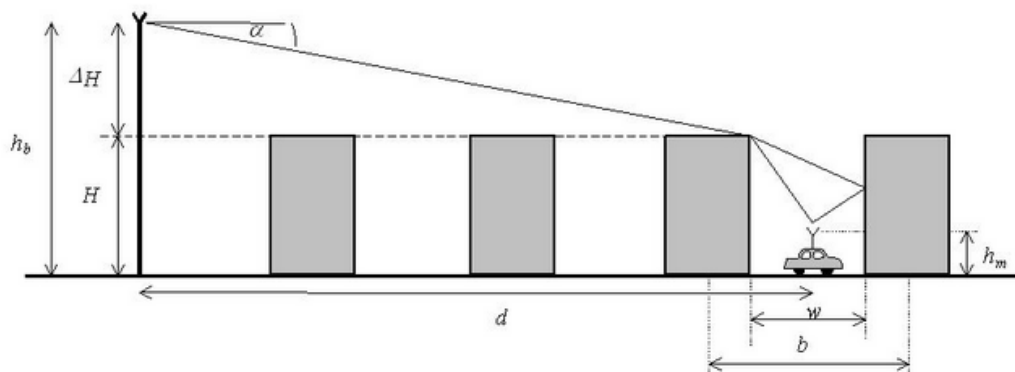


Figure 2.13. Walfisch and Bertoni model representation.

2.4.2 Empirical Models

Empirical methods (also called statistical) provide fast estimate of propagation loss or, alternatively, the field strength at any point around a transmitter. They are quick and easy to use, but obviously they have not a lot of accuracy. These models are based on measurements. They are usually a set of equations derived from extensive field measurements.

Several empirical models have been developed based on measured data and use curve-fit equations to model propagation in areas of urbanization. Often empirical models are city specific and tied to urban land-use maps. The London model of M. F. Ibrahim and J. D. Parsons is an example of such a model [7,8]. Another, more generalized, hence more commonly used, empirical model is that of Y. Okumura [9]. Their model is based on extensive measurements in Tokyo, Japan.

These models are recommended when no high accuracy is required. A great disadvantage of empirical models is that they cannot be used for different environments without modification.

2.4.3 Deterministic Models

Deterministic models or geometrical models estimate the field strength (or signal power) directly from the path profile (profile of the environment between the transmitter and the receiver). Besides free space losses, these models also take account of losses due to diffraction, reflection and scattering in cases where there is insufficient clearance within the radio path. Accordingly, geometrical models require a detailed knowledge of the scenario.

These methods are based on numerical approaches involving either solution of Maxwell's equations using full-wave simulation techniques, such as MoM and FDTD [10], or, using geometrical approximations such as Ray Launching (RL) [11] and Ray Tracing (RT) [12].

Previously, RL and RT were both classified as ray tracing methods, although more recently both methods are distinguished. RL technique principle is that the transmitter launches thousands of test rays in a solid angle and the true path is determined by looking for the rays arriving at the receiver. In the other hand, RT methods compute propagation paths using 3D environment geometry and determining the path loss and phase shift of each ray using electromagnetic analysis.

The RT model uses either the Shooting and Bouncing Rays (SBR) method or the Image method. For the case SBR, a representation is depicted in Figure 2.14.

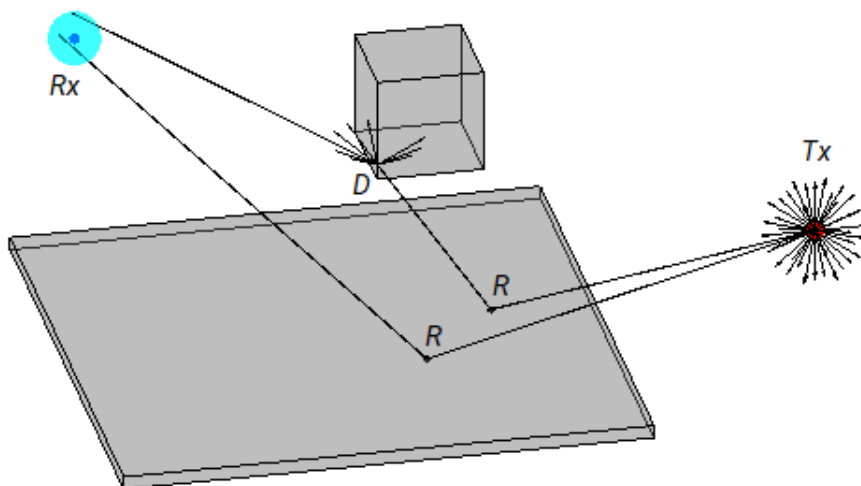


Figure 2.14. SBR Ray Tracing method principle.

In this Thesis, the wireless characterization of complex indoor scenarios was required. For these cases, Ray Tracing and Ray Launching methods offer a good trade-off between accuracy and computational resources needed, providing quite accurate RF power estimations. On account of this, an in-house developed Ray Launching algorithm has been used to analyse the radio propagation behaviour in the environments under study in this work.

It is important to mention that the subsection of propagation mechanism was included and detailed in this chapter because the way of EM waves propagation is affected by these phenomena are crucial topics for this thesis, specially to understand the simulation process using the 3D RL algorithm where these propagation mechanisms are taken into account.

Chapter 3

MIMO Systems Theory

THE current world, where every day new and present wireless communication technologies are demanded to provide more transmission bit rate, improved delay and better reliability during the communication is established, is forcing these technologies to evolve in a faster way. This evolution is traduced in the development of new technologies to increase the performance of the systems; in the physical layer of the system, the most relevant technique being implemented and researched is the MIMO (Multiple Input Multiple Output) technology. This chapter is mainly focused on the explanation of wireless channel characterization and its importance for MIMO systems. Initially, a historical outlook to the origin of MIMO is presented in section 3.1. Then, in section 3.2, we explained the meaning of MIMO communications and the channel models used for its study. The MIMO channel is clearly described in section 3.3, which is highly important for the development of this thesis. Finally, in section 3.4, four space-time coding techniques are reviewed in detail, and in section 3.5 the application of these techniques in the thesis is commented.

3.1 Historical Outlook to MIMO

MIMO (Multiple-Input Multiple-Output) technology since the beginning was of great interest mainly because it allows increasing the amount of information we transmit, but also, as in classical diversity systems, can increase the reliability of link, or make a trade between these functionalities.

The unequivocal advantage and importance of integrating MIMO technology in a wireless system, is evidenced by its use in existing and emerging wireless communication standards such as WiFi (802.11b/g/n/ac/ax), Long Term Evolution (LTE), 5G NSA/SA and so on.

Interestingly, like many other brilliant solutions developed in these years in the field of digital communications, the MIMO concept is not a new idea but dated back to the 1970s and was studied as a model for multipair telephone cables [13].

At the time that MIMO increases the transmission bit rate, it also occupies the same bandwidth allotment as in standard Single-Input Single-Output (SISO) technology, improving this way the bandwidth efficiency, which is highly important for mobile network operators, for example, where the amount of available bandwidth is limited. The bandwidth efficiency, also called spectral efficiency, is a measure of how well a certain frequency band employed to transmit data is used. The higher this value, the better used that band is. See next Equation.

$$\text{Spectral efficiency} = \frac{\text{Throughput (bps)}}{\text{Channel Bandwidth (Hz)}} \quad (3.1)$$

It is likely for this reason why the first concrete analysis of a MIMO implementation was done in a cellular network scenario by Winters in [14]. This scenario was composed by a base station equipped with multiple antennas and one antenna in the mobile terminals, transmitting in the same frequency band. In that work, Minimum Mean Squared Error (MMSE) linear processing (also known as optimum combining) was applied to remove the co-channel interference caused by the simultaneous transmission of the mobile terminals.

In 1996, Foschini introduced his now well-known concept of Layered Space-Time (LST) architecture [15]. Since then, the implementation of multiple transmit and multiple receive antennas has been amongst the most important fields of study for the design of wireless communication systems. In this work, he proposed an architecture for a point-to-point MIMO communication system where the data stream generated by the source was divided in several branches and encoded without sharing any information with each other. The algorithm was later dubbed Bell Laboratories Layered Space-Time (BLAST).

Foschini's work is considered one of the first space-time multiplexing technique, and of course was the motivation of developing new studies in space-time coding.

Few time later of Foschini contribution, a space-time trellis coding was introduced by Tarokh in [16]. In this work, symbols are encoded according to the antennas through which they are simultaneously transmitted and are decoded using a maximum likelihood decoder. This scheme is very effective in providing considerable performance gains, but with the handicap that requires additional processing, which increases exponentially as a function of bandwidth efficiency and the required diversity order.

Another approach, that avoids this complexity in processing, was presented by Alamouti in 1998 [17], the simplest space-time algorithm applicable to a system of two transmit antennas, and as minimum of one receive antenna. Alamouti scheme achieves the full diversity with a very simple maximum likelihood decoding algorithm. The main functionality of the scheme is the sequence of encoding, which applies orthogonality between the symbols transmitted by the two transmit antennas.

The Alamouti scheme is unique and is only applicable to a system with maximum of 2 antennas in diversity transmission.

After the remarkable scheme presented by Alamouti, a new work was presented by Tarokh applying the theory of orthogonal designs to create analogues of Alamouti's scheme, namely, Space-Time Block Codes [18], for more than two transmit antennas.

The space-time block codes are one of the most important class of space time coding, and are known as orthogonal space time codes because the encoding process. As compared to the uncoded single antenna systems, the STBC causes a rate loss, and only the Alamouti scheme achieve a full rate for all complex modulation scheme. Another systematic design method for high-rate optimized space-time block code was presented in [19] for complex constellations and arbitrary number of antennas in transmission.

Apart from STBCs, another interesting and novel scheme was presented by Joungh in [20], where CSI is only present in transmitter. These techniques are referred as Space-Time Line Code because the encoding structures.

After these works, many other contributions have been presented addressing the different aspect of the MIMO architecture and the interest on MIMO topics has been always high.

3.2 MIMO Communications

The available bandwidth, or the frequency range, is a very special and scarce resource in a given radio channel, and it is the needed assets to accomplish the transmission. Regulatory entities of countries strictly regulate the allotment of bandwidth to civilian entities, such as cell phone services providers. Given a constant transmission rate for each user in a network, providers want to maximize the number of users within their allotted bandwidth. Thus, the issue then becomes one of bandwidth efficiency.

MIMO technology base is that, in the transmitter, each antenna broadcasts an independent signal on the same bandwidth. The two signals are combined in the channel, and each receive antenna captures an independently faded version of the combined signals. See Figure 3.1.

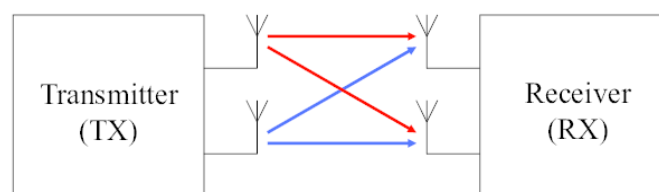


Figure 3.1 Basic representation of MIMO system.

In this way we increase our chances that at least one Antenna at the receiver does not suffer from multipath fading. By increasing the number of Antennas at the receiver, we better the odds.

A MIMO system has the ability to translate increased spatial diversity into increased channel capacity. The capacity of a MIMO channel is highly dependent on the spatial structure of the channel. MIMO channel models are an important tool in understanding the potential gains of a MIMO system.

In the next section, the MIMO channel models will be reviewed.

3.2.1 MIMO Channel Models

Research works have probed that, depending on the environment, the capacity of a measured channel often falls short of the limit given by Foschini. Space-time algorithms that focus on approaching the MIMO capacity bound rely heavily on the multipath diversity of the channel. As a result, their overall performance is highly dependent on the environment. Thus, there is need to accurately model the MIMO channel to evaluate properly the performance gains of MIMO versus diversity or single antenna systems.

MIMO channel models have two purposes:

- MIMO channel model can be used in the design of a MIMO system. This includes the design of an optimal signalling scheme, detection scheme, and space-time code. The same model can often be used to test a given system. In this case, the model acts as channel simulator.
- The most important purpose of a MIMO channel model is to gain some insight into the underlying physics of the channel. At higher level, an accurate channel model can tell us a lot about the behaviour of a given channel.

Two of most representative MIMO channel models are briefly described in the following subsection.

3.2.1.1 Cluster Models

These are a compromise between stochastic and ray tracing models. They use rays, called multipath components, to simulate reflected energy in a channel. Then, the multipath components are stochastically modelled using a number of parameters measured from real-life channels. To simplify the model, the multipath components are grouped into *Clusters*, with multipath components in each *Cluster* having similar statistic. *Clusters*, in turn, simulate the behaviour of objects in the channel [21].

3.2.1.2 Correlative Models

This model attempt to approximate the spatial structure of the channel by modelling the correlation between paths in a MIMO channel. These models bias a “white” channel matrix with correlation matrices at the transmitter and receiver to approximate the correlation between scatterers at both link ends. The white channel matrix consists of uncorrelated complex-Gaussian elements [21]. The three main correlative channel Models:

- Kronecker
- Weichselberger
- Structured Models

Due to its simplicity, the Kronecker model is by far the most popular MIMO channel model in the literature. It greatly simplifies channel analysis, as it holds that scatterers around the transmitter fade independently of those around the receiver. Despite its popularity, the Kronecker model has been shown to be inaccurate. The Weichselberger model uses the eigen-value decomposition (EVD) of the channel as its parameters, and, in most cases, is more accurate than the Kronecker model. The Structured Model is an extension of the Weichselberger model to the wideband MIMO channel. It uses tensors to express the wideband MIMO channel in an elegant fashion, often with fewer parameters than the Kronecker model.

In general, channel models for wireless systems have been primarily concerned with modelling the effects of the following parameters on the transmitted signal: path loss, delay spread, shadowing, doppler spread, and Rician K-factor. Parameters of specific interest to the MIMO channel are the *Joint Antenna Correlations* and *Channel Matrix Singular-value Distribution*. Also, of interest in the MIMO channel is the spatial diversity, which can be measured by analysing the H-matrix singular-value distribution. In this way, the MIMO channel can be decomposed into a number of parallel SISO channels whose channel gains are directly related to the singular values of H-matrix. By analysing the distribution of the singular values in different environments, we can assess the performance gain of MIMO over other signalling techniques.

The MIMO channel models explained before are very good tools to estimate the behaviour of a MIMO systems in different environment. Those are a great choice when no other technique is available and that is why was important to present this subsection.

In this thesis, the wireless channel characterization was accomplished by an in-house 3D Ray Launch tool, obtaining the most accurate estimation of behaviour of MIMO channel in very specific indoor complex scenarios.

3.3 The MIMO Channel

In all communication system, the channel is the central part that engineers can't master. In wireless systems, the channel is the air or any other medium who allows the propagation of EM (electromagnetic) waves. The signal carrying the information travels in the form of EM waves, and the behaviour and modification of this signal when is propagated over the channel, is determining for the overall performance of a wireless communication system.

Most wireless communication channels consist of multiple signal paths travelling from transmit antenna to receive antenna. These *multiple paths* are caused by the presence of objects in the route of the signal journeying along the environment that, through the mechanisms of propagation such as free space propagation, reflection, diffraction, and

scattering, alter the path of radiated energy. These objects are referred to as Scatterers [21]. Figure 3.2 shows a multipath channel representation.

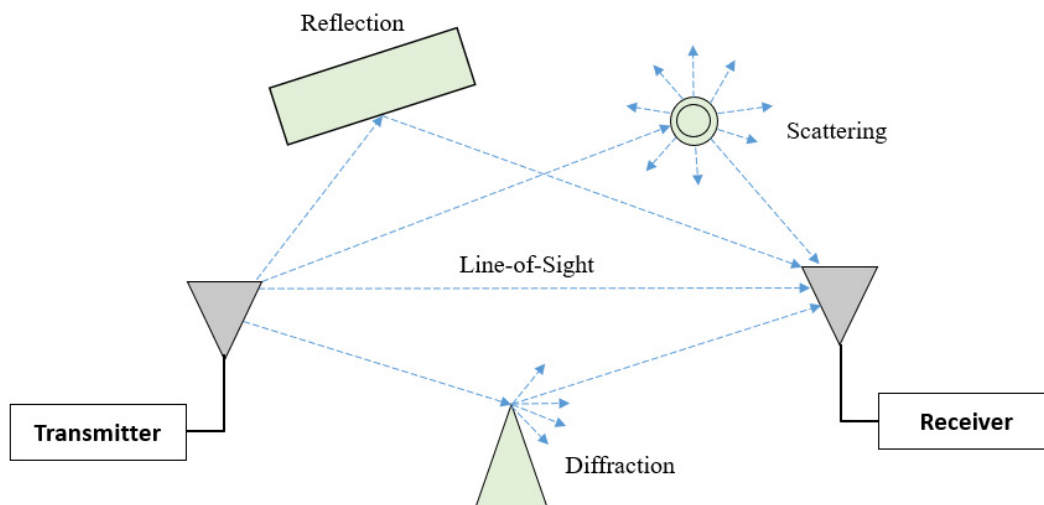


Figure 3.2 Multipath channel representation. Effect of mechanisms of propagation over a wireless signal.

These multipath components of the signal have different amplitudes and phases when arriving to receiver, of course because the paths travelled have different length. In some cases, the multiple signals add destructively at the receiver, creating points in space where the composite received signal is greatly attenuated. This is referred to as *multipath interference* [21].

For long, communication systems designers were fighting this multipath interference in different ways, because depending on the physical environment characteristics, this interference could prevent the establishment of stable communication. MIMO technology take advantage of multipath channels by broadcasting independent bit streams or signals from different transmit antennas on the same frequency and bandwidth. Because the multipath richness, each signal transmitted from each different antenna, have the chance to suffer less or different fading in the travel to the receiver.

Before MIMO technology development, it was impractical such transmission scheme, because the signals are combined in the channel, and each receive antenna captures an independently faded version of the combined signals. It was after the different MIMO coding methods appearance, that transmitted streams captured at the receiver could be

separated from the combined signal. Figure 3.3 shows an example of a 2 x 2 MIMO system.

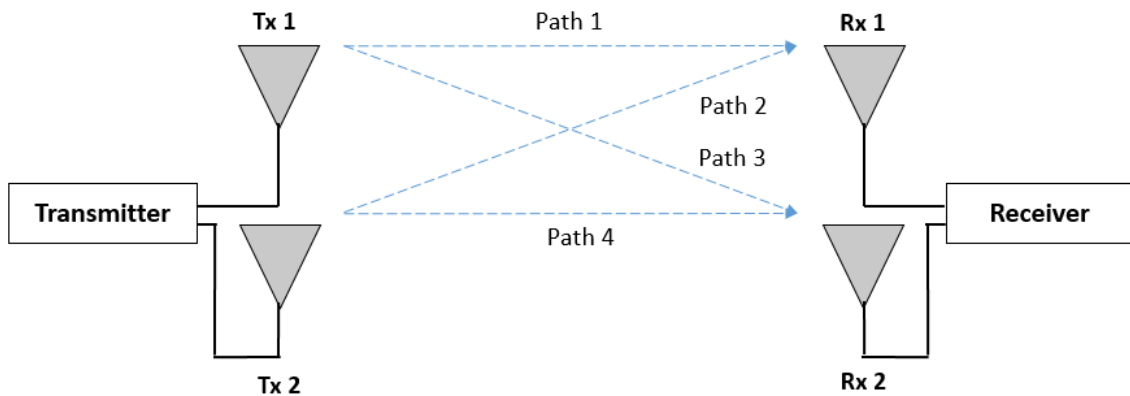


Figure 3.3 Example of a 2 x 2 MIMO system. Each Rx antenna capture the combined signals radiated from both Tx antennas.

The MIMO channel can be viewed as a collection of many SISO channels. One SISO channel exists between each transmit-receive pair. Each SISO channel is often referred to as path or parallel channel [21]. We often refer a MIMO channel as being composed of many paths, see Figure 3.3.

Generally, we use a complex gain to characterize each path, then, we express all complex gains as a Matrix H , see Equation 3.2.

$$H = \begin{bmatrix} h_{11} & \cdots & h_{1N} \\ \vdots & \ddots & \vdots \\ h_{M1} & \cdots & h_{MN} \end{bmatrix} \quad (3.2)$$

We refer to H as *H-Matrix*, and thus to the MIMO channel as the matrix channel. Each element of H is the complex gain h_{MN} between receive-antenna M , and transmit-antenna N .

The performance of a MIMO system is dependent on the characteristics of the radio environment, given by the values of the *H-Matrix* [22]. We can measure this performance as a function of the capacity of the channel. Thanks to the contribution of Foschini [15], where he firstly presented his famous formula, we can calculate this capacity, see Equation 3.3.

$$C = B \log_2 \det \left(I_M + \frac{snr}{N} H H^H \right) \quad (3.3)$$

Where; I_M is the $M \times M$ identity matrix, snr is the Signal-to-Noise Ratio per receive antenna, $()^H$ is the Hermitian transpose, H is a matrix whose entries are the $M \times N$ channel gains (H -matrix), M and N denotes the number of receive-antenna and transmit-antenna, respectively.

3.4 Space-Time Coding

The main advantage that MIMO provides is probably the increase in link capacity. This can be characterized as multiplexing gain and arises because the MIMO channel is able to transmit multiple data streams simultaneously over the same bandwidth, using N transmit antennas spatially separated; hence, the term spatial multiplexing that is usually used to denote MIMO. Additional to the spatial aspect, and depending on the coding scheme, the coded data streams will be transmitted using a specific number of symbol periods, thus the transmission is done across both space and time.

In a Space-Time coding technique, the bit/data stream is firstly modulated using a specific digital modulation scheme such as QPSK, 16-QAM, and so on. Using the symbols generated by the modulator, the Space-Time encoder generates a code-specific, scaled unitary transmission matrix U_x [23] to be transmitted by N transmit antennas. Figure 3.4 depict a block diagram of a digital transmitter employing Space-Time coding and N transmit antennas.

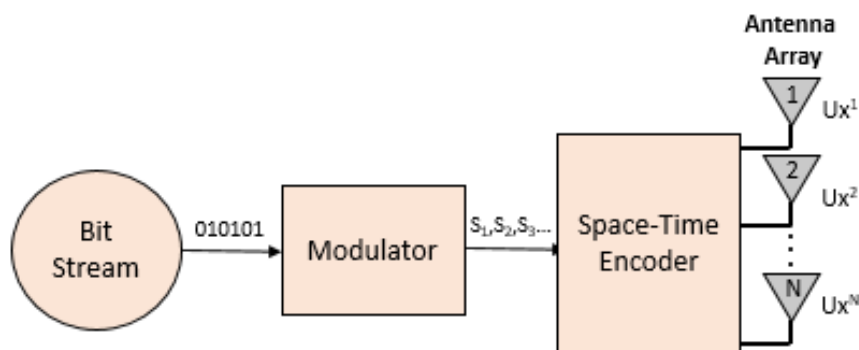


Figure 3.4 Block Diagram of transmitter employing Space-Time Coding. With N antennas in transmission.

In the context of wireless communications, and as It was stated before, with the implementation of these techniques, we wish to improve the transmission system's spectral efficiency defined as,

$$\eta = \frac{r_b}{B} \text{ bits/s/Hz} \quad (3.4)$$

Where r_b is the data rate of information-carrying bits at system input and B is the available frequency bandwidth of the transmission channel. This spectral efficiency η depends on and varies according to the Space-Time code technique implemented in the wireless communications system.

We can find numerous of coding techniques that have been presented from different authors, including Space-Time Block Codes (STBC), Space-Time Trellis Codes (STTC), Space-Time Line Code (STLC), Space-Time Turbo Trellis Codes, Layered Space-Time (LST) Codes and so on. In this work, we will focus our analysis using STBC, STTC and STLC.

In the next four subsections, we will review the Space-Time Block Coding technique, Space-Time Trellis Codes and Space-Time Line Code. Beginning with the Alamouti Scheme which is considered the simplest block coding applicable to a diversity system of 2 Tx antennas and 2 Rx antennas, MIMO 2x2. We also will briefly review the generalization of STBC for diversity systems with more of 2 transmit antennas. Then, we will discuss and evaluate STTC using a practical example. Finally, the STLC will be presented.

3.4.1 The Alamouti Scheme

In the remarkable work presented by Siavash Alamouti, He proposed a simple, yet fundamentally new Space-Time coding method with $N = 2$ transmit antennas and, as a minimum, $M = 1$ receive antennas [17]. This work, known as the Alamouti scheme, also triggered a large number of theoretical and practical investigations into the research areas of space-time coding, optimal transmit matrices, rate and performance analyses, etc. [23].

The key feature of the scheme is that it achieves a full diversity gain with a simple maximum-likelihood decoding algorithm [24]. In order to explain the Alamouti scheme, let's use a transmit diversity system with 2 transmit antennas and 2 receive antennas, Figure 3.5 shows a block diagram of the scheme.

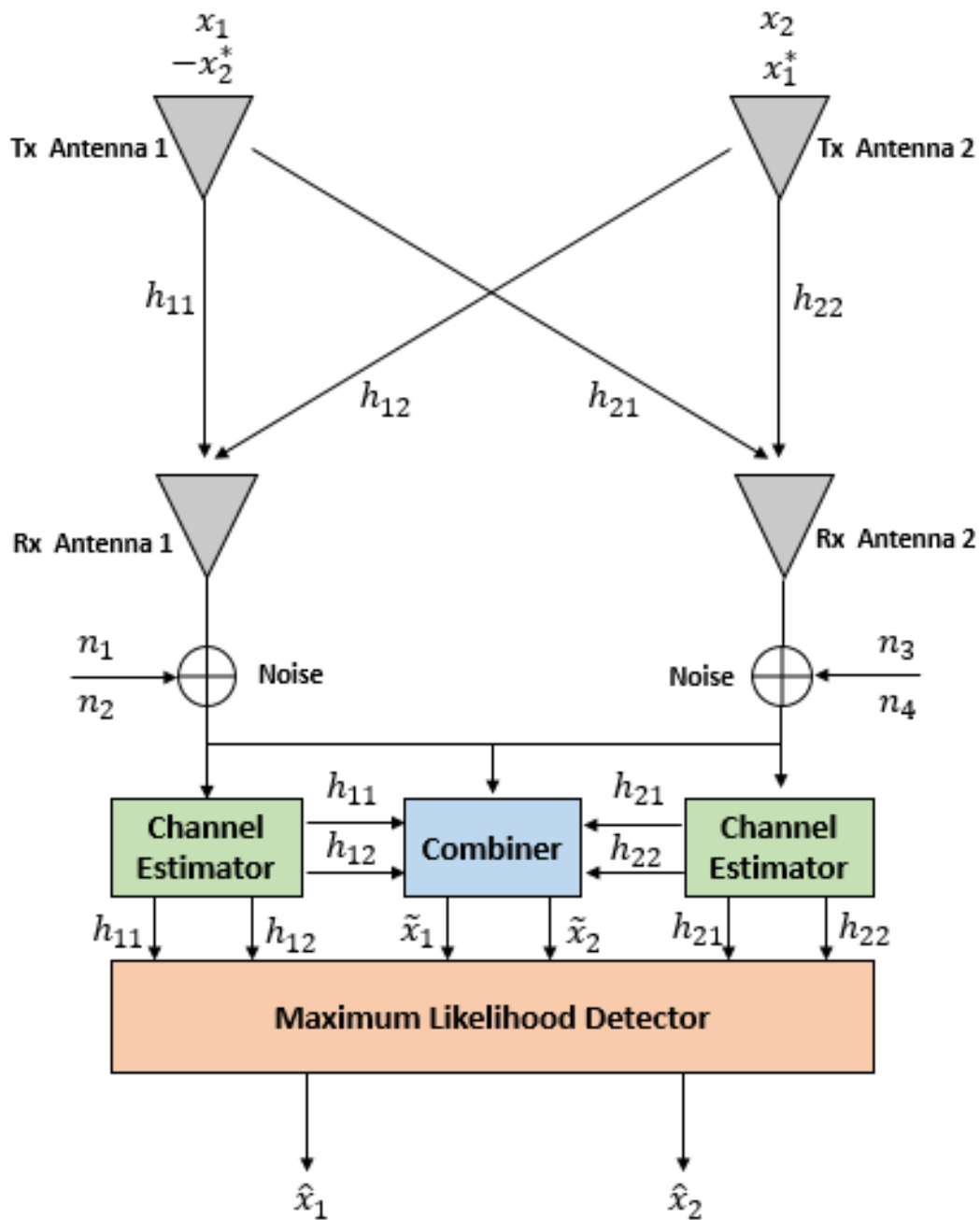


Figure 3.5 Block Diagram of Alamouti Scheme. Using two-branch transmit diversity with two receivers.

This scheme may be defined by the following three functions:

- Encoding and transmission sequence,
- Combining scheme at receiver and,
- Maximum likelihood decision rule.

3.4.1.1 The Encoding and Transmission Sequence

In order to explain the encoding process, let's say that an M -ary modulation scheme is firstly used to modulate the bits stream in groups of m bits, where $m = \log_2 M$. Then, the encoder takes a block of two modulated symbols to be transmitted at a given symbol period simultaneously by the two transmit antennas. The signal transmitted from antenna one is denoted by x_1 and from antenna two by x_2 . In the next symbol period signal $-x_2^*$ is transmitted from antenna one, and signal x_1^* is transmitted by antenna two. Note that $*$ is the complex conjugate operation. This process and sequence are shown in Table 3.1.

Table 3.1 The encoding and transmission sequence for the scheme

| | Tx Antenna 1 | Tx Antenna 2 |
|--------------|---------------------|---------------------|
| time t | x_1 | x_2 |
| Time $t + T$ | $-x_2^*$ | x_1^* |

The channel response or channel coefficients at time t may be modeled by a complex multiplicative distortion h_{MN} , where h denoting the fading coefficient for the path from transmit antenna N to receive antenna M . Assuming that the fading coefficients are constant across two consecutive symbol periods, they can be express as

$$\begin{aligned}
 h_{11}(t) &= h_{11}(t + T) = h_{11} = |h_{11}|e^{j\theta_{11}} \\
 h_{12}(t) &= h_{12}(t + T) = h_{12} = |h_{12}|e^{j\theta_{12}} \\
 h_{21}(t) &= h_{21}(t + T) = h_{21} = |h_{21}|e^{j\theta_{21}} \\
 h_{22}(t) &= h_{22}(t + T) = h_{22} = |h_{22}|e^{j\theta_{22}}
 \end{aligned} \tag{3.5}$$

Where $|h_{MN}|$ and θ_{MN} , are the amplitude gain and phase shift for the path from transmit antenna N to receive antenna M , and T is the symbol duration. Table 3.2 shows the channel definition of the scheme.

Table 3.2 The definition of channels between transmit and receive antennas.

| | Tx Antenna 1 | Tx Antenna 2 |
|---------------------|---------------------|---------------------|
| <i>Rx Antenna 1</i> | h_{11} | h_{12} |
| <i>Rx Antenna 2</i> | h_{21} | h_{22} |

At the receive antennas, the received signals over the two consecutive symbols periods, denoted by r_1 and r_2 for time t and $t + T$, respectively, for receive antenna 1, and r_3 and r_4 for time t and $t + T$, respectively, for receive antenna 2, can be expressed as

$$\begin{aligned}
 r_1 &= h_{11}x_1 + h_{12}x_2 + n_1 \\
 r_2 &= -h_{11}x_2^* + h_{12}x_1^* + n_2 \\
 r_3 &= h_{21}x_1 + h_{22}x_2 + n_3 \\
 r_4 &= -h_{21}x_2^* + h_{22}x_1^* + n_4
 \end{aligned} \tag{3.6}$$

Where n_1, n_2, n_3 and n_4 are independent complex variables with zero mean and power spectral density $N_0/2$ per dimension, representing Additive White Gaussian Noise (AWGN) at time t and $t + T$, at receive antenna 1 and receive antenna 2, respectively. Table 3.3 depicts the arrival order of received signals.

Table 3.3 The received signals at the two receive antennas.

| | Rx Antenna 1 | Rx Antenna 2 |
|-------------------|---------------------|---------------------|
| <i>time t</i> | r_1 | r_3 |
| <i>Time t + T</i> | r_2 | r_4 |

3.4.1.2 The Combining Scheme

If the channel fading coefficients, h_{MN} , can be perfectly recovered at the receiver, the decoder will use them as the Channel State Information (CSI). The combiner shown in Figure 3.5 builds the following two combined signals using the received signals and the Channel State Information, that are sent to the Maximum Likelihood Detector:

$$\begin{aligned}\tilde{x}_1 &= h_{11}^* r_1 + h_{12} r_2^* + h_{21}^* r_3 + h_{22} r_4^* \\ \tilde{x}_2 &= h_{12}^* r_1 - h_{11} r_2^* + h_{22}^* r_3 - h_{21} r_4^*\end{aligned}\quad (3.7)$$

Substituting (3.5) and (3.6) into (3.7) we get

$$\begin{aligned}\tilde{x}_1 &= (|h_{11}|^2 + |h_{12}|^2 + |h_{21}|^2 + |h_{22}|^2)x_1 + h_{11}^* n_1 + h_{12} n_2^* + h_{21}^* n_3 \\ &\quad + h_{22} n_4^* \\ \tilde{x}_2 &= (|h_{11}|^2 + |h_{12}|^2 + |h_{21}|^2 + |h_{22}|^2)x_2 - h_{11} n_2^* + h_{12}^* n_1 - h_{21} n_4^* \\ &\quad + h_{22}^* n_3\end{aligned}\quad (3.8)$$

3.4.1.3 Maximum Likelihood Decision Rule

Finally, a Maximum Likelihood Detector (MLD) is employed to find the two signal points closest to the transmitted ones.

Assuming that all the signals in the modulation constellation are equiprobable, the maximum likelihood detector chooses a pair of signals (\hat{x}_1, \hat{x}_2) from the signal modulation constellation to minimize the distance metric

$$\begin{aligned}& d^2(r_1, h_{11}\hat{x}_1 + h_{12}\hat{x}_2) + d^2(r_2, -h_{11}\hat{x}_2^* + h_{12}\hat{x}_1^*) + \\ & d^2(r_3, h_{21}\hat{x}_1 + h_{22}\hat{x}_2) + d^2(r_4, -h_{21}\hat{x}_2^* + h_{22}\hat{x}_1^*) \\ &= |r_1 - h_{11}\hat{x}_1 - h_{12}\hat{x}_2|^2 + |r_2 + h_{11}\hat{x}_2^* - h_{12}\hat{x}_1^*|^2 + \\ & |r_3 - h_{21}\hat{x}_1 - h_{22}\hat{x}_2|^2 + |r_4 + h_{21}\hat{x}_2^* - h_{22}\hat{x}_1^*|^2\end{aligned}\quad (3.9)$$

over all possible values of \hat{x}_1 and \hat{x}_2 . Substituting (3.6) into (3.9), the maximum likelihood detector can be represented as

$$(\hat{x}_1, \hat{x}_2) = \arg \min_{(\hat{x}_1, \hat{x}_2) \in C} (|h_{11}|^2 + |h_{12}|^2 + |h_{21}|^2 + |h_{22}|^2 - 1)(|\hat{x}_1|^2 + |\hat{x}_2|^2) + d^2(\tilde{x}_1, \hat{x}_1) + d^2(\tilde{x}_2, \hat{x}_2) \quad (3.10)$$

where C is the set of all possible modulated symbol pairs (\hat{x}_1, \hat{x}_2) , \tilde{x}_1 and \tilde{x}_2 are the two decision statistic constructed by the combiner using the received signals and CSI explained before and depicted in (3.8).

For a given channel realization h_{11} , h_{12} , h_{21} and h_{22} , the decision statistics \tilde{x}_1 and \tilde{x}_2 , are only a function of x_1 and x_2 . Thus, the maximum likelihood decision rule (3.10) can be expressed in two independent decision rules as follow

$$\begin{aligned} \hat{x}_1 &= \arg \min_{\hat{x}_1 \in C} (|h_{11}|^2 + |h_{12}|^2 + |h_{21}|^2 + |h_{22}|^2 - 1)|\hat{x}_1|^2 + d^2(\tilde{x}_1, \hat{x}_1) \\ \hat{x}_2 &= \arg \min_{\hat{x}_2 \in C} (|h_{11}|^2 + |h_{12}|^2 + |h_{21}|^2 + |h_{22}|^2 - 1)|\hat{x}_2|^2 + d^2(\tilde{x}_2, \hat{x}_2) \end{aligned} \quad (3.11)$$

For M -PSK signals, where energy constellations are equal for all signal points, the decision rule in (10) can be simplified to

$$\begin{aligned} \hat{x}_1 &= \arg \min_{\hat{x}_1 \in C} d^2(\tilde{x}_1, \hat{x}_1) \\ \hat{x}_2 &= \arg \min_{\hat{x}_2 \in C} d^2(\tilde{x}_2, \hat{x}_2) \end{aligned} \quad (3.12)$$

3.4.2 Space-Time Block Codes (STBC)

As stated by Tarokh, band-limited wireless channels are narrow pipes that do not accommodate rapid flow of data. Deploying multiple transmit and receive antennas broadens this data pipe [16]. One interesting approach for deploying multiple transmit and receive antennas is the Space-Time Trellis Coding presented by Tarokh in [16], this proposal combines signal processing at the receiver with coding techniques appropriate to multiple transmit antennas. With this scheme an important handicap appears, when the number of transmit antennas is fixed, the decoding complexity increases exponentially with transmission rate.

In order to address this complexity of decoding, the before presented Alamouti scheme achieves the full diversity with a very simple maximum-likelihood decoding algorithm. In fact, the Alamouti scheme is the first Space-Time Block Code.

The key feature of the scheme is the orthogonality between the sequences generated by the encoder and transmitted by the two transmit antennas. This scheme was generalized to an arbitrary number of transmit antennas by applying the theory of orthogonal designs. The generalized schemes are referred to as Space-Time Block Codes (STBCs) [18].

3.4.2.1 The Coding Scheme

In general, a Space-Time Block Code is defined by an $p \times N$ transmission matrix X . where N represents the number of transmit antennas and p presents the number of time periods for transmission of one block of coded symbols.

Let us assume that transmission at the baseband employs a complex constellation C with of 2^m points. At each encoding operation, a block of km information bits is mapped into the signal constellation to select k modulated signals x_1, x_2, \dots, x_k , where each group of m bits selects a constellation signal. The k modulated signals are encoded by a Space-Time block encoder to generate N parallel signal sequence of length p according to the transmission matrix X . These sequences are transmitted through N transmit antennas simultaneously in p time periods [19].

We can represent this process by the next matrix notation in (3.13)

$$\begin{array}{c}
 \text{transmit antennas} \\
 \xrightarrow{\hspace{10em}} \\
 \begin{array}{c}
 \text{time periods} \\
 \downarrow \\
 \begin{bmatrix}
 X_{11} & X_{12} & \cdots & X_{1N} \\
 X_{21} & X_{22} & \cdots & X_{11} \\
 \vdots & \vdots & & \vdots \\
 X_{p1} & X_{p2} & \cdots & X_{pN}
 \end{bmatrix}
 \end{array}
 \end{array}
 \quad (3.13)$$

A generalized orthogonal design of size n is the $p \times N$ matrix where the entries are linear combinations of the k modulated symbols, $\pm x_1, \pm x_2, \dots, \pm x_k$, and their conjugated $\pm x_1^*, \pm x_2^*, \dots, \pm x_k^*$, that satisfies (3.14) in order to achieve the full transmit diversity of N ,

$$X \cdot X^H = (|x_1|^2 + |x_2|^2 + \cdots + |x_k|^2)I_N \quad (3.14)$$

where X^H is the Hermitian of X and I_N is a $N \times N$ identity matrix.

The orthogonality of the design allows the receiver to decouple the signals transmitted from different antennas and consequently, a simple maximum likelihood decoding, based only on linear processing of the received signals.

Space-Time Block Codes can be classified into real signals and complex signals STBC, depending on the signal constellations implemented. In order to understand the technique, and for abbreviation, We will present some transmission matrix examples using complex signals.

STBC for 2 transmit antennas:

$$X_2^C = \begin{bmatrix} x_1 & x_2 \\ -x_2^* & x_1^* \end{bmatrix} \quad (3.15)$$

This case corresponds to the Alamouti scheme. This scheme provides the full diversity of 2 and the full rate of 1. The scheme is unique in that it is the only Space-Time Block Code with an $N \times N$ complex transmission matrix to achieve the full rate [18].

STBC for 3 transmit antennas:

$$X_{3,1/2}^C = \begin{bmatrix} x_1 & x_2 & x_3 \\ -x_2 & x_1 & -x_4 \\ -x_3 & x_4 & x_1 \\ -x_4 & -x_3 & x_2 \\ x_1^* & x_2^* & x_3^* \\ -x_2^* & x_1^* & -x_4^* \\ -x_3^* & x_4^* & x_1^* \\ -x_4^* & -x_3^* & x_2^* \end{bmatrix} \quad (3.16)$$

$$X_{3,3/4}^C = \begin{bmatrix} x_1 & x_2 & \frac{x_3}{\sqrt{2}} \\ -x_2^* & x_1^* & \frac{x_3}{\sqrt{2}} \\ \frac{x_3^*}{\sqrt{2}} & \frac{x_3^*}{\sqrt{2}} & \frac{(-x_1 - x_1^* + x_2 - x_2^*)}{2} \\ \frac{x_3^*}{\sqrt{2}} & -\frac{x_3^*}{\sqrt{2}} & \frac{(x_2 + x_2^* + x_1 - x_1^*)}{2} \end{bmatrix} \quad (3.17)$$

The two above transmission matrices (3.16) and (3.17) achieve a rate of $\frac{1}{2}$ and $\frac{3}{4}$ respectively. These matrices show why coding for more of two transmit antennas achieve less rate, is the only way of complying with orthogonality design.

STBC for 4 transmit antennas:

$$X_{4,1/2}^C = \begin{bmatrix} x_1 & x_2 & x_3 & x_4 \\ -x_2 & x_1 & -x_4 & x_3 \\ -x_3 & x_4 & x_1 & -x_2 \\ -x_4 & -x_3 & x_2 & x_1 \\ x_1^* & x_2^* & x_3^* & x_4^* \\ -x_2^* & x_1^* & -x_4^* & x_3^* \\ -x_3^* & x_4^* & x_1^* & -x_2^* \\ -x_4^* & -x_3^* & x_2^* & x_1^* \end{bmatrix} \quad (3.18)$$

$$X_{4,3/4}^C = \begin{bmatrix} x_1 & x_2 & \frac{x_3}{\sqrt{2}} & \frac{x_3}{\sqrt{2}} \\ -x_2^* & x_1^* & \frac{x_3}{\sqrt{2}} & -\frac{x_3}{\sqrt{2}} \\ \frac{x_3^*}{\sqrt{2}} & \frac{x_3^*}{\sqrt{2}} & \frac{(-x_1 - x_1^* + x_2 - x_2^*)}{2} & \frac{(-x_2 - x_2^* + x_1 - x_1^*)}{2} \\ \frac{x_3^*}{\sqrt{2}} & -\frac{x_3^*}{\sqrt{2}} & \frac{(x_2 + x_2^* + x_1 - x_1^*)}{2} & -\frac{(x_1 + x_1^* + x_2 - x_2^*)}{2} \end{bmatrix} \quad (3.19)$$

The two above transmission matrices (3.18) and (3.19) achieve a rate of $\frac{1}{2}$ and $\frac{3}{4}$ respectively. With both presented transmission matrices $X_{N,3/4}^C$ in (3.17) and (3.19), for the cases of 3 and 4 transmit antennas with rate of $\frac{3}{4}$, there is a particular issue that they have uneven power among the symbols transmitted. This means that the signal does not have a constant envelope and the transmission power in each antenna must vary, both of which are undesirable.

There are improved versions of these transmission matrices with rate of $\frac{3}{4}$ that solve the uneven transmission power and exhibit the same power in all the antennas over all the time periods. This Space-Time Block Code for 3 transmit antennas was presented in [25] and is depicted in (3.20), and the case for 4 transmit antennas was presented in [26] and is depicted in (3.21).

STBC with rate of $\frac{3}{4}$ for 3 and 4 transmit antennas and even transmission power:

$$X_{3,3/4}^c = \begin{bmatrix} x_1 & -x_2 & -x_3 \\ x_2^* & x_1^* & 0 \\ x_3^* & 0 & x_1^* \\ 0 & -x_3^* & x_2^* \end{bmatrix} \quad (3.20)$$

$$X_{3,3/4}^c = \begin{bmatrix} x_1 & -x_2 & -x_3 \\ x_2^* & x_1^* & 0 \\ x_3^* & 0 & x_1^* \\ 0 & -x_3^* & x_2^* \end{bmatrix} \quad (3.21)$$

3.4.2.2 The Decoding Algorithm

Next, we consider the decoding algorithm. Clearly, the rows of transmission matrix X are all permutations of first row of X with possible different signs. Let $\epsilon_1, \dots, \epsilon_n$ denote the permutations corresponding to these rows and let $\delta_k(i)$ denote the sign of x_i in the k th row of X . Then $\epsilon_k(p) = q$ means that x_p is up to a sign change the (k,q) th element of X .

We assume that the channel coefficients $h_{MN}(t)$ are constant over p symbols periods.

$$h_{MN}(t) = h_{MN}, \quad t = 1, 2, \dots, p \quad (3.22)$$

In deriving the maximum likelihood decoding, similar to the one from Alamouti scheme, we can construct the decision statistics for the transmitted signal x_i as

$$\tilde{x}_i = \sum_{t=1}^N \sum_{j=1}^M \delta_t(i) \cdot r_t^j \cdot h_{j, \epsilon_t(i)}^* \quad (3.23)$$

for all $i = 1, 2, \dots, N$ and decide in favor of x_i among all the constellation symbols x if

$$\hat{x}_i = \arg \min_{\tilde{x}_i \in C} |\tilde{x}_i - x_i|^2 + \left(-1 + \sum_{t=1}^N \sum_{j=1}^M |h_{j,t}|^2 \right) |x_i|^2 \quad (3.24)$$

This is a very simple decoding strategy that provides diversity.

3.4.3 Space-Time Trellis Code

Space-time trellis code (STTC) is a type of Space-Time code that transmits multiple, redundant copies of a generalized TCM (Trellis Coded Modulation) signal distributed over time and a number of antennas ('space'). These multiple, 'diverse' copies of the data are used by the receiver to attempt to reconstruct the actual transmitted data. For an STC to be used, there must necessarily be multiple transmit antennas, but only a single receive antennas is required; nevertheless, multiple receive antennas are often used since the performance of the system is improved by the resulting spatial diversity.

In contrast to Space-Time Block Codes (STBCs), they are able to provide both coding gain and diversity gain and have a better bit-error rate performance. In essence they marry single channel continuous time coding with the signaling protocol being used and extend that with a multi-antenna framework. However, that also means they are more complex than STBCs to encode and decode; they rely on a Viterbi decoder at the receiver where STBCs need only linear processing. Also, whereas in a single transmitter, single receiver framework the Viterbi algorithm (or one of the sequential decoding algorithms) only has to proceed over a trellis in a single time dimension, in here the optimal decoding also has to take into consideration the number of antennas, leading to an extraneous polynomial complexity term.

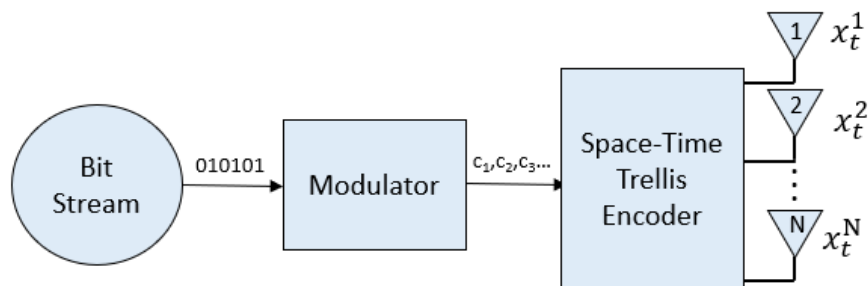


Figure 3.6 Block diagram of space-time trellis implementation.

STTC was first introduced by Tarokh, Seshadri and Calderbank [16]. It was widely discussed and explored in the literature as STTC can simultaneously offer a substantial coding gain, spectral efficiency, and diversity improvement on flat fading channels.

Next, we will review how STTC is implemented.

3.4.3.1 Encoder Structure for STTC

In the space-time trellis code, the encoder maps binary data to modulation symbols, where the mapping functions is described by a trellis diagram.

Let us consider an encoder of space-time trellis coded M -PSK modulation with n_T transmit antennas as shown in Figure 3.7 The input message stream, denoted by c , is given by

$$c = (c_0, c_1, c_2, \dots, c_t, \dots) \quad (3.25)$$

where c_t is a group of $m = \log_2 M$ information bits at time t and given by

$$c_t = (c_t^1, c_t^2, \dots, c_t^m) \quad (3.26)$$

The encoder maps the input sequence into a M -PSK modulated signal sequence, which is given by

$$X = (X_0, X_1, X_2, \dots, X_t, \dots) \quad (3.27)$$

where X_t is the *space-time symbol* at time t and given by

$$X_t = (x_t^1, x_t^2, \dots, x_t^{n_T})^T \quad (3.28)$$

The modulated signals, $x_t^1, x_t^2, \dots, x_t^{n_T}$, are transmitted simultaneously through n_T transmit antennas.

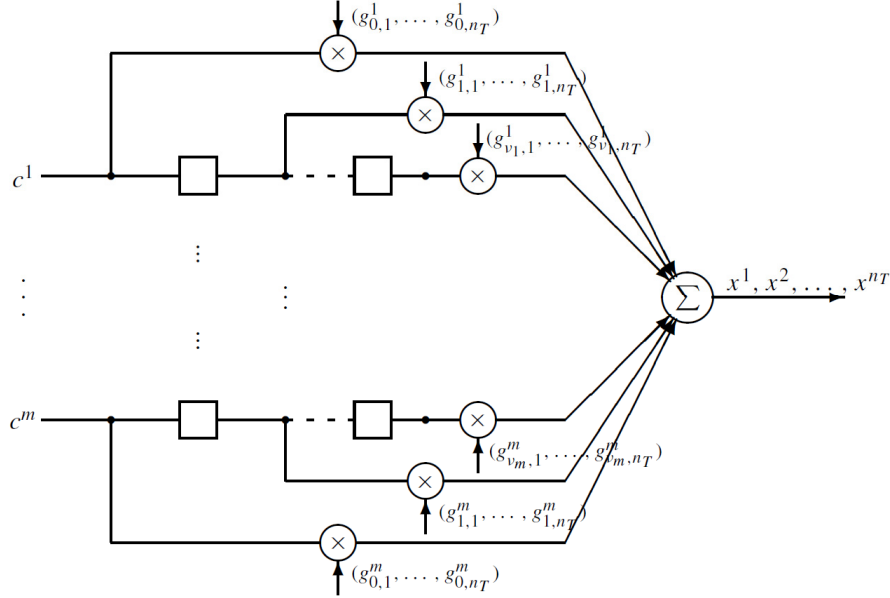


Figure 3.7 Encoder for STTC.

3.4.3.2 Generator Description

In the STTC encoder as shown in Figure 3.6, m binary input sequences c^1, c^2, \dots, c^m are fed into the decoder, which consists of m feedforward shift registers. The k -th input sequence $c^k = (c_0^k, c_1^k, c_2^k, \dots, c_t^k, \dots)$, $k = 1, 2, \dots, m$, is passed to the k -th shift register and multiplied by an encoder coefficient set. The multiplier outputs from all shift registers are added modulo M , giving the encoder output $X = (X^1, X^2, \dots, X^{n_T})$. The connections between the shift register elements and the modulo M adder can be described by the following m multiplication coefficient set sequences

$$\begin{aligned}
 g^1 &= [(g_{0,1}^1, g_{0,2}^1, \dots, g_{0,n_T}^1), (g_{1,1}^1, g_{1,2}^1, \dots, g_{1,n_T}^1), \dots, (g_{v1,1}^1, g_{v1,2}^1, \dots, g_{v1,n_T}^1)] \\
 g^2 &= [(g_{0,1}^2, g_{0,2}^2, \dots, g_{0,n_T}^2), (g_{1,1}^2, g_{1,2}^2, \dots, g_{1,n_T}^2), \dots, (g_{v2,1}^2, g_{v2,2}^2, \dots, g_{v2,n_T}^2)] \\
 &\vdots \\
 &\vdots \\
 g^m &= [(g_{0,1}^m, g_{0,2}^m, \dots, g_{0,n_T}^m), (g_{1,1}^m, g_{1,2}^m, \dots, g_{1,n_T}^m), \dots, (g_{vm,1}^m, g_{vm,2}^m, \dots, g_{vm,n_T}^m)]
 \end{aligned} \tag{3.29}$$

where $g_{j,i}^k$, $k = 1, 2, \dots, m, j = 1, 2, \dots, vk, i = 1, 2, \dots, n_T$, is an element of the M -PSK constellation set, and vk is the memory order of k -th shift register.

The encoder output at time t for transmit antenna i , denoted by x_t^i , can be computed as

$$x_t^i = \sum_{k=1}^m \sum_{j=0}^{vk} g_{j,i}^k c_{t-j}^k \bmod M, i = 1, 2, \dots, n_T \quad (3.30)$$

These outputs are elements of an M -PSK signal set. Modulated signals form the space-time symbol transmitted at time t

$$X_t = (x_t^1, x_t^2, \dots, x_t^{n_T})^T \quad (3.31)$$

The space-time trellis coded M -PSK can achieve a bandwidth efficiency of m bits/s/Hz. The total memory order of encoder, denoted by v , is given by

$$v = \sum_{k=1}^m vk \quad (3.32)$$

where vk , $k = 1, 2, \dots, m$, is the memory order for the k -th encoder branch. The value of vk for M -PSK constellations is determined by

$$vk = \left\lceil \frac{v + k - 1}{\log_2 M} \right\rceil \quad (3.33)$$

The total number of states for the trellis encoder is 2^v . The m multiplication coefficient set sequences are also called the *generator sequences*, since they can fully describe the encoder structure.

3.4.3.2 Generator Polynomial Description

The STTC encoder can also be described in generator polynomial format. Let us consider a space-time encoder with two transmit antennas as shown in Figure 3.8. The input binary sequence to the upper shift register can be represented as

$$c^1(D) = c_0^1 + c_1^1 D + c_2^1 D^2 + c_3^1 D^3 + \dots \quad (3.34)$$

Similarly, the binary input sequence to the lower shift register can be written as

$$c^2(D) = c_0^2 + c_1^2 D + c_2^2 D^2 + c_3^2 D^3 + \dots \quad (3.35)$$

where $c_j^k, j = 0, 1, 2, 3, \dots, k = 1, 2$, are binary symbols 0, 1. The feedforward generator polynomial for the upper encoder and transmit antenna i , where $i = 1, 2$, can be written as

$$G_i^1(D) = g_{0,i}^1 + g_{1,i}^1 D + \dots + g_{v_1,i}^1 D^{v_1} \quad (3.36)$$

where $g_{j,i}^1, j = 0, 1, \dots, v_1$ are non-binary coefficients that can take values 0, 1, 2, 3 for QPSK modulation and v_1 is the memory order of the upper encoder. Similarly, the feedforward generator polynomial for the lower encoder and transmit antenna i , where $i = 1, 2$, can be written as

$$G_i^2(D) = g_{0,i}^2 + g_{1,i}^2 D + \dots + g_{v_2,i}^2 D^{v_2} \quad (3.37)$$

where $g_{j,i}^2, j = 0, 1, \dots, v_2$, are non-binary coefficients that can take values 0, 1, 2, 3 for QPSK modulation and v_2 is the memory order of the lower encoder. The encoded symbol sequence transmitted from antenna i is given by

$$X^i(D) = c^1(D)G_i^1(D) + c^2(D)G_i^2(D) \quad \text{mod } 4 \quad (3.38)$$

The relationship in (3.38) can be written in the following form

$$X^i(D) = [c^1(D) \quad c^2(D)] \begin{bmatrix} G_i^1(D) \\ G_i^2(D) \end{bmatrix} \text{ mod } 4 \quad (3.39)$$

A systematic recursive STTC can be obtained by setting

$$G_1(D) = \begin{bmatrix} 2 \\ 1 \end{bmatrix}$$

which means that the output of the first antenna is obtained by directly mapping the input sequences c^1 and c^2 into a QPSK sequence.

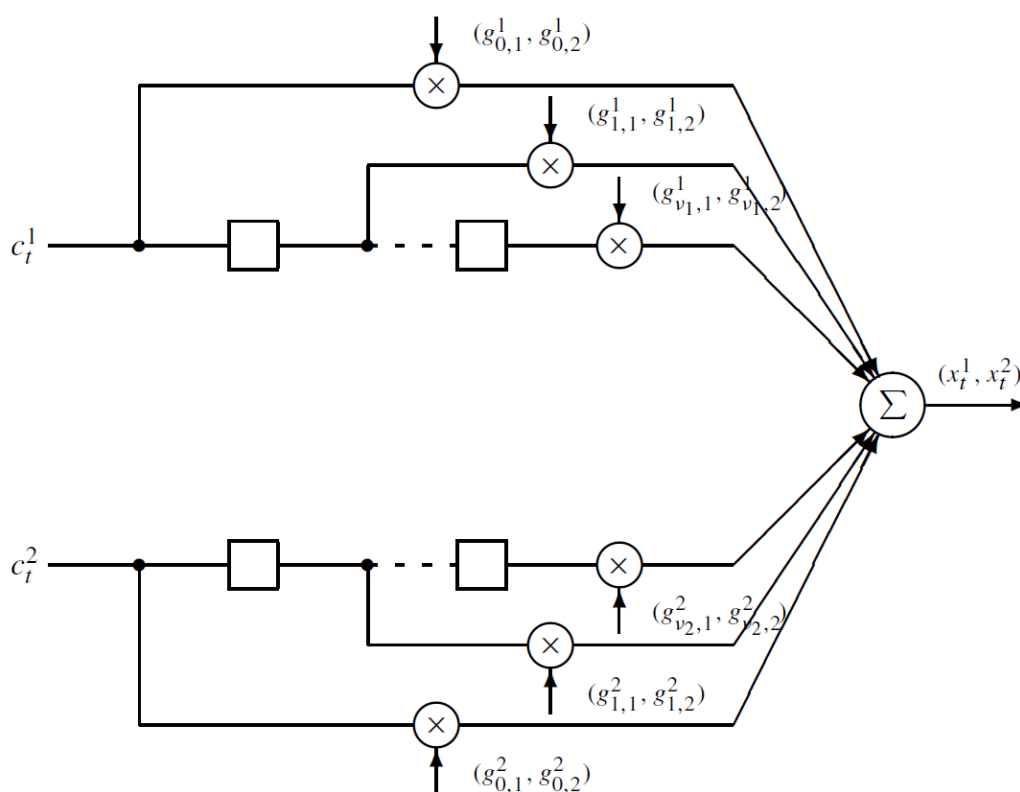


Figure 3.8 STTC encoder for two transmit antennas.

In order to have a deeper understanding of the STTC code construction, we will examine a practical example of implementation:

Let us assume that the generator sequences of a 4-state space-time trellis coded QPSK scheme with 2 transmit antennas are

$$g^1 = [(02), (20)]$$

$$g^2 = [(01), (10)]$$

The trellis structure for the code is shown in Fig. 3.9. The trellis consists of $2^v = 4$ states, represented by state nodes. The encoder takes $m = 2$ bits as its input at each time. There are $2^m = 4$ branches leaving from each state corresponding to four different input patterns. Each branch is labelled by $c_t^1 \ c_t^2 / x_t^1 \ x_t^2$, where c_t^1 and c_t^2 are a pair of encoder input bits, and x_t^1 and x_t^2 represent two coded QPSK symbols transmitted through antennas 1 and 2, respectively. The row listed next to a state node in Fig. 3.9 indicates the branch labels for transitions from that state corresponding to the encoder inputs 00, 01, 10, and 11, respectively.

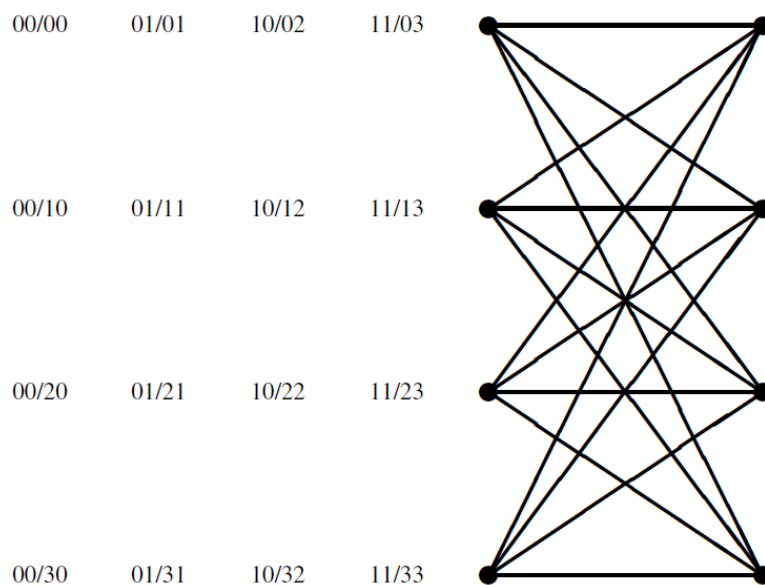


Figure 3.9 Trellis structure for a 4-state space-time coded QPSK with 2 antennas.

Assume that the input sequence is

$$\mathbf{c} = (10, 01, 11, 00, 01, \dots)$$

The output sequence generated by the space-time trellis encoder is given by

$$\mathbf{x} = (02, 21, 13, 30, 01, \dots)$$

The transmitted signal sequences from the two transmit antennas are

$$\mathbf{x}^1 = (0, 2, 1, 3, 0, \dots)$$

$$\mathbf{x}^2 = (2, 1, 3, 0, 1, \dots)$$

Note that this example is actually a delay diversity scheme since the signal sequence transmitted from the first antenna is a delayed version of the signal sequence from the second antenna.

For STTC, the decoder employs the Viterbi algorithm to perform maximum likelihood decoding. Assuming that perfect CSI is available at the receiver, for a branch labelled by $(x_t^1, x_t^2, \dots, x_t^{n_T})$, the branch metric is computed as the squared Euclidean distance between the hypothesized received symbols and the actual received signals as

$$\sum_{j=1}^{n_R} \left| r_t^j - \sum_{i=1}^{n_T} h_{j,i}^t x_t^i \right|^2 \quad (3.40)$$

The Viterbi algorithm selects the path with the minimum path metric as the decoded sequence [27].

3.4.3 Space-Time Line Code

This coding technique was developed as a fundamental attempt to look for a counter part to the previously presented Space-Time Block Code (STBC). The full spatial-diversity gain can be achieved through various techniques using multiple antennas depending on what is known about the CSI (Channel State Information) at the transmitter and/or receiver [20]. A classical Maximum Ratio Combining (MRC) technique achieves full diversity when, for example, a receiver with multiple antennas knows the CSI [28-32]. As a counterpart of the MRC, a Maximum Ratio Transmission (MRT) technique was established that also achieves full spatial-diversity gain when a transmitter with multiple antennas knows the CSI [33-35]. Finally, the STBCs techniques also achieve full spatial-diversity when transmitter and receiver have multiple antennas but the CSI is available at the receiver only [17,18].

This novel rate-one full spatial-diversity achieving STC scheme, referred to as Space-Time Line Code (STLC), solved the fundamental design question for MIMO systems where the CSI is available at the transmitter only. In the proposed scheme, two information symbols are encoded using the multiple channel gains (*space*) and are transmitted consecutively (*time*). Given that the coded symbols are transmitted sequentially through a single transmit antenna, they are a *line*-shaped compared to the block shape of STBC, justifying the name of this new STC scheme as Space-Time Line Code (STLC). The STLC can be directly extended to a system with multiple transmit antennas. In this case, multiple independent STLCs are implemented in parallel lines. Full diversity can be achieved by a simple decoding scheme, i.e., a direct combining scheme of the received signals at two receive antennas in two symbol times. An STLC receiver does not need full CSI for the decoding. Just the sum of all channel gain, which is a single real value variable, is required; however, even this is not necessary for the detection of phase-shift keying (PSK) constellation signals [20].

Since the full CSI is required solely for a transmitter, the STLC scheme is a relevant strategy for communications between high-capable (complex) transmitters and minimal-function (simple) receivers. For example, Internet of Things (IoT) and wearable devices are the applications of the simple receivers, for which low cost, low complexity, and low power

consumption are required [36]. This full spatial-diversity achieving structure, in which full CSI is available only at the complex device, relieves the simple device from frequent channel estimations and complex decoding and enables minimal-function operation by jointly operating the STLC and STBC schemes, which is called an STBLC.

For abbreviation, we will present the scheme considering a system with two transmit and two receive antennas. The channel gains from the two transmits and two receive antennas are depicted in Table 3.4, the transmitter has CSI, yet the receiver does not.

Table 3.4 The definition of channels between transmit and receive antennas.

| | Tx Antenna 1 | Tx Antenna 2 |
|---------------------|---------------------|---------------------|
| <i>Rx Antenna 1</i> | h_1 | h_3 |
| <i>Rx Antenna 2</i> | h_2 | h_4 |

3.4.4.1 Encoding and Transmission sequence

Denote the STLC symbol transmitted at time t by s_t . As stated, two information symbols x_1 and x_2 are encoded and transmitted consecutively. Let's then establish the STLC encoding for M transmit antennas that can be written as follows:

$$[S_{1,1}^* \ S_{1,2} \ \dots \ S_{m,1}^* \ S_{m,2} \ \dots \ S_{M,1}^* \ S_{M,2}]^T = C_{(1:2M)} \begin{bmatrix} x_1^* \\ x_2 \end{bmatrix} \quad (3.41)$$

where $s_{m,t}$ is the transmitted symbol through the m th transmit antenna at time t , and the STLC encoding matrix $C_{(1:2M)} \in \mathbb{C}^{2M \times 2}$ is constructed as

$$C_{(1:2M)} = \left[C_{(1,2)}^T \ \cdots \ C_{(2m-1,2m)}^T \ \cdots \ C_{(2M-1,2M)}^T \right]^T \quad (3.42)$$

Here, $C_{(2m-1,2m)}$ is an STLC encoding matrix that consists of h_{2m-1} and h_{2m} . In this scheme, $C_{(1:2M)}$ fulfills an orthogonality property as

$$\mathbf{C}_{(1:2M)}^H \mathbf{C}_{(1:2M)} = \sum_{m=1}^M \mathbf{C}_{(2m-1,2m)}^H \mathbf{C}_{(2m-1,2m)} = \gamma_{2M} \mathbf{I}_2 \quad (3.43)$$

where γ_α is the sum of all channel gains involved in the communication with diversity order α and I_x represents a x -by- x identity matrix.

The decoding structure depends on the STLC encoding structure. The details are introduced with the example of a 2x2 STLC system, as depicted in Fig. 3.10. The notations for the channel gains for a 2x2 STLC are shown in Table 3.4

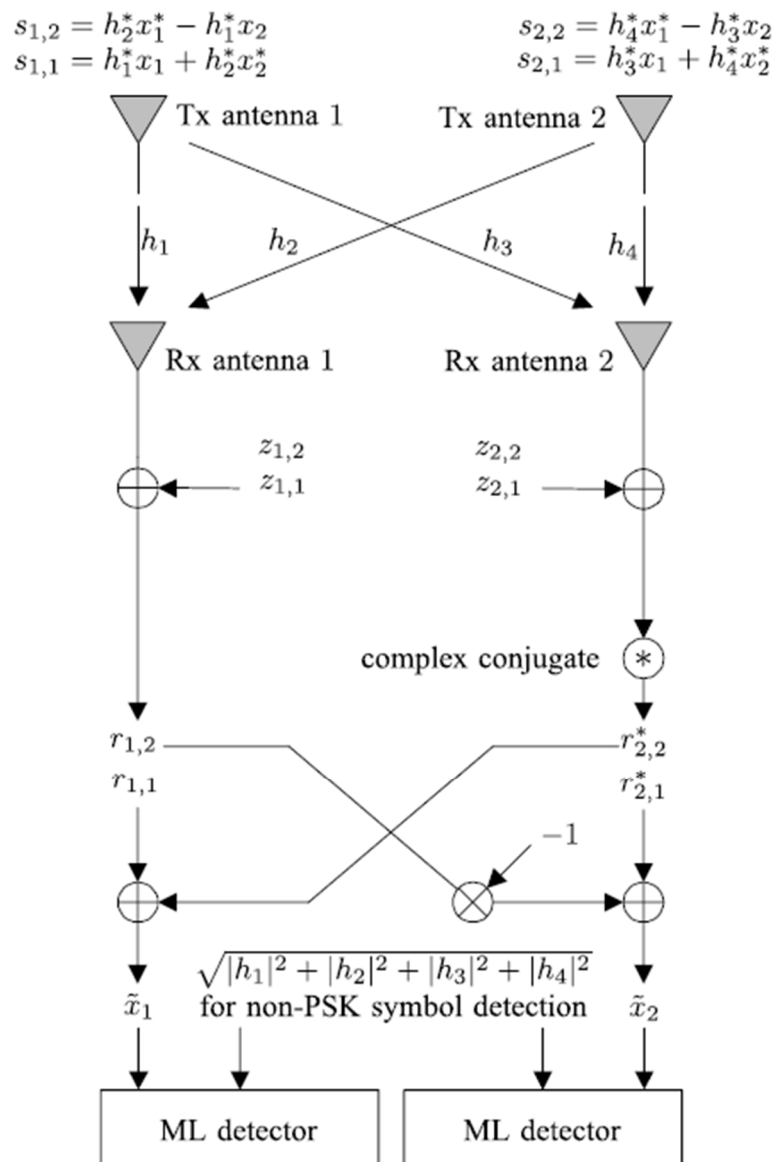


Figure 3.10 Example of full spatial-diversity 2x2 STLC system.

For STLC with two transmit antennas, we apply an STLC encoding matrix $C_{(1,2)}^a$ and a Type-2 structure, please see Appendix B, to each transmit antenna, i.e., $C_{(2m-1,2m)} = C_{(2m-1,2m)}^a$ for all $m \in \{1,2\}$, with decoding functions $f^*(\cdot, \cdot)$ and $f(\cdot, \cdot)$ are used for estimating x_1 and x_2 , respectively. Thus, the encoding with x_1 and x_2 is written as follows:

$$\begin{bmatrix} s_{1,1}^* \\ s_{1,2} \\ s_{2,1}^* \\ s_{2,2} \end{bmatrix} = \begin{bmatrix} C_{(1,2)}^a \\ C_{(3,4)}^a \end{bmatrix} \begin{bmatrix} x_1^* \\ x_2 \end{bmatrix} = \begin{bmatrix} h_1 & h_2 \\ h_2^* & -h_1^* \\ h_3 & h_4 \\ h_4^* & -h_3^* \end{bmatrix} \begin{bmatrix} x_1^* \\ x_2 \end{bmatrix} \quad (3.44)$$

The resultant STLC symbols are shown in the following Table 3.5.

Table 3.5 Encoding and transmit sequence for the STLC with two transmit antennas.

| | Tx time $t = 1$ | Tx time $t = 2$ |
|---------------------|-------------------------------------|-------------------------------------|
| <i>Tx Antenna 1</i> | $S_{1,1} = h_1^* x_1 + h_2^* x_2^*$ | $S_{1,2} = h_2^* x_1^* - h_1^* x_2$ |
| <i>Tx Antenna 2</i> | $S_{2,1} = h_3^* x_1 + h_4^* x_2^*$ | $S_{2,2} = h_4^* x_1^* - h_3^* x_2$ |

To satisfy transmit power constraint σ_x^2 , being this the transmitted symbol energy, the transmitter normalize $S_{1,t}$ and $S_{2,t}$, according to η . The normalization factor η can be readily derived as $\eta = 1/\sqrt{\gamma_4}$ such that $E|\eta S_{1,t}|^2 + E|\eta S_{2,t}|^2 = \sigma_x^2$ for all t . The transmitter then transmits $\eta S_{1,t}$ and $\eta S_{2,t}$ through transmit antennas 1 and 2, respectively, simultaneously at time t . Concurrently, the receive symbols defined in Table 3.6 can be expressed as follows:

$$\begin{bmatrix} r_{1,1} & r_{1,2} \\ r_{2,1} & r_{2,2} \end{bmatrix} = \begin{bmatrix} h_1 & h_3 \\ h_2 & h_4 \end{bmatrix} \frac{1}{\sqrt{\gamma_4}} \begin{bmatrix} \underbrace{s_{1,1} \ s_{1,2}}_{STLC1} \\ \underbrace{s_{2,1} \ s_{2,2}}_{STLC2} \end{bmatrix} + \begin{bmatrix} z_{1,1} & z_{1,2} \\ z_{2,1} & z_{2,2} \end{bmatrix} \quad (3.45)$$

Table 3.6 Notations for the STLC received signals.

| | Rx time $t = 1$ | Rx time $t = 2$ |
|---------------------|-----------------|-----------------|
| <i>Rx Antenna 1</i> | $r_{1,1}$ | $r_{1,2}$ |
| <i>Rx Antenna 2</i> | $r_{2,1}$ | $r_{2,2}$ |

where $z_{n,t}$ is AWGN at n th receive antenna at time t with zero mean and σ_z^2 variance.

3.4.4.2 Decoding Scheme

Because STLC decoding structure follows the encoding structure, specifically STLC encoding matrix $C_{(1,2)}^a$ with a Type-2 structure, from Appendix B, the decoding scheme is readily determined as follows:

$$\begin{aligned} f^*(r_{1,1}^*, r_{2,2}) &= r_{1,1} + r_{2,2}^* = \sqrt{\gamma_4}x_1 + z_{1,1} + z_{2,2}^*, \\ f(r_{2,1}^*, -r_{1,2}) &= r_{2,1}^* - r_{1,2} = \sqrt{\gamma_4}x_2 + z_{2,1}^* - z_{1,2} \end{aligned} \quad (3.46)$$

The combiner is shown in Fig. 3.10. Note that both equations in (3.46) are only a function of x_1 or x_2 respectively. Thus, two separate ML detections of x_1 and x_2 are possible, as in STBC decoder. Here, we reemphasize that the receiver does not need full CSI to combine the received signals, yet it requires the effective channel gain $\sqrt{\gamma_4}$ for the ML detection of non-PSK symbols in the sequel. This effective channel gain can be estimated by using the blind SNR estimation techniques [37]. Thus, (3.46) is called a *blind combining* technique.

The encoding and decoding structures (3.44) and (3.46) are not unique. Examples of possible STLC encoding and decoding structures are listed in Appendix B.

The multiple transmit antenna STLC scheme described in this section can be applied to a massive MIMO system. In [38], it was shown that the M -by-2 STLC system asymptotically achieves optimal (maximum) SNR as M increases, and it achieves stable SNR, regardless of the spatial correlation, and considerable robustness against channel uncertainty at the transmitter. The STLC was also exploited to improve secure MIMO communications [39].

3.5 Application on This Work

In this chapter has been explained the basic aspects of MIMO systems, not without firstly navigate in the history of this amazing technology and all the effort that many scientists have made through the years. We also explained the different MIMO channels models and its importance for the design of system where MIMO will be implemented. These models become more relevant when no other wireless channel estimation tools are available.

This thesis makes use of a deterministic method to estimate the behavior of the MIMO channel, more specifically, an in-house developed 3D Ray Launching algorithm. . In this way, wireless channel characterization in terms of received power levels and time domain parameters for the different scenarios under analysis are obtained.

Additionally, this chapter presented a deep explanation of more relevant space-time coding, such as, Space-Time Clock Codes, Space-Time Trellis Code and Space-Time Line Code. Including the Alamouti scheme which is a kind of STBC applicable only to 2x2 MIMO systems.

After obtaining the wireless channel characterization, and using these parameters obtained; a programed-apart matlab scripts have been developed to implement STBC, coding technique best suitable for our scenarios, to complete the analysis of MIMO performance in the three different use cases later presented in this thesis.

Chapter 4

Simulation Methodology

RAY theory is a very accurate model and technique continuously under development and already implemented in simulation tools to obtain wireless channel characterization. This accuracy is mainly due to the fact that this methodology implies a complete and detail geometric description of the environment where propagation paths are computed. This full 3D geometric description suppose that processing time and computational resources are demanding but fair enough according to the usefulness of results obtained. In this thesis we make use of a deterministic 3D ray launching simulation tool in complex indoor scenarios. This chapter in focused on explaining the complete simulation methodology employed in the development of this thesis. In section 4.1, the principles of ray theory are presented and the logic of the algorithm as well. Then, in section 4.2, the way of creating the simulation environment is explained, including the description of how the simulation tool implement the ray theory. In this section we also present the approach we use these simulation results to analyse MIMO performance.

4.1 3D Ray Launching Technique

There are multiple methodologies in the field of wireless communications to accomplish a channel characterization, these can be classified depending on accuracy, computational resources required, and the parameters or information needed in the undergoing analysis or study. One of them providing a good trade-off between computational resources and useful simulation results, is the deterministic model based on Ray Theory.

Ray theory includes ray launching and ray tracing techniques. In the RL approach, the Tx sends thousands of rays in a solid angle and the algorithm follows the propagation of each ray until it either arrives at the Rx or becomes so weak to be significant. In RT, it estimates the principal radio wave propagation regions and rays are traced in such regions [40].

With the aim to estimate frequency/time radio channel characteristics in a volumetric scenario, an in-house developed deterministic 3D Ray Launching (3D-RL) simulation technique has been used. The algorithm is based on Geometrical Optics (GO) approach and the Uniform Theory of Diffraction (UTD).

The ray launching (RL) technique is based on recognizing a single point of the radiated wave with a ray that propagates along the space following a combination of optic and electromagnetic theories. RL techniques can be used in environments where the wavelength of the frequency of interest is much smaller than the dimensions of the surroundings. See Figure 4.1.

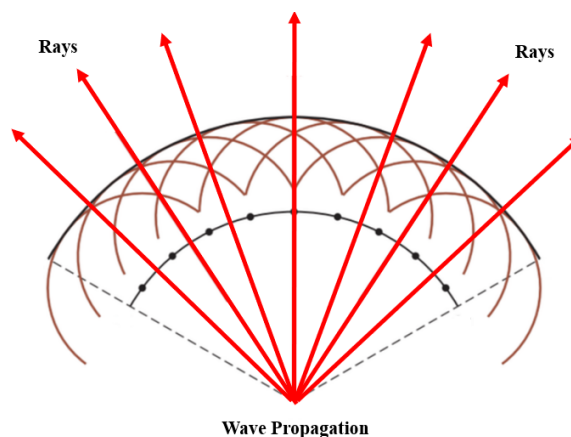


Figure 4.1 Wave front propagation associated with launched rays.

The rays considered in GO are direct, reflected, and refracted rays. Because of this, abrupt transitions areas may occur, corresponding to the boundaries of the regions where these rays exist. To complement the GO theory, the diffracted rays are introduced with the Geometrical Theory of Diffraction (GTD) and its uniform extension, the Uniform GTD (UTD). The purpose of these rays is to remove the field discontinuities and to introduce proper field corrections, especially in the zero-field regions predicted by GO [41].

The scenario that will be analysed is divided into a uniform hexahedral mesh with cuboids of a given dimension, this dimension should be in the order of wavelength of operation frequency to allow the parameters obtained to be representative and accurate.

The very initial process consists of launching a set of rays with predefined transmission RF power, then they go through a path from the transmitter to the receiver with a given angular resolution, for both horizontal and vertical planes with a given solid angle, and the resulting power levels along the path are calculated and stored in the respective cuboids. This process considers geometric specifications and geometrical optics principles as well as their corresponding electromagnetic phenomena such as free-space propagation, reflection, diffraction, and scattering [42], see Figure 4.2.

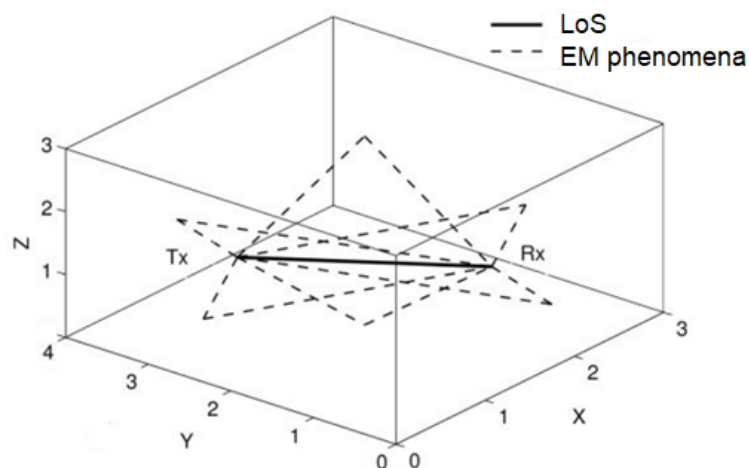


Figure 4.2 Principle of operation for 3D Ray Launching method.

Each ray propagates in the space as a single optic ray. The electric field E created by GO is calculated by [43]:

$$E_i^\perp = \sqrt{\frac{Prad D_t(\theta_t, \phi_t) \eta_0}{2\Pi} \frac{e^{-j\beta_0 r}}{r}} X^\perp L^\perp \quad (4.1)$$

$$E_i^\parallel = \sqrt{\frac{Prad D_t(\theta_t, \phi_t) \eta_0}{2\Pi} \frac{e^{-j\beta_0 r}}{r}} X^\parallel L^\parallel \quad (4.2)$$

Where $\beta_0 = 2\pi f_c \sqrt{\varepsilon_0 \mu_0}$, $\varepsilon_0 = 8.854 \times 10^{-12}$ F/m, $\mu_0 = 4\pi \times 10^{-7}$ H/m and $\eta_0 = 120\pi$ ohms. $Prad$ is the radiated power of the transmitter antenna, $D_t = (\theta_t, \phi_t)$ is the directivity, (X^\perp, X^\parallel) are the polarization ratio, (L^\perp, L^\parallel) the path loss coefficients for each polarization, r the distance in the free space and f_c the transmission frequency.

When this ray finds an object in its path, two new rays are created: a reflected ray and a transmitted ray. See Figure 4.3.

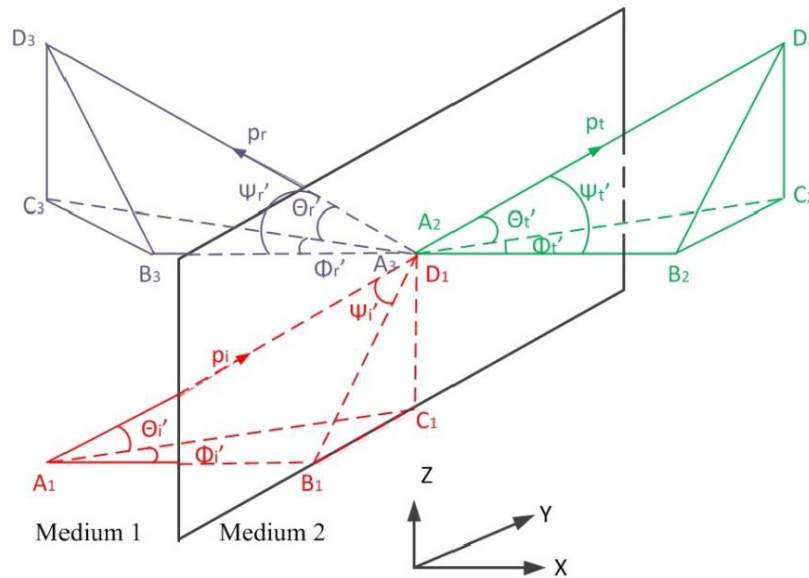


Figure 4.3 Reflection and transmission by plane interface at the oblique wave incidence.

These rays have new angles provided by Snell's law [44]. According to the Snell's law, see Figure 4.4, the reflection coefficient R^\perp and transmission coefficient T^\perp are calculated by

$$T^\perp = \frac{E_t^\perp}{E_i^\perp} = \frac{2\eta_2 \cos(\psi_i)}{\eta_2 \cos(\psi_i) + \eta_1 \cos(\psi_t)} \quad (4.3)$$

$$R^\perp = \frac{E_r^\perp}{E_i^\perp} = \frac{\eta_2 \cos(\psi_i) - \eta_1 \cos(\psi_t)}{\eta_2 \cos(\psi_i) + \eta_1 \cos(\psi_t)} \quad (4.4)$$

where $\eta_1 = 120\pi/\sqrt{\epsilon_{r1}}$, $\eta_2 = 120\pi/\sqrt{\epsilon_{r2}}$ and ψ_i , ψ_r and ψ_t are the incident, reflected and transmitted angles respectively.

Snell's law:
 $\eta_1 \sin \psi_1 = \eta_2 \sin \psi_t$

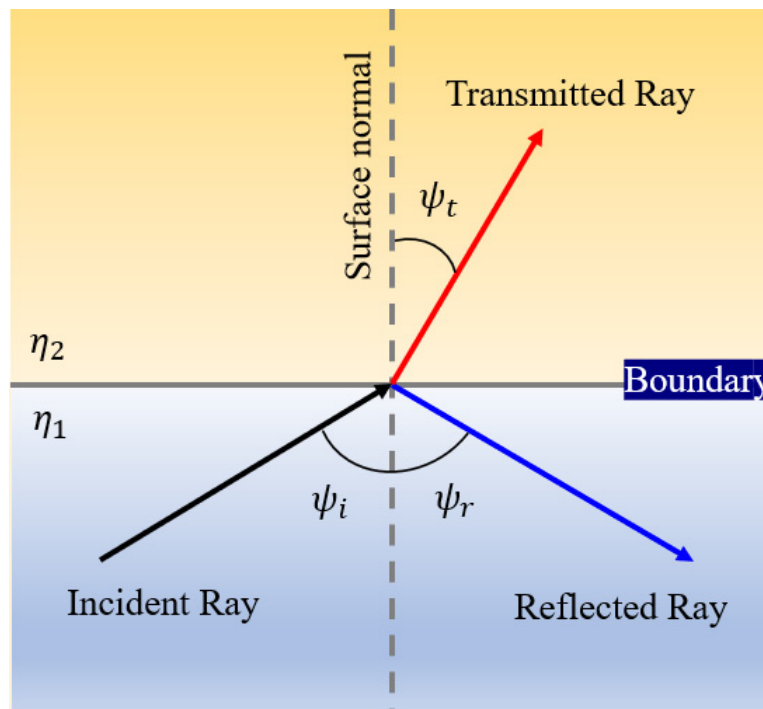


Figure 4.4 Representation of Snell's law.

For the parallel (or magnetic) polarization the magnetic field vector of the incident wave is perpendicular to the plane of incidence. Then, the reflection and transmission coefficients R^{\parallel} and T^{\parallel} can be calculated by

$$R^{\parallel} = \frac{E_r^{\parallel}}{E_i^{\parallel}} = \frac{\eta_1 \cos(\psi_i) - \eta_2 \cos(\psi_t)}{\eta_1 \cos(\psi_i) + \eta_2 \cos(\psi_t)} \quad (4.5)$$

$$T^{\parallel} = \frac{E_t^{\parallel}}{E_i^{\parallel}} = \frac{2\eta_2 \cos(\psi_i)}{\eta_1 \cos(\psi_i) + \eta_2 \cos(\psi_t)} \quad (4.6)$$

Once the parameters of transmission T and reflection R are calculated and the angle of incidence ψ_i and ψ_t the new angles (θ_r, Φ_r) of the reflected wave and (θ_t, Φ_t) of the transmitted wave can be calculated. A general case where a ray impinges with an obstacle with (θ'_i, Φ'_i) angles, is represented in Figure 4.3. Considering all the possible angles of incidence, the new angles for the reflected and transmitted wave are calculated, as it is shown for a general case in Figure 4.3.

The diffracted field is calculated by [45]:

$$E_{UTD} = e_0 \frac{e^{-jks_1}}{s_1} D^{\perp\parallel} \sqrt{\frac{s_1}{s_2(s_1 + s_2)}} e^{-jks_2} \quad (4.7)$$

where s_1 , s_2 are the distances represented in Figure 4.5, from the source to the edge and from the edge to the receiver point. $D^{\perp\parallel}$ are the diffraction coefficients given by [45-47] as:

$$D^{\parallel\perp} = \frac{-e^{(-j\pi/4)}}{2n\sqrt{2\pi k}} \left\{ \begin{array}{l} \cot\left(\frac{\pi + (\Phi_2 - \Phi_1)}{2n}\right) F(kLa^+(\Phi_2 - \Phi_1)) \\ + \cot\left(\frac{\pi - (\Phi_2 - \Phi_1)}{2n}\right) F(kLa^-(\Phi_2 - \Phi_1)) \\ + R_0^{\parallel\perp} \cot\left(\frac{\pi - (\Phi_2 + \Phi_1)}{2n}\right) F(kLa^-(\Phi_2 + \Phi_1)) \\ + R_n^{\parallel\perp} \cot\left(\frac{\pi + (\Phi_2 + \Phi_1)}{2n}\right) F(kLa^+(\Phi_2 + \Phi_1)) \end{array} \right\} \quad (4.8)$$

where $n\pi$ is the wedge angle, F , L and a^\pm are defined in [45], $R_{0,n}$ are the reflection coefficients for the appropriate polarization for the 0 face or n face, respectively. The Φ_2 and Φ_1 angles in Equation (4.8) would refer to the angles in Figure 4.5.

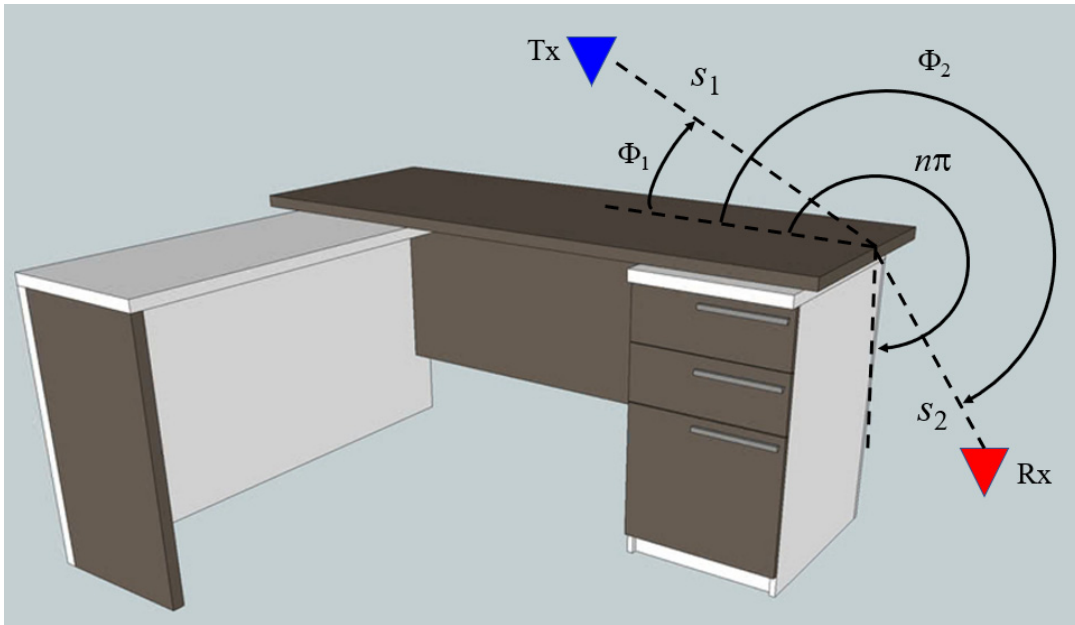


Figure 4.5 Geometry for edge diffraction coefficients.

The information kept in each cuboid in the whole scenario under simulation allow the calculation of the received power considering the losses of propagation through a medium (ϵ, μ, σ) at a distance d , with the attenuation constant α (Np/m), and the phase constant β (rad/m). The received power is calculated with the sum of incident electric vector fields in an interval of time Δt inside each cuboid of the defined mesh.

Based on this theory, the main attribute of the ray-launching technique is that it provides the impulse response of the channel $h(r, f_c, \Delta f, d)$ for each transmitter, at a given carrier frequency, f_c , at a given bandwidth ($f_c \pm \Delta f$), where the materials have a similar response and at a given position. With this information, a stationary channel can be completely characterized [48].

The power levels for the whole volume of the scenario are obtained, in addition to delay spread maps, power delay profiles and signal to noise ratio levels.

4.2 The Algorithm

The algorithm is an in-house developed code created at the Universidad Publica de Navarra. In subsection 4.1 It has been widely explained the mathematical and physics principles bases for RT and RL theory employed in the simulation process of the algorithm.

As stated before, the code exploits the use of volumetric ray launching, in which the simulation scenario is divided in uniform sized cuboids to perform the calculations [49]. The dimensions of the cuboids are determined by the wavelength of the frequency of interest for the system under analysis [50], this way we guarantee that the channel characterization estimated for a particular point in the space, is relevant for the analysis.

The simulation tool is developed in matlab and takes into account the complete topo-morphological characterization such as size, shape and the frequency dispersive material properties (dielectric permittivity and loss tangent at the frequency of operation) of all the elements within the scenario, such as tables, chairs, walls, doors, columns and simplified human body models.

The algorithm has been created with the target of being able to evaluate wireless communications in complex indoor scenarios, for this, this algorithm has the following characteristics [51]:

- Simulation of a realistic multipath propagation.
- Three-dimensional modelling of all types of rooms with different shapes and sizes.
- Create complex environments as large as desired, multiple floors, multiple buildings.
- Characterization and modelling of any type of object (windows, tables, chairs, walls, etc.) by its three-dimensional shape and its dielectric constant.
- Modelling of reflection, refraction, and diffraction.
- Calculation of the interactions between rays and objects considering the polarization of the wave.
- Modelling of any type of transceiver.
- Duration of the simulation of a given ray characterizable by number of reflections and maximum delay.
- Analysis of the scenario by extracting parameters such as electric field, power levels, signal/interference, power delay, dispersion, etc.

In the following subsection 4.2.1 the process for creation the scenario of simulation will be explained, but essentially the scenarios are created in the way of rooms with all objects inside described and including the necessary transmitters and receivers in the analysis.

The algorithm operates in an iterative manner, starting with the first room available and the first transmitter within, then considering a ray launch and its reflections and storing the created rays for processing later the diffraction contribution. Figure 4.6 shows the different steps for the simulation process of the algorithm.

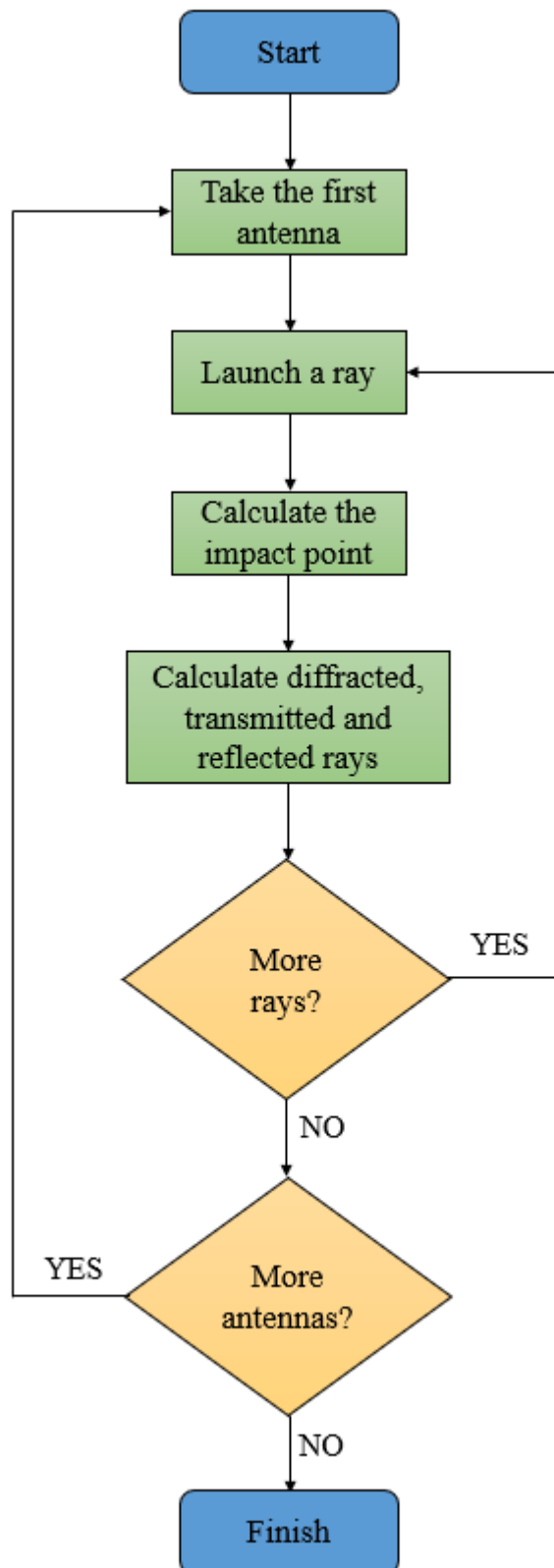


Figure 4.6 Process diagram for 3D RL algorithm during simulation iterations.

The 3D-RL algorithm provides results for the whole volume of the scenario. Results are obtained for the complete scenario volume and are later particularized to specific height planes to simplify result evaluation.

It is important to remark that this algorithm has been validated in the literature for propagation prediction at complex indoor environments, achieving a good trade-off between results accuracy and computational load [52].

4.2.1 Scenario Creation

We have already described the principles of the 3D ray launching technique, including how the rays are used to simulate the propagation of EM wave and the way they interact with the objects or scatterers, then causing the appearance of the electromagnetic phenomena of propagation mechanisms. Moreover, a brief explanation of the logical process that the algorithm executes to perform the simulation iterations has also been presented.

Before the algorithm begins the simulation, the complex indoor scenario that will be analysed is created in a very early stage of the in-house simulation tool. The scenario is created with the information which characterized the room and the objects in it, the interconnections of the different rooms and all the information which characterizes the transmitters and receivers. The tool provides a set of functions to create all the objects inside the rooms, including its dimensions and dielectric properties.

The room's characterization is given by its size. In this tool, the rooms are defined as different hexahedra with different dimensions in the x-axis, y-axis, and z-axis. Besides, the material which is inside the room can be defined. Normally, this material is air, but it is possible to consider any material for the room. Figure 4.7 depict a typical scenario created with the tool to be used in the simulations.

In the following figure we can see how complex and complete a scenario created with tool could be. This allows us to do the analysis and wireless channel characterization of almost any kind of indoor environment.

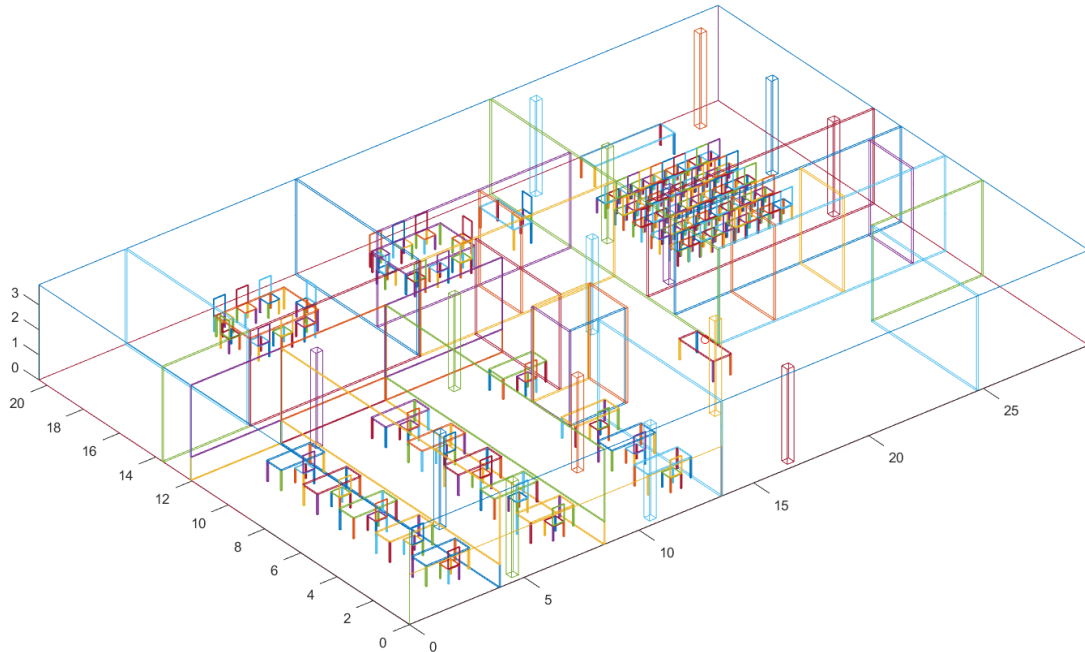


Figure 4.7 Schematic view of a scenario created with the 3D Ray Launching simulation tool.

In the tool, the objects are made up of hexahedrons. Each of these hexahedrons is defined by its center position in coordinates relative to the room it is in, the width of the object on each axis, and the material the object is made of. By means of this basic geometric shape, it is possible to easily create a multitude of much more complex objects, see Figure 4.8, such as tables, chairs, or shelves, and place them in the room.

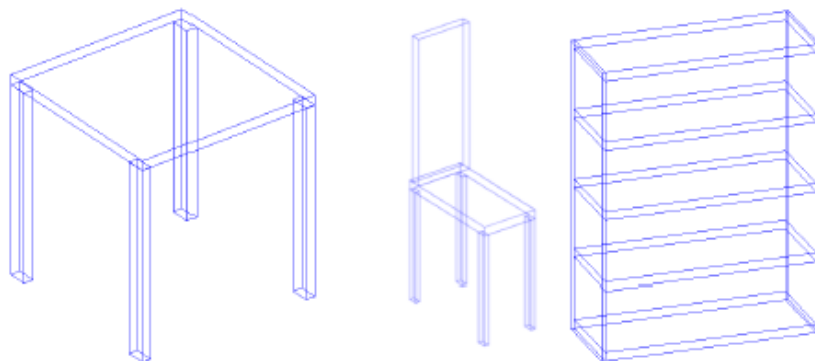


Figure 4.8 Schematic view of objects created with simulation tool.

The 3D Ray Launching simulation tool also includes the following material and its dielectric characteristics to be used in the creation of objects inside the scenario under study:

Table 4.1 Objects material included in the simulation tool.

| Code | Material |
|------|--------------|
| 0 | Air |
| 1 | Wood |
| 2 | Brick wall |
| 3 | Plasterboard |
| 4 | Doors |
| 5 | Glass |
| 6 | Aluminum |
| 7 | Concrete |

As stated before, the calculated parameters are stored in the cuboids that fill the entire volume of the scenario under analysis. For this reason, when a ray arrived a specific cuboid, these parameters are stored in a matrix with the value of the received power and the time of arrival. This happens until the ray reach the number of reflections specified (i.e. impacts on objects) or it exceeds the propagation time set, both parameters defined by the user.

An important aspect to remark is the cuboid resolution where the parameters are estimated, as stated earlier, the cuboid size should be in the order of the wavelength of the simulation frequency to be representative, but it should be selected in a careful way because as smaller cuboid resolution, more processing time and computational resources are needed.

In order to obtain accurate simulation results, the characteristics of the deployed wireless transceivers are predefined before the simulations in the tool. Following, the main parameters of the transmitter as well as the receiver transceivers are shown, between other parameters:

- Operation frequency (Hz).
- Output RF power level (Watt).
- Cuboid resolution (m).
- Maximum reflection events.
- Angular resolution for rays.
- Antenna type and directivity.
- Antenna gain.

At last, to summarize; the scenario created is composed of four variables:

- *Rooms*: This variable has the necessary information to characterize each one of the rooms and the objects that are inside them.
- *Interconnections*: This variable defines the way the rooms are interconnected.
- *Transmitters*: It has information that characterizes each of the transmitters.
- *Receivers*: Characterizes each of the receivers in the scenario.

One of the advantages of dividing the scenario into rooms is that by simulating each room separately, the algorithm just has to have in processing memory the room that is being simulated in that moment. Therefore, it does not matter how big the simulation environment is, because in memory it will be only necessary to have the room of the current simulation iteration.

Once the scenario has been created, the simulation is performed by the 3D Ray Launching algorithm.

4.2.2 Analysis Process

Once the scenario has been simulated, a master matrix of dimension ($Resx \times Resy \times Resz$) is obtained and each element of this master matrix has in turn another matrix with the information of each of the rays that has passed through that location or cuboid.

The information that has been saved from each ray is:

- Time it took for the ray to arrive (τ).
- Distance traveled by the ray (d).
- Loss coefficient in each polarization (L^\perp, L^\parallel).
- Direction of the beam at the transmitter (θ_t, Φ_t).
- Direction of the ray at the receiver (θ_r, Φ_r).
- Transmitting antenna (n).

With all these parameters the algorithm, at the final stage, calculates the received power levels, power delay profiles and E field in each cuboid for the complete volume of scenario.

As stated before, the data is collected for the whole volumetric space of the environment, according to the cuboid resolution or size defined previous the simulations. Afterward, the data extracted is particularized to specific height planes of interest to perform the result evaluation.

In this thesis, where MIMO performance analysis is accomplished, the results obtained from the 3D ray launching tool are employed to estimate wireless channel characterization in terms of received power levels and time domain parameters.

The following Figure depicts the complete simulation methodology implemented in thesis, including the use of the 3D Ray Launching algorithm explained in the chapter.

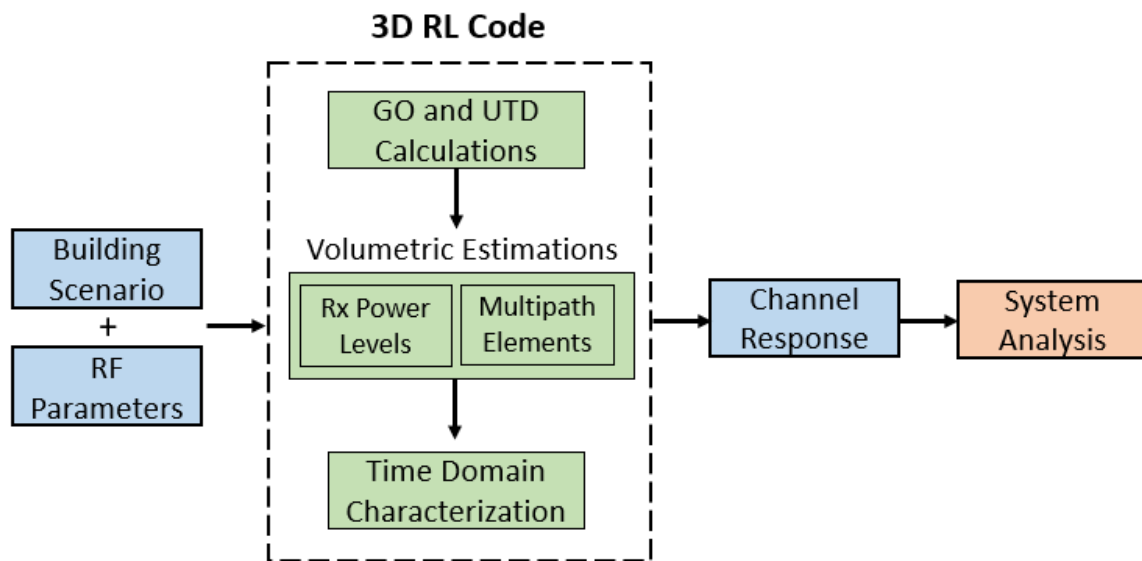


Figure 4.8 Block diagram of simulation methodology implemented.

Furthermore, very valuable analysis in the context of multipath propagation can also be done with the results obtained from the simulation process. For instance: in each scenario studied in this thesis, we can determine the values of the corresponding radio channel matrix, *H-Matrix*, from the power levels transmitted, power levels received and the corresponding channel response.

These *H-Matrix* values, including other results from the algorithm such as power delay profiles, are then employed in a separately developed matlab scripts to estimate accurate MIMO performance by means of STBC functions.

Chapter 5

Deterministic MIMO Performance Analysis

ANALYZING the performance of MIMO systems in a variety of complex indoor scenarios with different topology and morphology properties, and under different wireless communication parameters and technologies, is one of the main objectives of this thesis. In relation with this, the study of radio channel characteristics and its influence on the accomplishment of wireless networks, specially while implementing MIMO, is a research field of great interest, representing another motivation for the realization of this thesis. Having into account all of these, this thesis fulfilled a deterministic MIMO performance analysis in three relevant study cases. In this chapter, we firstly present in section 5.1, the effect of different antenna element spacing in the performance of MIMO system in a volumetric analysis. Then, section 5.2 presents and analyses the influence of human scattering in complex indoor scenarios. Last but not least, in section 5.3, a complete phase evolution analysis is accomplished in the context of IoT and IIoT applications focused in receive diversity.

5.1 Antenna Spacing Effect in MIMO Performance

The progressive implementation of applications that make use of more demanding transmission bit rates, require the use of techniques with aim of maximizing spectral efficiency whilst controlling interference levels in order to comply with coverage/capacity requirements. In this sense, multiple solutions have been proposed, at the physical layer as well as in network definition and orchestration. One of these approaches is the use of different MIMO (Multiple Input Multiple Output) techniques (conventional MIMO, multi-user, massive, etc.) in order to increase channel capacity by means of combined Space-Time Coding and signal transmission [53,21].

The achievable performance, which increases owing to multiple transmit-receiver links is strongly dependent on the wireless channel environment, which determine the values of the corresponding radio channel matrix, as well as on the antenna element spacing employed. In this study case, the effect of variable antenna spacing will be studied and presented considering complex indoor scenarios, in which all the scattering elements will be considered. In this way, wireless channel characterization in terms of received power levels and time domain parameters for the complete volume of the scenario under analysis will be obtained, for 5G NR FR1 frequency band at 3.7 GHz.

5.1.1 Scenario Description

As explained in Chapter 4, in order to estimate frequency/time radio channel characteristics in a volumetric scenario, a deterministic method is employed, launching several simulation iterations based on an in-house developed 3D Ray Launching algorithm. As already delineated, with the purpose of performing the estimations, the scenario is built based on cuboids, with size determined in function of the wavelength of the frequency we need to analyse. The principle of operation of the algorithm was also explained in Chapter 4, and its optimizations to reduce computational complexity are given in [42,54,55].

In order to accomplish this study case, an indoor scenario has been implemented, corresponding to a medium-size *Conference Room* with dimensions 10m L x 8.75m W x 3.5m H located inside the Jeronimo de Ayanz Building at the Universidad Pública de Navarra.

The 3D model of this scenario has been implemented in order to perform wireless channel estimations with the aid of the 3D-RL algorithm, see Figure 5.1. The 3,4 – 3,8 GHz band is considered to be the main band for introducing 5G NR FR1 based services in Europe [56], so a frequency of operation of 3,7 GHz is employed in the simulation studies performed.

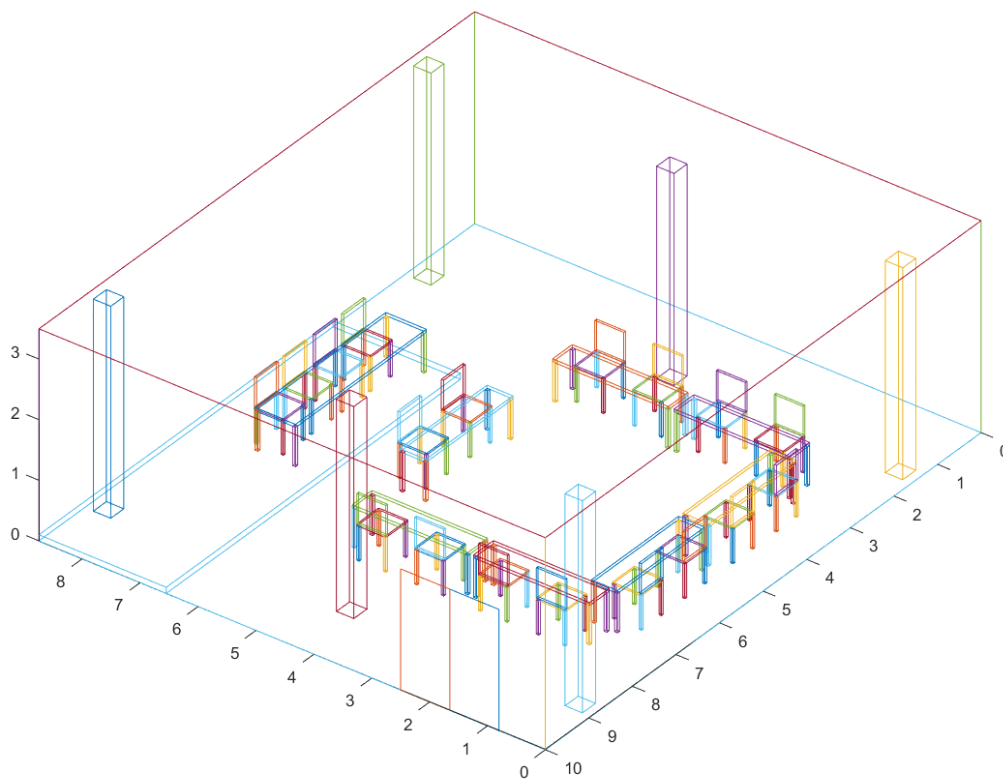


Figure 5.1 Implemented scenario under test in the 3D RL simulation tool.

The complex indoor scenario has been built with the most details as possible, making use of the functions to create objects available in the simulation tool. This implies the inclusion of as much physical characteristics as possible to obtain a result data very accurate. In Figure 5.2, a realistic view of the scenario is depicted, showing how complex the model can be.



Figure 5.2 Realistic description of the 3D complex scenario implemented.

A list of relevant parameters used in the simulations can be found in Table 5.1, based on previous convergence analysis studies for the 3D RL simulation code.

Table 5.1 Simulations parameters

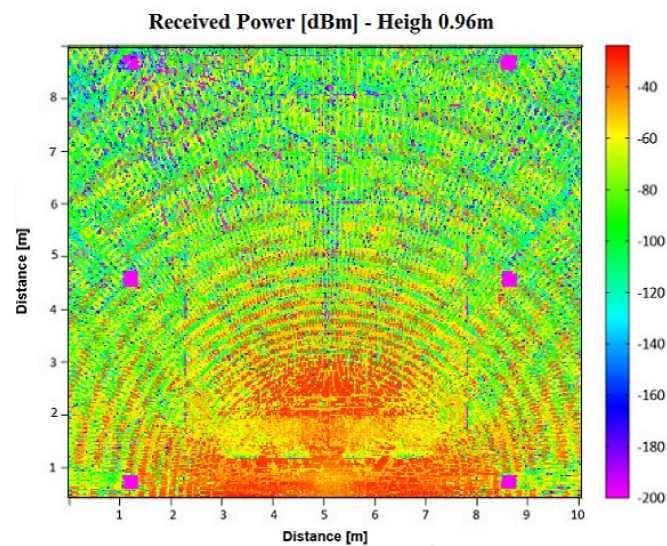
| Parameter | Value |
|-------------------------------|-----------------|
| Operation Frequency | 3,7 GHz |
| Output RF Power Level | 9 dBm |
| Cuboid Resolution | 3cm × 3cm × 3cm |
| Maximum Reflections Simulated | 6 |
| Antenna Type and Gain | Monopole, 0 dBi |

In this specific scenario, we take into account the complete topomorphological characterization of all elements within the scenario. This includes shape, size, and electric properties (i.e., frequency dispersive dielectric constant and conductivity) of all objects inside the environment including walls, doors, ceiling, columns, etc.

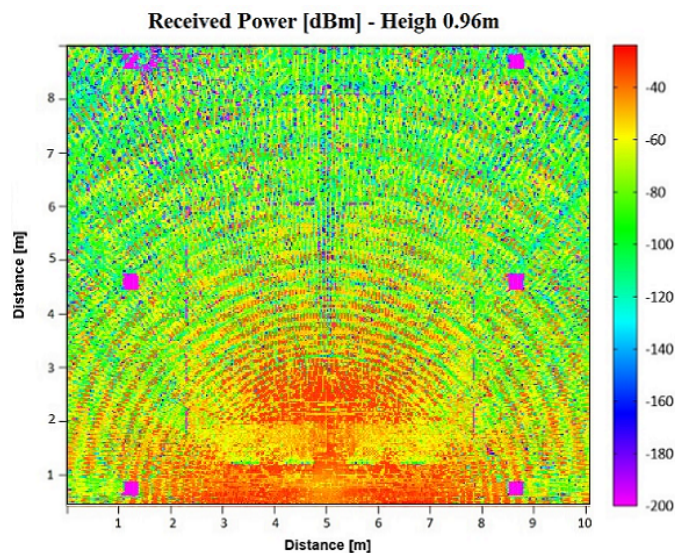
5.1.2 MIMO Performance Analysis

5.1.2.1 3D RL Simulation Analysis

With the aid of the 3D RL algorithm, wireless channel characterization parameters are obtained for the complete volume of the scenario under analysis. The simulation process for this scenario is done in two parts, corresponding to the results required for Transmission Antenna 1 and Transmission Antenna 2.



(a)



(b)

Figure 5.3 Bidimensional coverage estimation for a 0.96m heigh plane for (a) Tx1 and (b) Tx2 in the simulation scenario.

We firstly depicts in Figure 5.3, the bi-dimensional distribution of received power levels, for a height plane of 96 cm for the complete area of the scenario, and corresponding to the results for Tx1 and Tx2.

The focus of the radio channel characterization in this work is the evaluation of Space-Time diversity performance. With this purpose, the results depicted in the following Figure 5.4 correspond to the combined RF power distribution radiated from two transmitter antennas located at a height of 2m.

Figure 5.4 also depicts the bi-dimensional distribution of received power levels, for a height plane of 96 cm corresponding to the potential location of a wireless receiver device, for example a laptop, that can be located on one of the tables of the scenario. As initial visual verification, using the heatmap scale, we clearly notice the power increase with the two transmit antennas combined (MIMO).

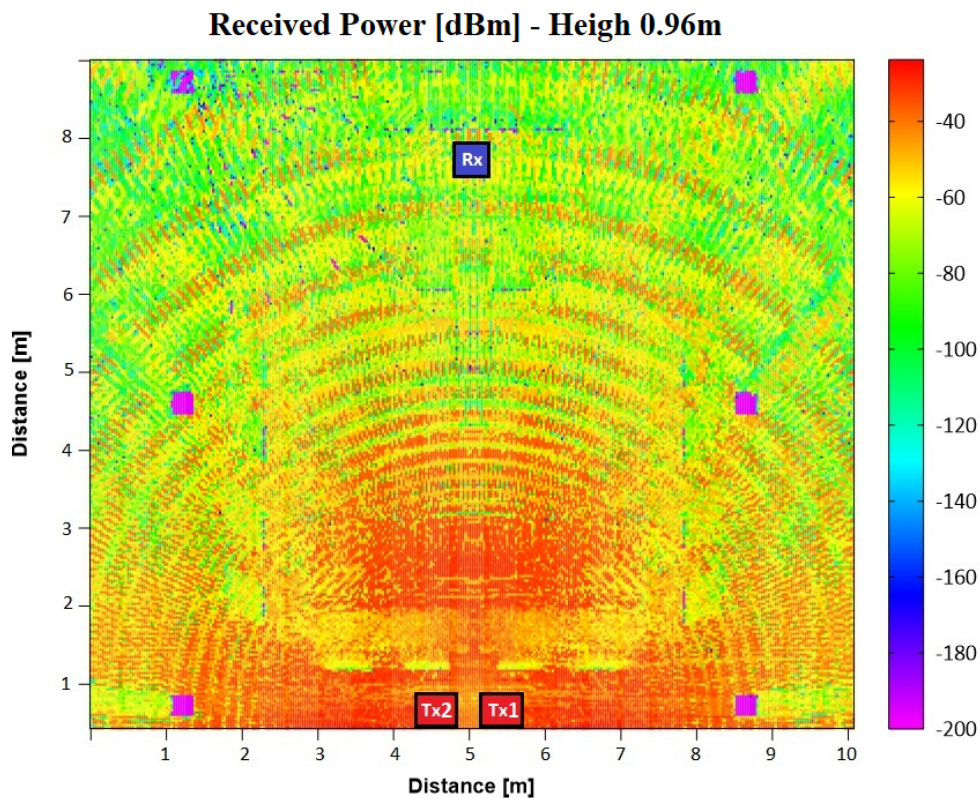


Figure 5.4 Bidimensional coverage estimation for a 0.96m heigh plane of 2 x Tx in the simulation scenario.

Tx antennas are represented by red rectangles (Tx) whereas the potential receiver (laptop) is represented by a blue rectangle (Rx).

The power levels distribution in the horizontal plane will be only dependent on the distance between the User Equipment or Terminal Device and Transmitter.

The location of the transmitters (i.e., 2m height) corresponds to the potential location of a 5G femtocell within the scenario under test. A visual representation of Receiver and Transmitter (with two transmit antennas) locations in this case can be found in Figure 5.5.

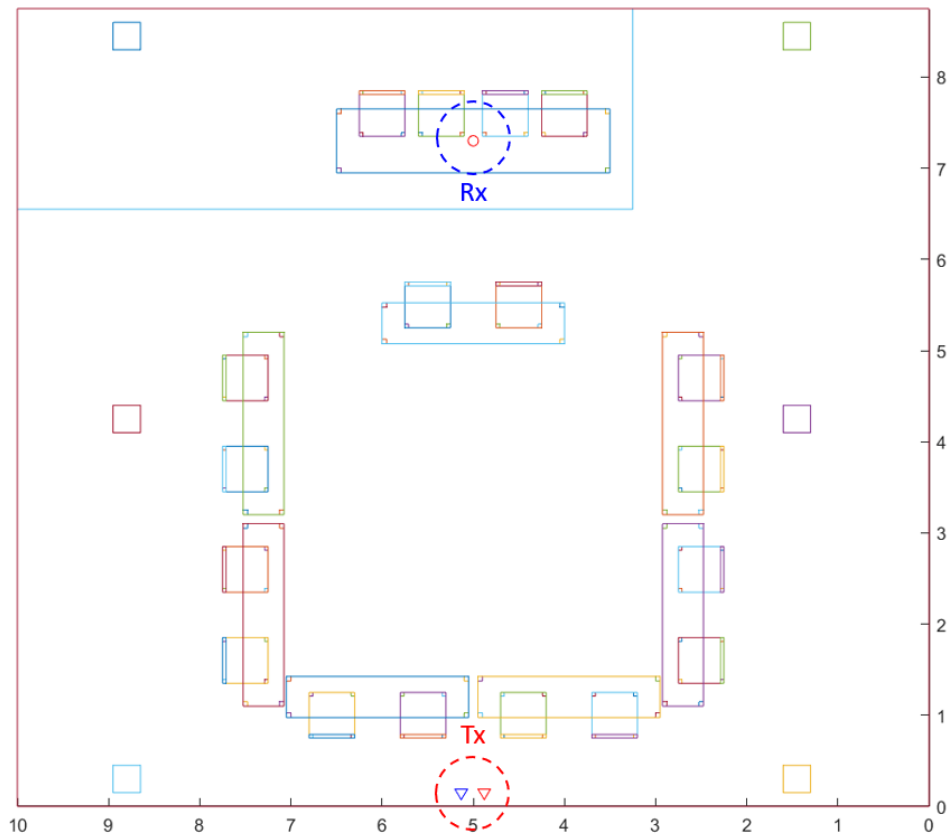


Figure 5.5 Schematic representation of Tx and Rx positions within the scenario.

The plant view depicted in Figure 5.5 is an example of a classical indoor scenario where femtocell or repeater will be deployed for 5G networks according to the EM propagation characteristics of 5G NR FR1 frequency band.

Time domain characterization in terms of Power Delay Profile (PDP) and Delay Spread have also been obtained. In Figure 5.6, the PDP estimation for the location of the laptop previously mentioned is depicted.

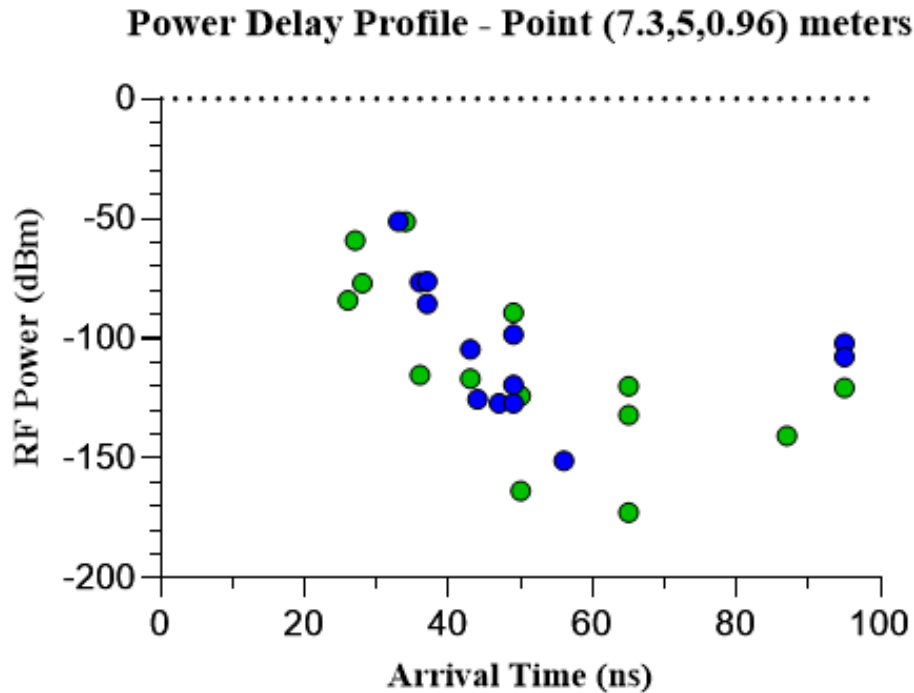


Figure 5.6 Power Delay Profile at a given cuboid. Green Bullets representing multipath elements from Tx1 and Blue Bullets from Tx2.

Space-Time coding approaches take advantage of the multipath interference for improving the data rate and/or the reliability of communications over fading channels [16]. The performance of a MIMO system is determined by the characteristics of the radio environment, given by the values of an $M \times N$ Radio Channel Matrix (*H-Matrix*). It has been seen that for low-band frequency, different received power values are obtained when the spatial configuration of the antennas is modified [50]. Taking into account the previously mentioned study, it is interesting to deterministically validate the effects of antenna spacing in the 5G NR FR1 frequency band.

In this study case, MIMO performance in the scenario under test will be analysed considering the effects on received power levels by modifying antenna spacing in transmission and considering an operating frequency in the 3.7 GHz band.

Received power level distributions have been obtained for 3 situations, in which the spacing between Tx1 and Tx2 has been varied in different multiples of the operating wavelength λ . Table 5.2 shows received power levels for each case under analysis, with the assumption that the UE (User Equipment) is a laptop with two receiver antennas with spacing fixed in 4λ , which is feasible for the 3,7 GHz operation frequency and the current physical dimensions of commercially available laptops.

Table 5.2 RF power estimations for different antenna spacing

| Channel Path | λ | 2λ | 3λ |
|--------------|-------------|-------------|-------------|
| | Power (dBm) | Power (dBm) | Power (dBm) |
| h_{11} | -61,96 | -50,89 | -43,16 |
| h_{12} | -75,16 | -59,16 | -48,64 |
| h_{21} | -67,52 | -52,08 | -42,31 |
| h_{22} | -71,02 | -63,29 | -58,26 |

It can be seen that when using a spacing of 1λ between two transmitter antennas, the received power on the two receiver antennas is highly affected for Tx2 [h_{12} and h_{22}] transmissions, due to the topo-morphological configuration of the environment. This behaviour persists in all the λ spacing under analysis, so it is clear that the scattering distribution in the scenario under test is affecting the multipath signals traveling from Tx2 toward the UE, decreasing received power levels. These results highlight the importance of this kind of studies in complex indoor scenarios, where small changes in the environment layout can impact drastically in the performance of a system.

The estimation of received power levels shown in Table 5.2 and the corresponding analysis are strongly dependent on the receiver location (e.g., laptop), where displacements in the order of $\lambda/2$ can be relevant [15].

In order to gain insight in relation with received power level distribution as a function of variable UE locations within the scenario under test, Figure 5.7 depicts the received power distribution for a cut-plane height of 96 cm with multiple laptops.

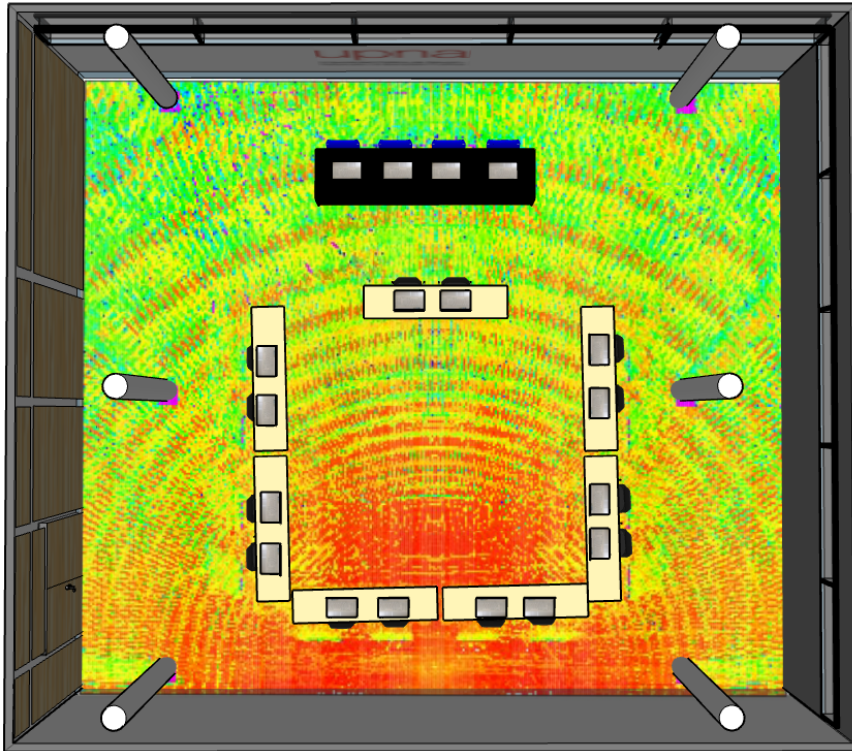


Figure 5.7 Schematic view of coverage estimation and RF power received by various laptops locations in the simulation scenario.

The results shown in Table 5.2 indicate that an antenna spacing of 3λ shows an evident improvement in received power levels in the observation point. This spatial diversity improvement is due to the distance between the two transmission elements, causing that the signals transmitted are sufficiently uncorrelated (less than 0,7 correlation) [17].

The frequency of operation plays a key role in the definition of antenna spacing and the design of MIMO systems. In the case of 5G networks frequencies, for example 3,7 GHz, spacing of more than 3λ would be hard to achieve because the dimensions of the femtocells are directly proportional to antenna spacing, and for the case of indoor scenarios this an important aspect to care of.

The use case under analysis implies that the 5G femtocell and laptop (UE) are surrounded by a similar scattering environment. Therefore, in both ends of the radio channel the two antenna elements must have a spacing in the order of 3λ to provide sufficient decorrelation [17]. Using the time domain characterization results depicted in Figure 5.6, the correlation coefficient ρ is obtained by using (5.1),

$$\rho_{xy} = \frac{\sum_{i=1}^n (x_i - \bar{x})(y_i - \bar{y})}{\sqrt{\sum_{i=1}^n (x_i - \bar{x})^2} \sqrt{\sum_{i=1}^n (y_i - \bar{y})^2}} \quad (5.1)$$

obtaining a value of $\rho = 0,54$ for the scenario under test, where n is the samples size, x_i, y_i are the individual sample point of multipath elements indexed i , and \bar{x}, \bar{y} are the samples mean.

In order to have deeper understanding of the performance of spatial multiplexing under analysis in this work, BER estimations have been obtained for a configuration of 2 Tx – 2 Rx antennas (MIMO channel) using antenna spacing of $\lambda, 2\lambda$ and 3λ .

The evaluation has been performed considering Additive White Gaussian Noise (AWGN) channel and assuming the channel being narrowband time-invariant, employing an orthogonal space-time block code transmission. The implementation of STBC was accomplished by means of a script developed in matlab and implementing QPSK modulated Alamouti OSTBC.

In this script we also make use of the previous power delay profiles estimations and received power levels obtained in Table 5.2. as main input to execute the OSTBC. Power delay profiles have been also extracted from the simulation results for the case of spacing of λ and 2λ .

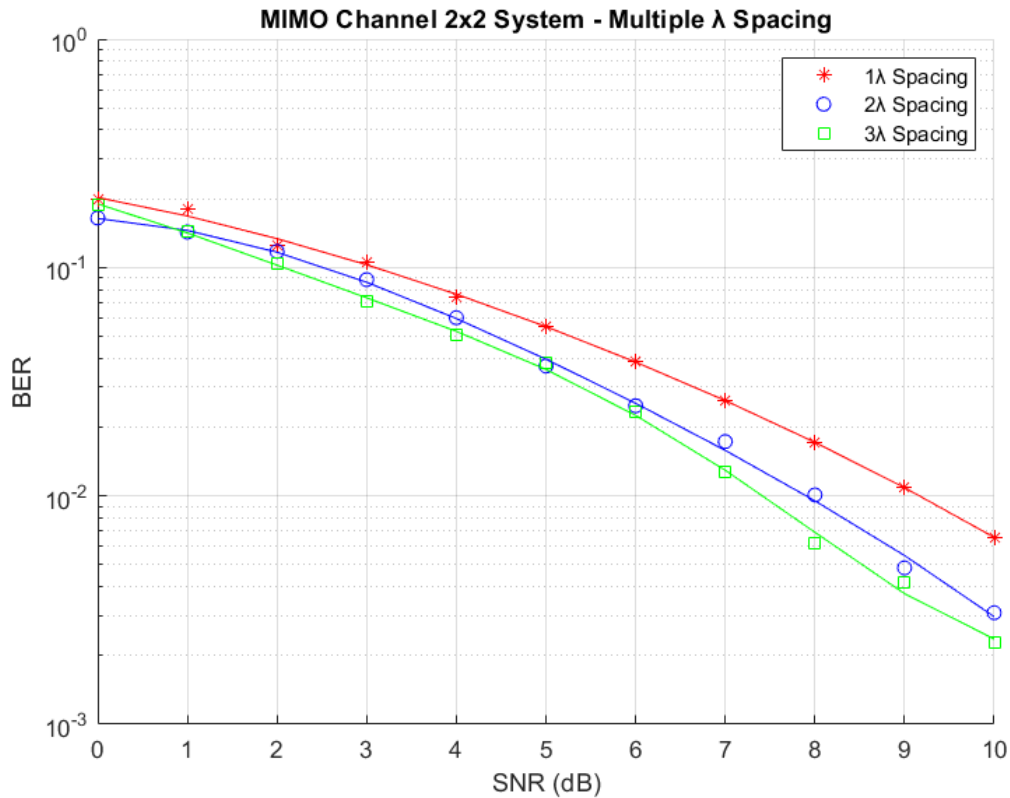


Figure 5.8 BER performance as a function of SNR for MIMO channels 2x2 in different antenna elements spacing.

From Figure 5.8, it can be seen that as the SNR values increase, BER estimations improve for all the antenna elements spacing settings. This is an expected result due to the protection that orthogonal space-time code adds to the system. It can also be seen that a spacing of 3λ offers an enhancement in the order of 2 dB over 1λ spacing in this particular scenario as SNR values increase. This improvement can be used in the system to enhance the transmission performance.

5.1.2.2 Wireless Channel Received Power Level Measurement

In order to provide initial validation of simulations previously presented, measurement results for received power levels have been obtained, for the real scenario under test.

A continuous wave transmitted test signal was generated by means of a VCO / Voltage-controlled Oscillator (model ZX95-3760-S+) in the frequency range of 3200 - 3760 MHz, to emulate 5G NR FR1 bands for future 5G deployments, coupled to a wideband omni-directional (300 MHz - 8 GHz) antenna. Received power levels have been measured with a similar antenna coupled to a portable spectrum analyser (FieldFox N9912A), as depicted in Figure 5.9. The receiver has been placed in the same UE location used in the 3D-RL simulations (laptop located at the central table of the podium – Point 7.3, 5, 0.96 meters).



Figure 5.9 Setup employed for the measurement campaign in the real scenario under test.

The measurement campaign has been carried out in the existing and real conference room corresponding to the same conference room model previously implemented in the 3D RL algorithm.

In order to emulate MIMO channel conditions, the transmitter has been located in six different points corresponding to the antenna Tx1 and Tx2 spacing variation of λ , 2λ and 3λ . The vertical position in the real scenario for the VCO was also fixed to a height of 2m as those employed for the transmitters in the 3D-RL simulations, corresponding once again to the location of a 5G indoor femtocell.

The received power level distribution is given in Table 5.3. Higher received power levels in the measurement results are observed as compared with simulation results previously presented, owing mainly to the gain of both antennas and in lesser extent, to inherent differences in between the simulation model and the real scenario. Transmission power was set to 9 dBm in the measurement trials performed.

Table 5.3 RF power measured in UE locations for different transmit point.

| | λ | 2λ | 3λ |
|-----|-------------|-------------|-------------|
| | Power (dBm) | Power (dBm) | Power (dBm) |
| Tx1 | -45,08 | -42,37 | -40,78 |
| Tx2 | -43,75 | -42,80 | -39,78 |

As we can see from Table 5.3, an improvement on the power levels received is clearly noticed when increasing antenna element spacing, in the order of 4 dB for both Tx antennas, consistent with decorrelation between Tx-Rx paths.

This data also validates the results obtained from the simulation tool using 3D ray launching, observing a pretty similar trend in received power levels for both environments, the real measured and the simulated one.

5.1.3 Results and Application

The topo-morphological characteristics of the surrounding environment as well as the configuration in terms of antenna spacing of a MIMO system plays a key role in the resulting performance.

In order to gain insight in the operation of a MIMO system in a complex indoor environment, a scenario under test has been implemented and tested by means of an in-house developed 3D RL code. Different results have been obtained in terms of frequency dependent received power levels as well as time domain characteristics, such as power delay profiles, for the complete volume of the scenario under analysis.

In this context, variations in the antenna spacing of a 2x2 MIMO system have been studied for a system operating at 5G NR FR1 compatible frequency of 3,7 GHz. Results show that as spacing is increased from 1λ to 3λ , there is an observable gain in the received power levels, which in turn are dependent on the specific configuration of the surrounding environment in terms of scattering distribution. Measurement results have also been obtained, showing a similar trend in relation with observable gain.

These results can help in the coverage and capacity radio planning tasks, in order to optimize overall system performance for the specific characteristics of the scenarios under analysis.

5.2 Human Scattering Influence in the Performance of MIMO Techniques

In recent years, with the deployment and development of the new 5G networks, a new research field related to the design of modern and more reliable indoor repeaters, e.g., femtocells, is at its boom. How people interconnect in urban areas and indoor environments will become increasingly important as we densify networks for 5G. Easy to install, low-cost and high performing solutions will be at the forefront of this densification, including small cells, femtocells, and so on.

When a system engineer will be planning coverage or capacity for a wireless network, for example 5G deployments, in these urban or indoor scenarios, the common factor in all the cases will be the dense present of human bodies in the environment, and this will represent a very challenging situation. For example, the RF planning in locations such as offices, shopping mall, stadium, and university campus, will be a strenuous task.

Wireless reliability requires, in part, that the signal be transmitted reliably. Ideally, EM waves will travel from the transmitter to the receiver with no loss in signal strength; this is, unfortunately, not possible in the real world. As soon as the RF signal leaves the transmitting antenna, the signal begins to degrade. Any object in the path of the signal will variously reflect, refract, diffract, or absorb the signal's energy [57]. Absorption is a common propagation characteristic. For example, water is a very efficient absorber of RF energy; it follows that the human body, which is over 70% water, will attenuate RF signal significantly.

Human body additionally to absorb signal energy, can cause any other wireless propagation mechanism such as scattering. The study and analysis of the human presence impact in these complex indoor scenarios is highly important in the planification task and system designing for wireless networks.

Making use of 5G NR FR1 frequency band at 3,7 GHz in this study case, the effect of human body scattering will be studied and presented considering complex indoor scenarios. Wireless channel characterization in terms of received power levels and time domain parameters for the complete volume of the scenario under analysis will be obtained, and MIMO performance analysis will also be presented.

5.2.1 Scenario Description

In the very initial stage of the analysis process, we need to build the complex indoor environment to be used in the simulations. As in the previous study case, we make use of the 3D RL tool to create the scenario based in cuboids and including all the scatterers inside.

The selected scenario corresponds to a medium-size *Conference Room* with dimensions 10m L x 8.75m W x 3.5m H located inside the Jeronimo de Ayanz Building at the Universidad Pública de Navarra. A 3D model of the scenario implemented is depicted in Figure 5.10.

Intending to provide a tool for the radio planning activity in emerging wireless technologies such as 5G mobile networks, we decided to do the study in the 3,4 – 3,8 GHz band, which is a frequency band of huge interest because is considered to be the main band for introducing 5G NR FR1 based services in Europe [56]. Then, a frequency of operation of 3.7 GHz is employed in the simulation studies performed.

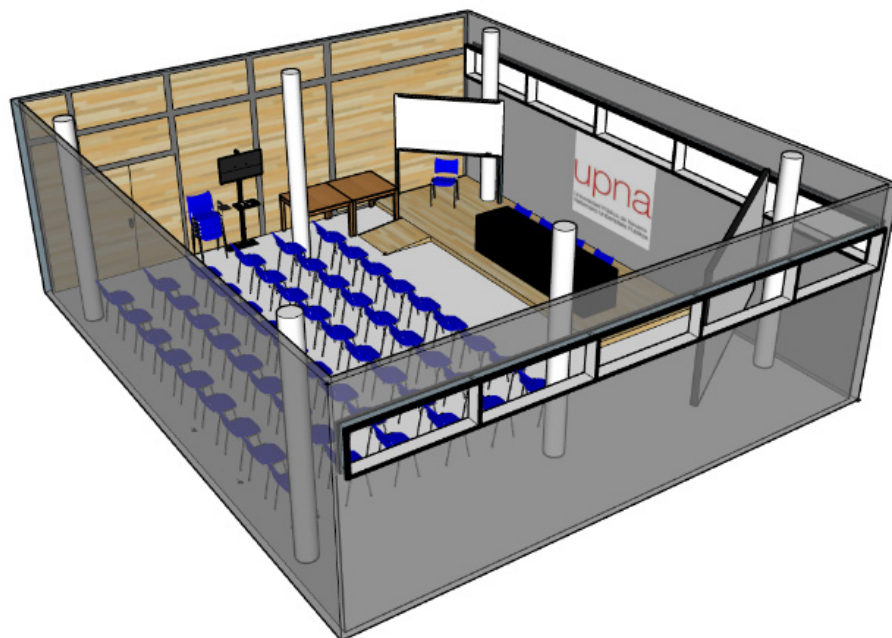


Figure 5.10 3D Model of the implemented scenario under test in the simulation tool, corresponding to a Conference Room.

Besides the frequency used for the code in the simulation iterations, there are more parameters as input for the computational process. A list of relevant parameters and their values used in the simulations can be found in Table 5.4.

Table 5.4 Simulations parameters.

| Parameter | Value |
|-----------------------------|-----------------|
| Operation Frequency | 3,7 GHz |
| Output RF Power Level | 26 dBm |
| Cuboid Resolution | 3cm x 3cm x 3cm |
| Maximum Reflection Events | 7 |
| Angular Resolution for Rays | 1° |
| Antenna Type and Gain | Monopole, 0 dBi |

The complex indoor scenario built for this study case is physically the same as used in the previous study in subsection 5.1. In this case we have implemented a layout completely different and using a composition of plenary kind instead of meeting format, as the previous case. Doing so, we can arrange the presence of much more human bodies inside de environment, very needed to accomplish the objective of this work.

This Conference Room, with the layout employed, has a capacity of 54 attendees plus 4 presenters at the podium. In order to evaluate the human scattering influence in the channel response and a MIMO system performance, 3 use cases has been performed with this scenario; 0%, 50% and 100% occupancy.

Additional to the new layout, we also make use of 26 dBm of output RF power in the transmitter as initial parameter for the simulation iterations. This corresponds with typical transmission power for current 5G femtocells and then allowing us to obtain the most accurate results possible.

5.2.2 MIMO Performance Analysis

After completing several simulation iterations, using the 3D RL code described before, we have the wireless channel characterization for the complete volume of the complex indoor environment. The wireless channel parameters obtained, such as received power levels distribution, and time domain characterization in the form of rays or multipath components arriving in every cuboid, are used to analyse the channel response and then the MIMO system performance for this specific scenario.

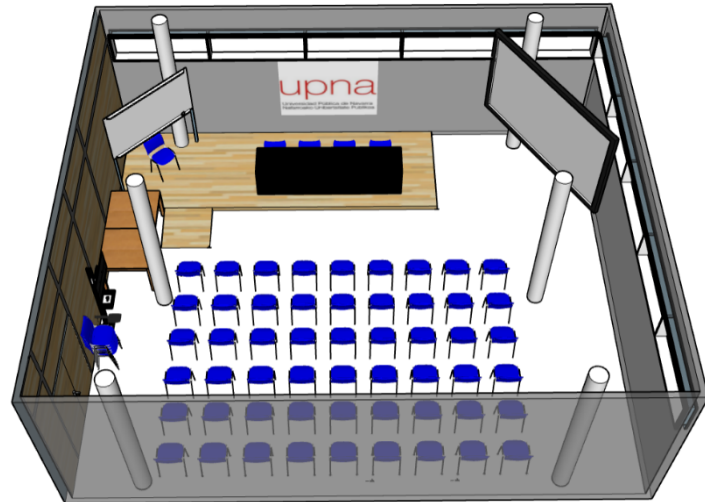
The main goal of this channel characterization is the evaluation of space-time diversity performance, for this reason, these simulation iterations have been performed using two transmit antennas with spacing between radiating elements of 3λ , antenna spacing showing better results in this kind of scenarios and operation frequency [22].

5.2.2.1 RF Power Coverage Estimations

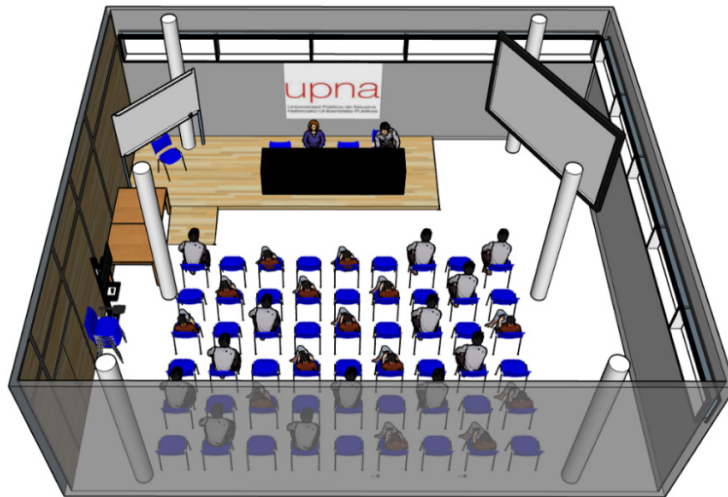
Having into account the dense presence of human bodies within the scenario selected and considering the great absorption effect that these scatterers impinge in the signal strength, the RF power levels is a highly important parameters to analyse when the signal is propagated.

It is important to remark that absorption is one of the factors that affect signal propagation in different environments and in different ways. The effect it causes is that part of the signal energy is transformed when it hits an object with absorption properties and part of the signal power is unexpectedly lost [58].

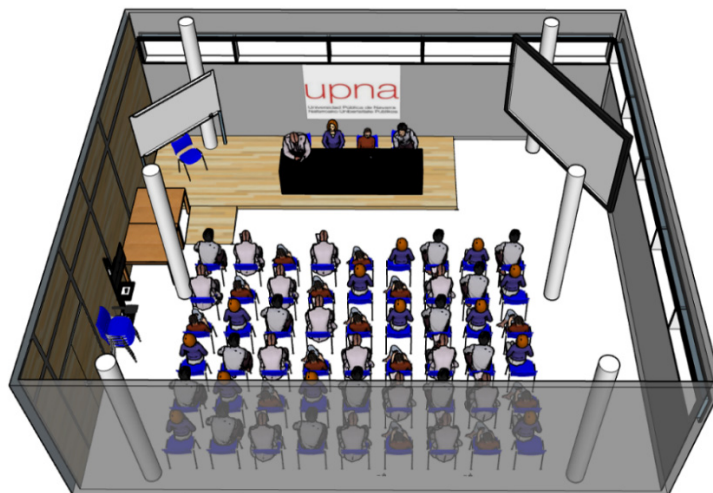
With the intention of better understanding the implications of the changes as human bodies have different occupancy level, we depict the three cases that will be analysed in Figure 5.11.



(a)



(b)



(c)

Figure 5.11 Schematic representation of human occupancy (a) 0% (b) 50% (c) 100% in the conference room.

According to the scenario model depicted in Figure 5.10 and Figure 5.11 under study, in order to do the analysis, we select a height plane of 0.78m corresponding to the potential location for a UE (User Equipment), for example a Tablet Device or Cellular Phone, hold by a person located anywhere in the auditorium area, see Figure 5.12.

In the horizontal plane, at cut-plane height of 0.78m, the power levels distribution will vary only depending on the distance from the observation point to the transmitter, and the effect of signal energy absorbed by human presence and scattering inducted.

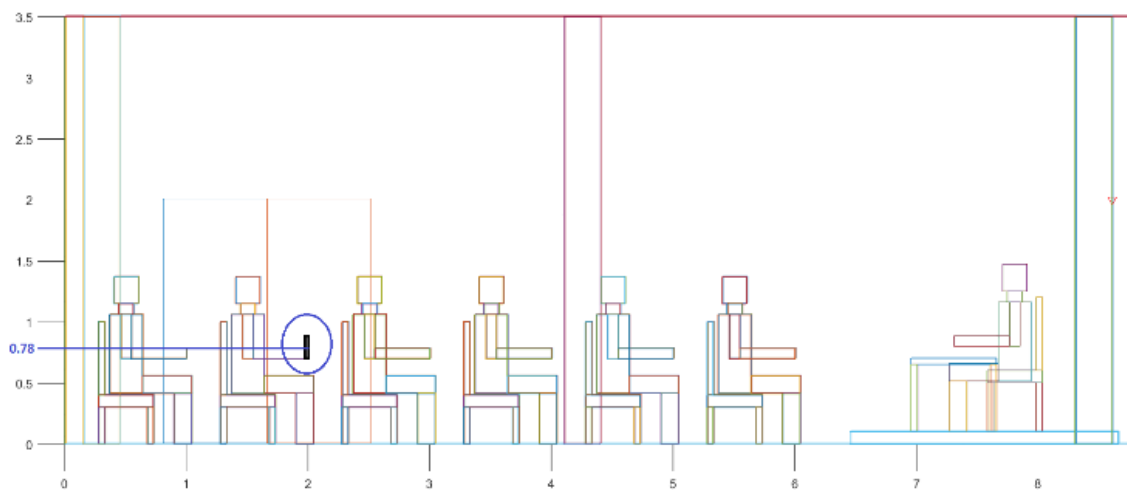
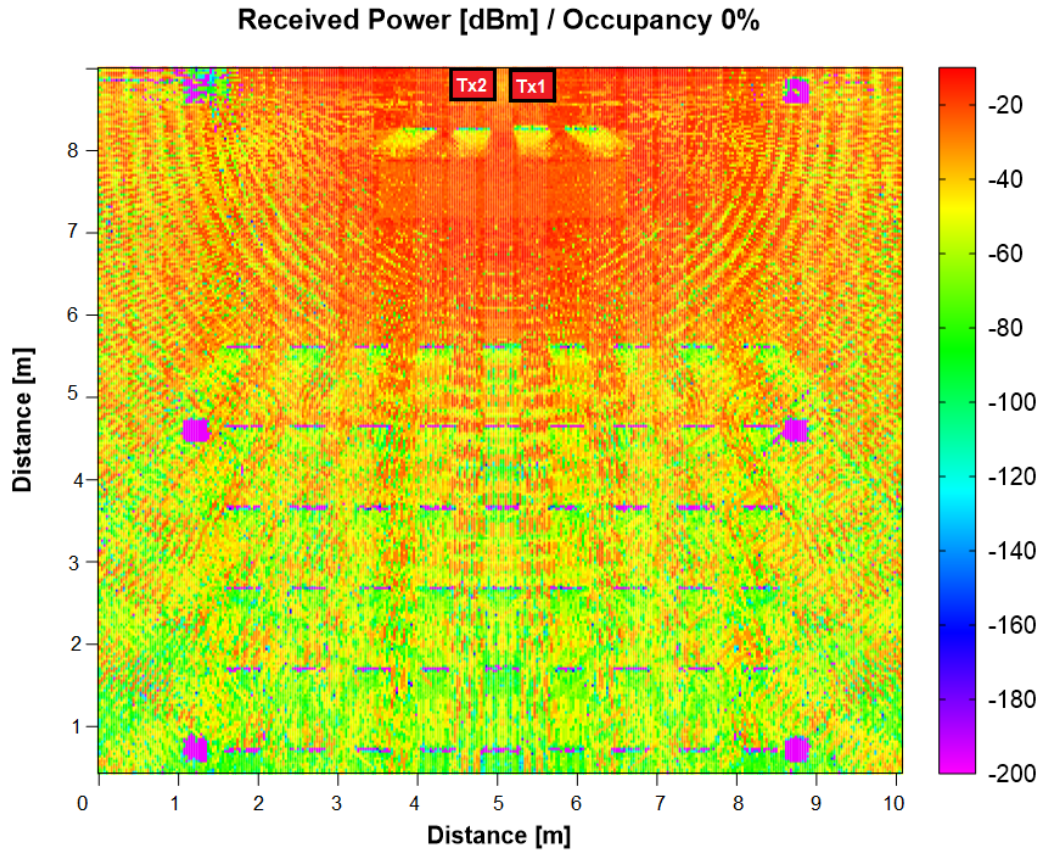


Figure 5.12 Schematic view of potential location and height position for a UE inside the indoor scenario.

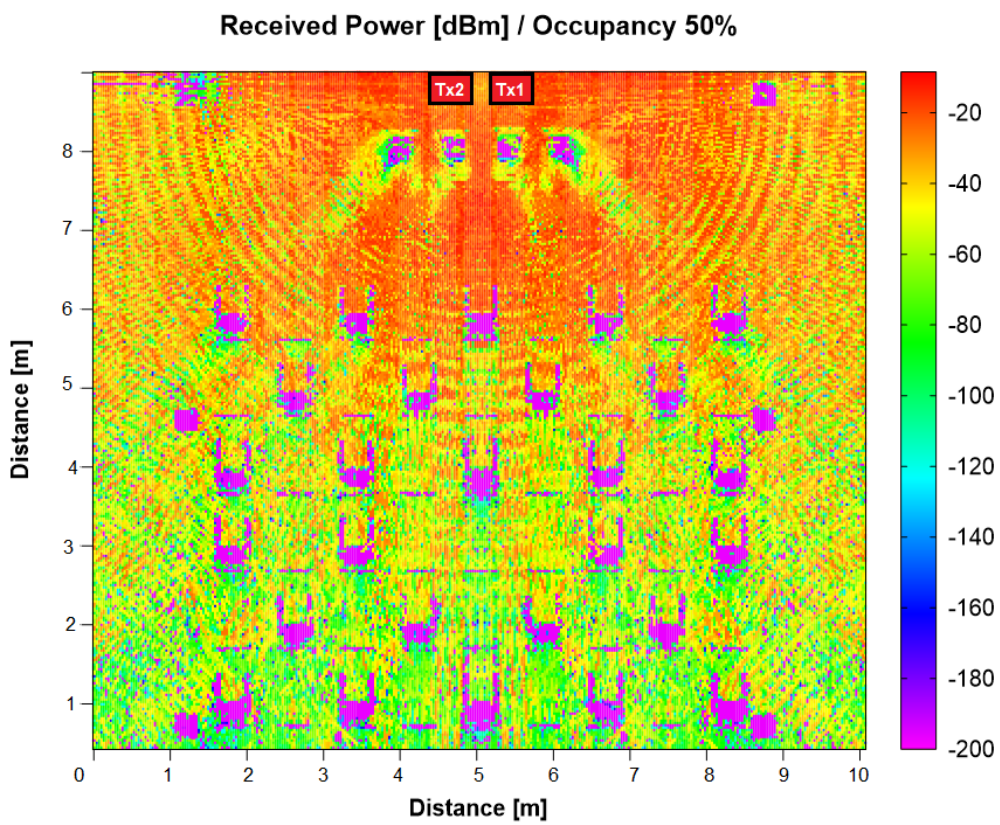
A bi-dimensional (XY-axes) distribution of received power levels, for a cut plane at height $h = 0.78\text{m}$, is depicted in Figure 5.13, for 3 use cases with 0%, 50% and 100% of human occupancy.

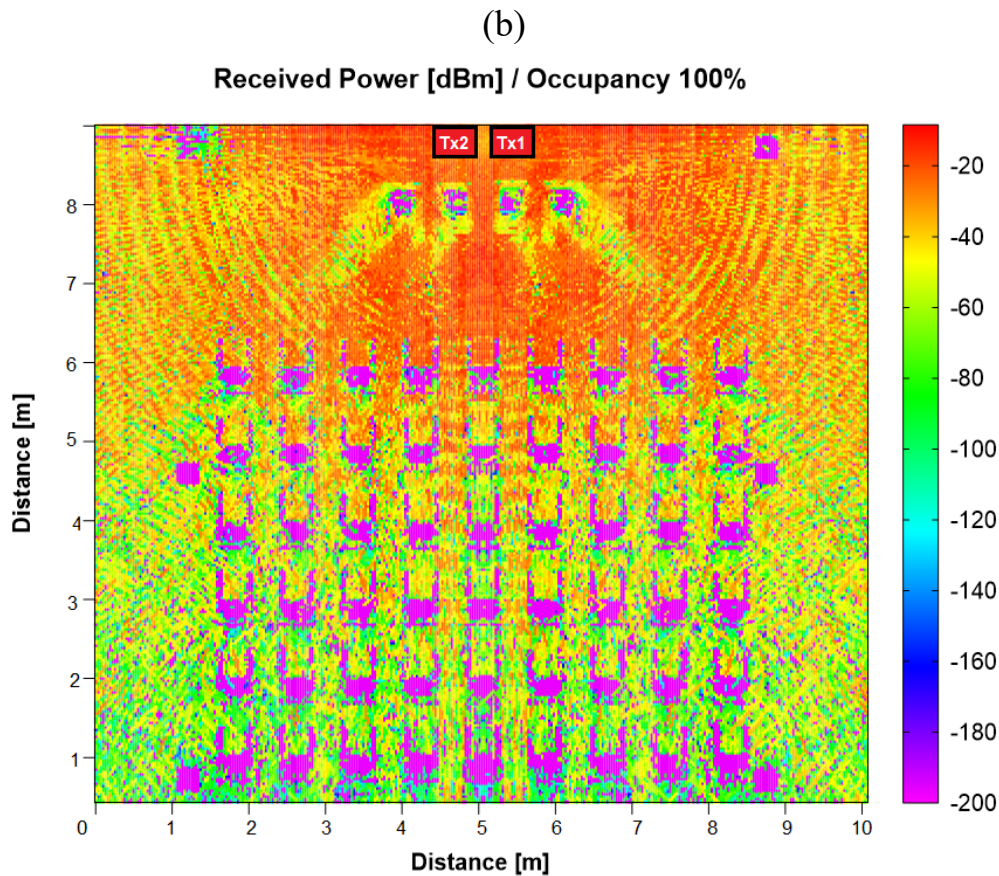
These estimations correspond to the combined RF power distribution radiated from two transmitter antennas located at a height of 2m in the simulated model. This position height matches the possible location for an indoor wireless transmitter or repeater such as a 5G femtocell equipment.

The Tx antennas are represented by red rectangles (Tx).



(a)





(c)

Figure 5.13 Bi-dimensional received power distribution at 0.78m height plane for (a) 0% human occupancy, (b) 50% human occupancy, (c) 100% human occupancy.

From Figure 5.13, we observe a clear graphic disturbance in the form of power distribution/levels modification as human bodies presence increase, in the 3 different use cases simulated.

In the interest of having a deeper understanding of human scattering influence, for example in power level received across the whole environment; we select a random but strategic and representative attendee location in the Conference Room. The location selected is the Point A, located at (5.8, 2, 0.78) coordinates, see Figure 5.14.

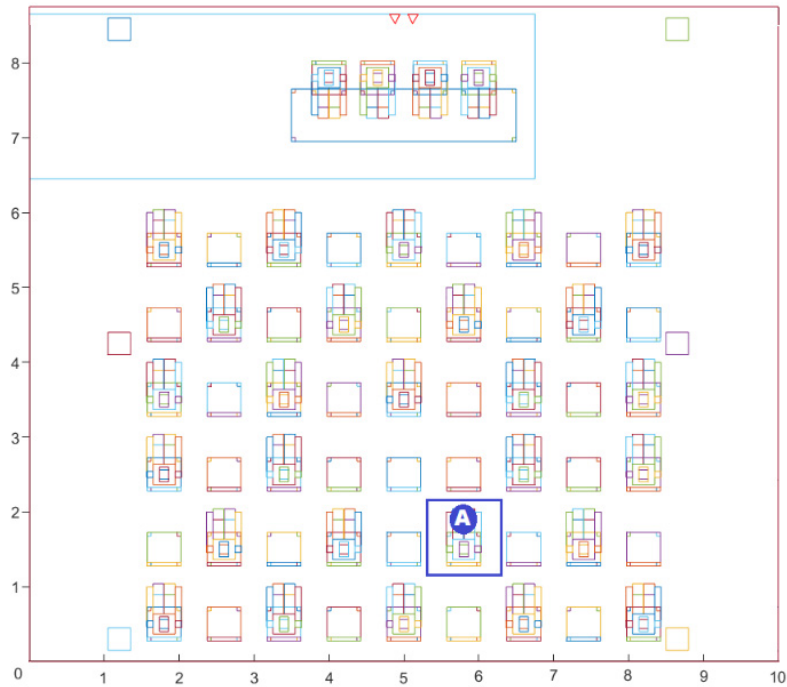


Figure 5.14 Schematic plant view of UE location at Point A (5.8, 2, 0.78) using use case of 50% human occupancy.

Received power levels at Point A for the 3 use cases, obtained by means of the 3D RL Simulations can be seen in Table 5.5.

Table 5.5 RF power estimations for 3 use cases at observation point A.

| RF Power [dBm] | 0% | 50% | 100% |
|----------------|--------|--------|--------|
| Tx1 | -45,96 | -54,78 | -62,11 |
| Tx2 | -46,96 | -58,57 | -64,30 |
| Total | -43,42 | -53,36 | -60,06 |

From these simulations results, we can observe an important decrease in total power levels received at Point A as quantity of person inside the scenario raises. There is a remarkable loss of around 10 dBm with 50% occupancy, another 6 dBm lost when Conference Room is complete comparing with 50% and a total of 16 dBm of loss between 100% occupancy over empty place.

In order to do a deeper clarification of human body scattering, and its impact on power levels received, let's state that scattering effect occurs when RF signal encounters some type of uneven surface and is reflected into multiple directions. The main signal dissipates into multiple reflected signals, causing substantial signal downgrade and may cause loss of received signal. It is evident, by the results shown in Table 5.5, that human bodies cause absorption but also scattering of the signal energy due to the morphology of the body itself.

One manner to model and verify this scattering could be to subtract from the RF power received with 0% and the ones obtained at 50% and 100% occupancy. From Table 5.6, It can be seen that the results of this operation prove that signal power degradation with 50% and 100% of occupancy are significant enough then the subtraction does not affect in a greatly manner the resulting power level estimation.

Table 5.6 RF power levels at observation point A subtracting 50% and 100% occupancy over 0% power received.

| RF Power 0% | Subtraction with | |
|-------------|------------------|--------|
| | 50% | 100% |
| -43,42 | -43,88 | -43,51 |

Moreover, Figure 5.15 shows received power level evolution as function of distance from transmitter for the complete Conference Room length in the 3 use cases.

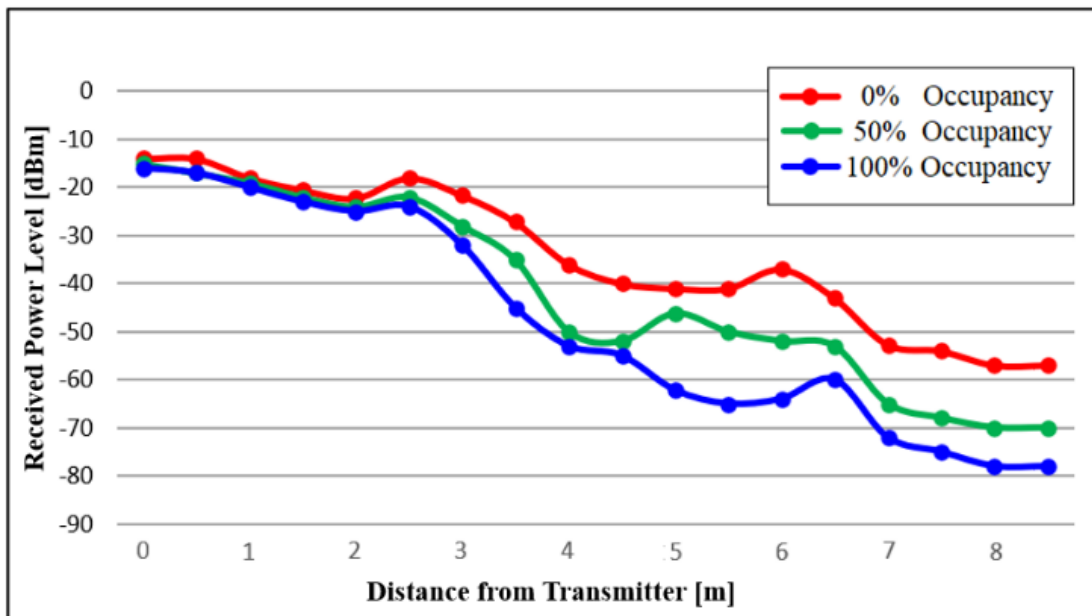


Figure 5.15 Received power evolution at 0.78m height plane as function of distance from Transmitter.

In Figure 5.15 we can identify a similar RF power curve trend till the meter 2.5 from transmitter for the 3 cases, at that moment power strength is mainly affected by the distance travelled in the propagation. After this point, the signal power for the 3 use cases begins to be affected by the presence of scatterers.

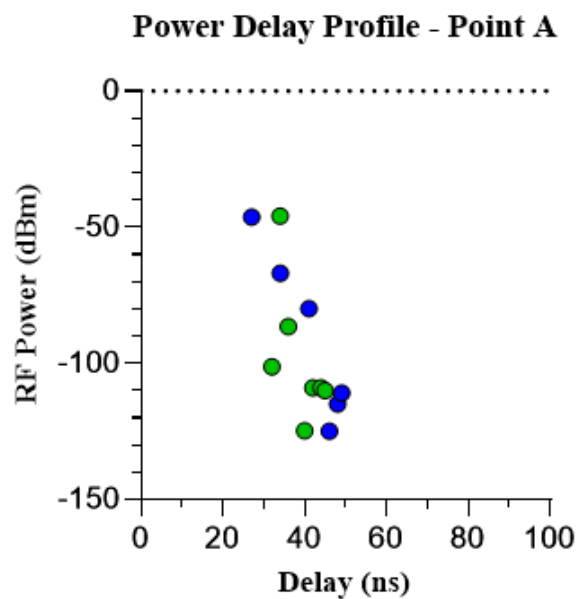
When the Conference Room has 0% occupancy, the signal is only affected by wood chairs, so, we notice a smoother curve trend change. After around meter 2.5 of distance from the transmitter, the signals for the use cases of 50% and 100% occupancy start to face scattering and signal energy absorption caused by human bodies, and the power decays faster keeping a similar trend between both of them.

5.2.2.2 Time Domain Characterization

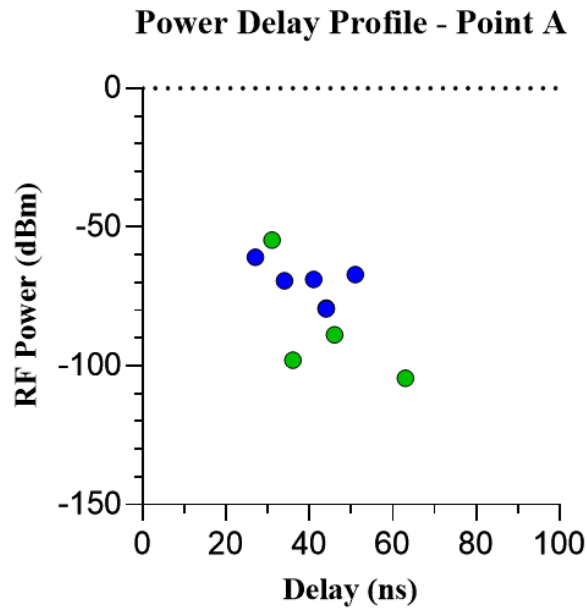
Time domain characterization in terms of Power Delay Profile (PDP) and Delay Spread have also been obtained. In Figure 5.16, the PDP estimation for the location of the UE previously mentioned is depicted.

This includes the time of arrival (τ) and power of each multipath component (rays) spread in the simulation. These characteristics of multipath components are completely dependent on physical channel composition, transmitted power and frequency simulated, spatial position of transmitter and observed cuboid under analysis.

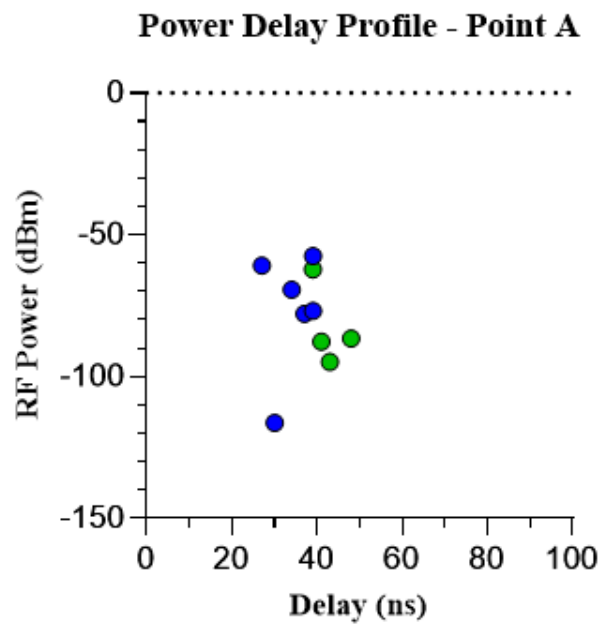
The graphical view of these rays arriving to point A, including their RF power, for the three cases under study, is a great tool to understand how the total signal is affected. This is, if delay spread is much marked between signal elements arriving, multipath interference could arise.



(a)



(b)



(c)

Figure 5.16 Power Delay Profile at Point A for (a) 0% human occupancy, (b) 50% human occupancy, (c) 100% human occupancy. Green bullets representing multipath components from Tx1 and blue bullets from Tx2.

As we can see from Figure 5.16, PDP shows less multipath components arriving at Point A for use cases of 50% and 100% comparing to 0% occupancy. This result is due to the number of scatters and their absorption effect in each use cases and, in lesser extent, to the limitation of 7 reflection events set in the simulation procedure to save computing time.

Additional to a different quantity of rays arriving in each cuboid, we also observe that in the presence of human scattering the delay spread is more noticeable, this is due to the more distance travelled by rays interacting with scatterers and the dielectric properties and shape of human bodies.

In the context of MIMO systems, a space-time multiplexing technique will take advantage of the multipath richness, where each signal transmitted from each different antenna, have the chance to suffer less or different fading in the travel to the receiver. A great measure of multipath richness is the correlation between the signals received from the two transmit antennas.

Using the time domain characterization results depicted in Figure 5.16 for the 3 use cases studied, the correlation coefficient ρ can be obtained by using (5.2),

$$\rho_{xy} = \frac{\sum_{i=1}^n (x_i - \bar{x})(y_i - \bar{y})}{\sqrt{\sum_{i=1}^n (x_i - \bar{x})^2} \sqrt{\sum_{i=1}^n (y_i - \bar{y})^2}} \quad (5.2)$$

where n is the samples size, x_i , y_i are the individual sample point of multipath components indexed i , and \bar{x} , \bar{y} are the samples mean.

Table 5.7 Correlation coefficient for three use cases at observation point A

| | 0% | 50% | 100% |
|--------------------------------|------|------|------|
| Correlation Coefficient ρ | 0,61 | 0,49 | 0,42 |

We can find correlation coefficients for the 3 use cases under test in Table 5.7. From this data is clearly noticed that as complex indoor scenario change, modifying for example the human scatterers distribution and quantity, there is better uncorrelation between the signals arrived from the two transmit antennas.

5.2.2.3 Space-Time Diversity Evaluation

Space-Time coding approaches take advantage of the multipath interference for improving the data rate and/or the reliability of communications over fading channels [16]. The performance of a MIMO system is dependent on the characteristics of the radio environment, given by the values of an $M \times N$ radio channel matrix, *H-matrix*.

For this evaluation, we will assume the location of a UE at Point A with two received antennas spaced by 2λ , which is feasible for current Tablet devices designed within the 3,7 GHz operation frequency.

Using the complete volumetric results provided by the 3D RL algorithm in the 3 use cases under analysis, we have the received power level for each transmit-receiver link as response of *H-matrix*, see Table 5.8.

Table 5.8 RF power estimations as channel response of *H-matrix* for 3 use cases

| Channel Path | 0% | 50% | 100% |
|--------------|-------------|-------------|-------------|
| | Power [dBm] | Power [dBm] | Power [dBm] |
| h_{11} | -45,19 | -56,37 | -63,67 |
| h_{12} | -45,87 | -54,81 | -62,18 |
| h_{21} | -49,25 | -59,43 | -68,91 |
| h_{22} | -47,82 | -58,97 | -69,39 |

In order to evaluate space-time diversity performance in the 3 use cases, we will estimate BER values between a configuration of 2 transmit antennas and 2 received antennas. The evaluation has been performed considering AWGN (Additive White Gaussian Noise Channel) and assuming the channel being Narrowband Time-Invariant, employing an orthogonal space-time block code transmission and using the previous PDP estimations depicted in Figure 5.16 and received power levels presented in Table 5.8.

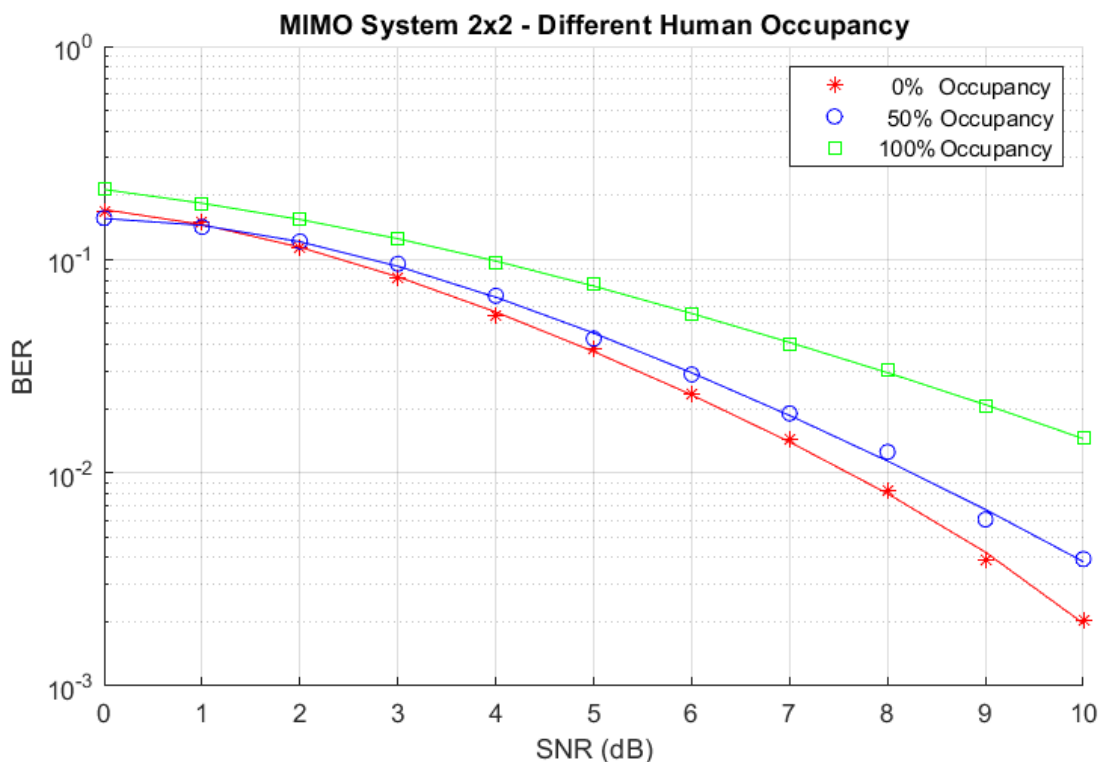


Figure 5.17 BER performance as function of SNR for MIMO system 2x2 in different human scattering scenarios.

We can observe from Figure 5.17 that the channel response with OSTBC encoding multiplexing for the 3 use cases, shows an improvement in BER values as SNR increases, this is due to the multipath channel characteristic and the effect of scatterers over the signal. It is important to highlight that 0% of human presence or occupancy has 3 dB enhancement over 100% occupancy as SNR grows. This result is mainly caused by the influence of human scattering and absorption effect as we concluded before analyzing the power levels results.

5.2.3 Results and Application

The EM waves propagation mechanisms and the corresponding interactions of the RF signal with the objects or scatterers inside the environment, are fundamental variables in the wireless channel characterization. Another phenomenon involved and related to these mechanisms is the absorption, which is more relevant in the presence of human bodies in the scenario. This due to the physical properties of human skin and body.

The MIMO performance analysis accomplished in this work was done by means of the implementation of a complex indoor scenario with the 3D RL tool described in early chapters. The wireless channel characterization was obtained in terms of power level distribution, Power Delay Profiles and Delay Spread. Furthermore, another important parameter in the sphere of multipath transmission such as correlation coefficient, has been also estimated.

Regarding to this, a variety of human occupancy of 0%, 50% and 100% have been studied for a MIMO system operating at 3,7 GHz. Results show that 0% of human occupancy has 3 dB enhancement over 100% occupancy when analyzing BER values. Besides, it was also observed an important decrease in total power levels received. There is a loss of around 10 dBm when 50% occupancy, another 6 dBm loss when premise is complete compering with 50% and a total of 16 dBm of loss between 100% occupancy over empty place.

The complete analysis developed in this work with aid of the 3D RL algorithms, can be useful for wireless coverage planification and throughput capacity forecast in bigger and complex indoor environments that will be mainly characterized by human presence, for example cinema, malls, offices, and so.

5.3 Phase Evolution Impact in Receive Diversity Applications

The advent of Internet of Things is foreseen to be given by the potentially massive deployment of multiple types of compact motes, with embedded wireless communication capabilities.

One of the future requirements is to provide low latency, provided by functionalities such as ultra-reliable low latency communications (uRLLC) within 5G communication systems. This can be the case for example in industrial environments, for tele-control and tele-command of different systems. In the case where moderate transmission bit rates are employed, massive Single Input Multiple Output (SIMO) systems exhibit more optimal performance for example in the detection of Channel State Information, especially for cases with low SNR and high mobility [59].

Energy based amplitude modulation approaches have been proposed in order to implement non-coherent massive SIMO communication schemes, applicable in conditions with large amount of devices, with cost, size and energy restrictions [60-61]. Channel estimation within SIMO systems is relevant, as the consideration of non-ideal effects, such as fading components or the impact of interference lead to an increase in general system noise levels [62]. Moreover, wireless channel analysis can also aid in foreseeing potential jamming attacks to SIMO systems, particularly in initial channel training phases [63].

In this work, the analysis of SIMO system operation in high node density indoor scenarios, where rich multipath effects are given, is presented.

Deterministic wireless channel estimation is performed by means of in-house 3D Ray Launching (3D RL) code, obtaining volumetric received power level distributions, as well as time domain characterization.

Received phase distributions as a function of cuboid distributions are obtained, which are then employed in order to analyse impact on $1 \times N$ SIMO channel performance, as a function of potential receiver locations.

5.3.1 Scenario Description

As the previously presented two use cases, a third complex indoor scenario is built using the coded functions included in the 3D RL tool based in cuboids. Using this tool, wireless channel characterization is obtained by means of simulation iterations and calculations are accomplished to estimate received power levels, power delay profiles and E field in each cuboid for the complete volume of scenario.

In order to perform the required wireless system analysis, volumetric phase variation behavior is obtained by processing received power levels and time domain characterization from the implemented indoor scenario model.

The scenario under analysis is a small *Meeting Room* with dimensions 3.2m L x 6.3m W x 3.1m H located within Los Tejos building of the Universidad Pública de Navarra. The 3D model of the scenario has been created for the 3D-RL simulations, see Figure 5.18.

The scenario consists of a single wooden table, different types of walls and two columns sticking out of the wall. The transmitter has been placed on the table (represented by a red circle).

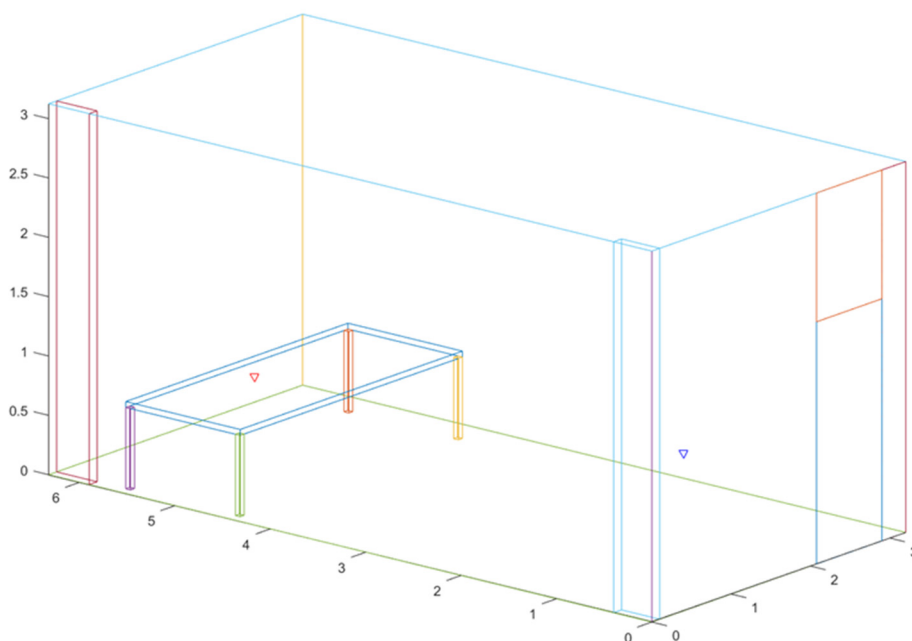


Figure 5.18 Meeting room scenario model created by the 3D-RL tool.

In order to obtain accurate RF power distribution results, real material properties have been considered: concrete columns and ceiling, wooden table, brick floor, plasterboard walls and a single glass wall (the one in front of the door). Another parameters are needed to execute the simulations and the summary of these is shown in Table 5.9.

Table 5.9 Simulations parameters.

| Parameter | Value |
|-------------------------------|-----------------|
| Operation frequency | 2,4 GHz |
| Output RF power level | 0 dBm |
| Cuboid resolution | 3cm × 3cm × 3cm |
| Permitted maximum reflections | 6 |
| Launched rays resolution | 1° |
| Antenna type and gain | Monopole, 0 dBi |

In this work, the frequency band of 2,4 GHz has been selected to do the simulations because is an ISM band implemented in use cases like industrial, scientific, and medical applications.

The analysis results can be relevant, for example, in deployments of Internet of Things (IoT) and Industrial Internet of Things (IIoT). The IIoT is a concept that involves incorporating smart objects, gadgets, and solutions into cutting-edge industrial operations to increase reliability, efficiency, and over-production costs [64].

A relevant technology that operates at 2,4 GHz is Zigbee, a protocol in the sphere of IoT and IIoT. Zigbee is a set of communication protocols between devices especially designed for IoT application. It is focused on applications that require secure communications with low data rate and maximizing the service life of its batteries. The domotic, home automation applications, medical sensors, toys are the areas in which this technology is stronger.

5.3.2 System Performance Analysis

5.3.2.1 Wireless Channel Characterization

The 3D-RL simulator provides results for the whole volume of the scenario. Results are obtained for the complete scenario volume and are later particularized to specific height planes to simplify result evaluation. As an example, Figure 5.19 shows a bi-dimensional plane of the estimated RF power distribution at the same height of the transmitter antenna (i.e., 0.85m).

The transmitter position is represented by a red rectangle (Tx) and a potential receiver location by a blue rectangle (Rx). The chosen operation frequency band of 2.4 GHz can emulate multiple systems (e.g., 802.11, 802.15/802.15.4, etc.) operating within the scenario.

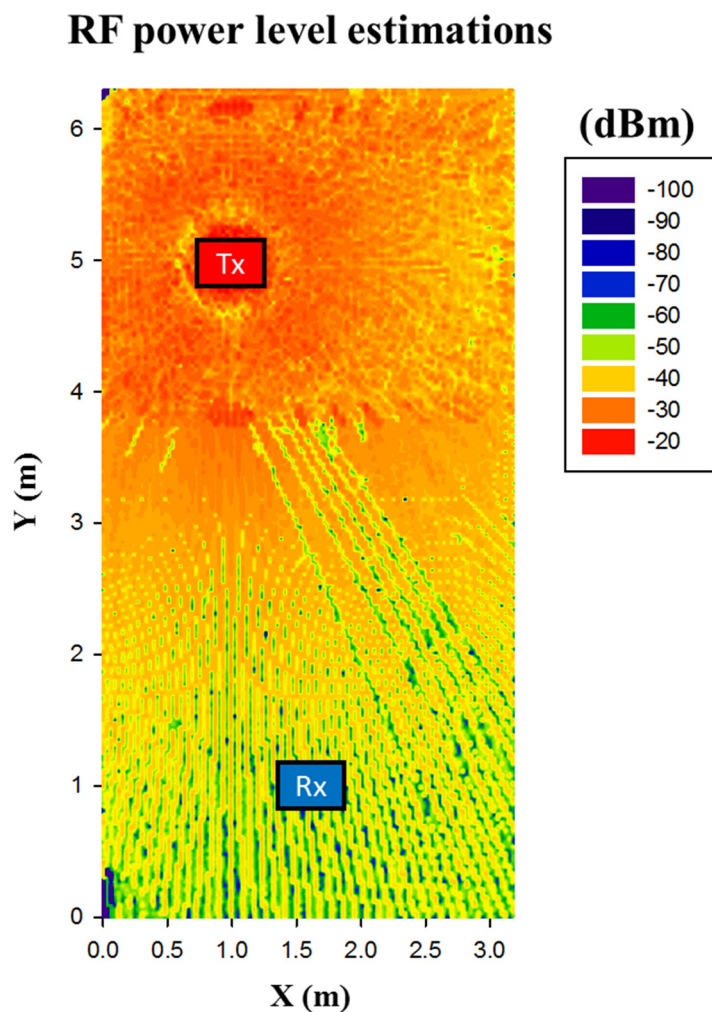


Figure 5.19 Received RF power level at the height plane of 0.85m.

Time domain characterization in terms of power delay profiles as well as delay spread are also obtained. An example for the specific receiver location selected within the scenario is depicted in Figure 5.20.

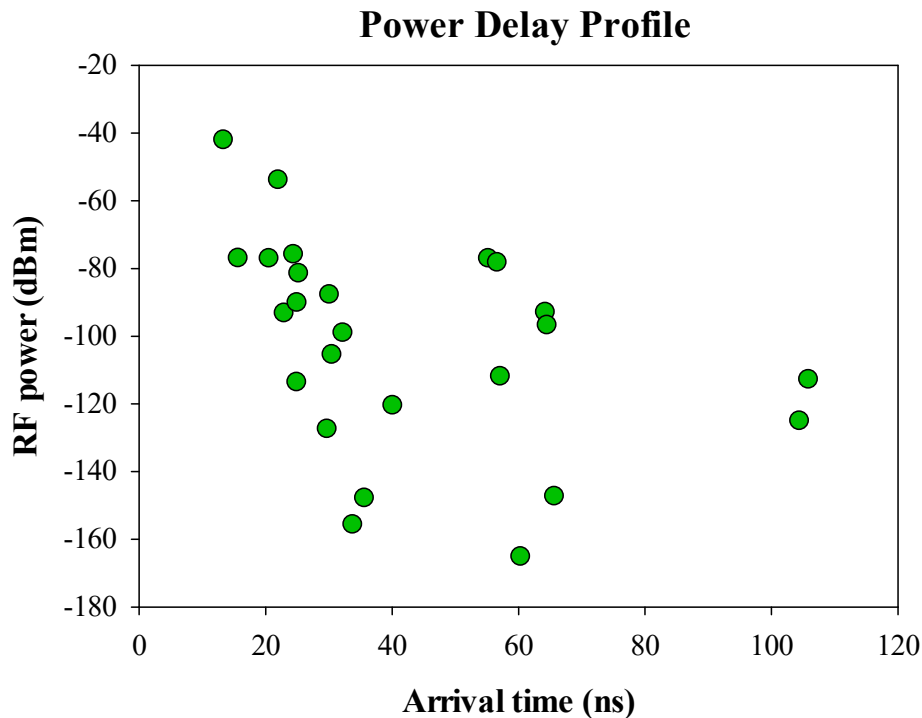


Figure 5.20 Power Delay Profile at the Rx position.

5.3.2.2 Phase Evolution Analysis

Using the 3D Ray Launching Algorithm, we obtain the Power Delay Profile (PDP) of the composite signal arriving to the cuboids composing the scenario. This includes the time of arrival (τ) and power of each Multipath Component (Ray) spread in the simulation. These characteristics of Multipath Components are completely dependent of physical channel composition, transmitted power and frequency simulated, and spatial position of transmitter and cuboid under analysis.

To estimate the phase of arrival of the composite signal, we initially calculate the phase of each multipath component to be vectorially summed and obtain the composite power and phase.

We use the angular speed (ω) of the signals and the arrival times (τ), to obtain the phases: $\beta = \omega * (\tau - t_0)$. We assume that t_0 is the initial time of simulation, so in this case $t_0 = 0$. The formula to calculate the phases is,

$$\beta = 2\pi f\tau \quad (5.3)$$

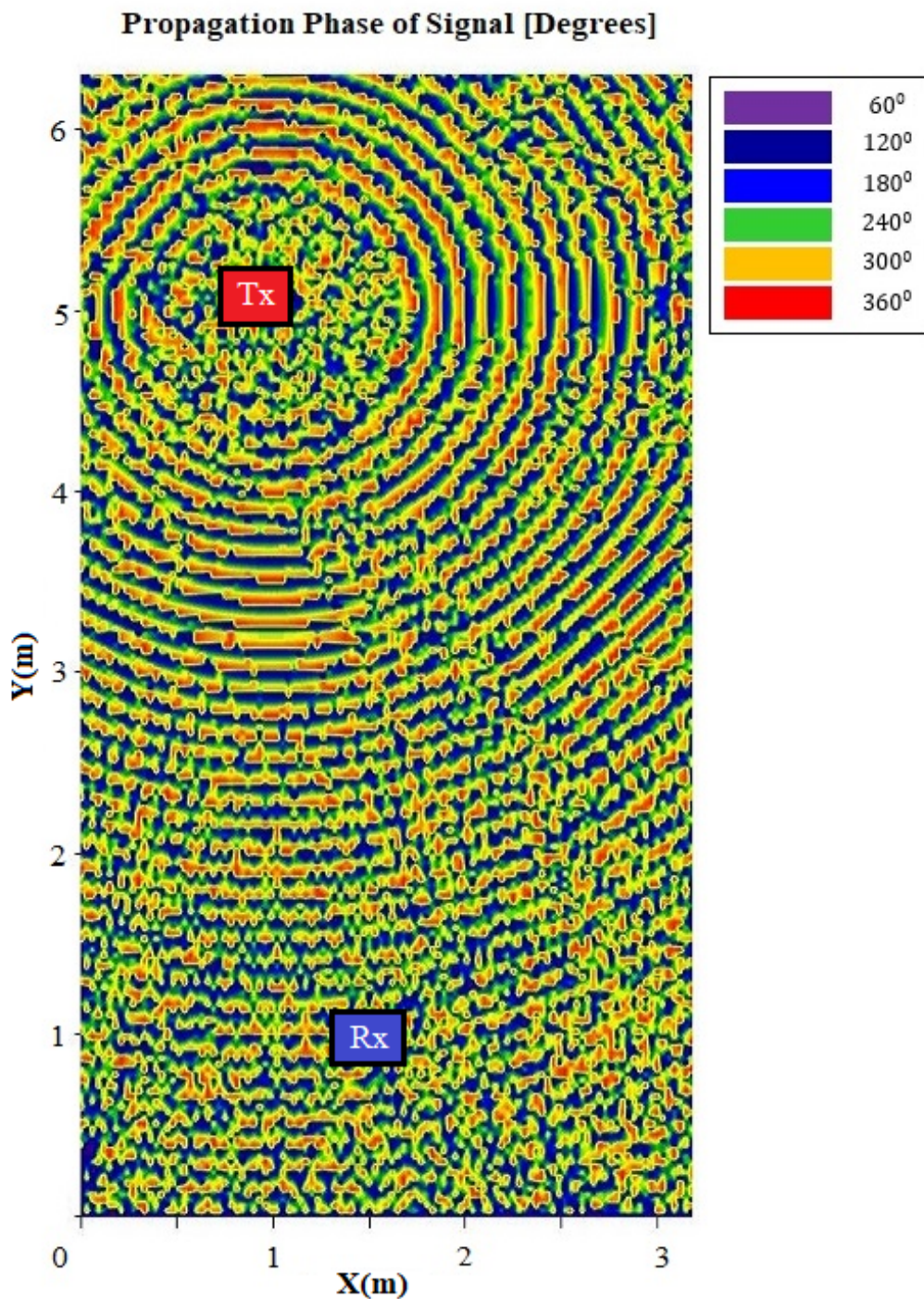


Figure 5.21 Bi-dimensional phase estimation of spread signal at 0.85m height plane in the simulation scenario.

The result is the total signal phase excursion in the path during interval τ . Figure 5.21 shows the estimated propagation phases of signals traveling from transmit antenna to the entire scenario. The expected phase/counter phase evolution derived from free space propagation is enriched with multiple zones with specific phase evolutions, derived from multipath, given by the multiple scattered components within the scenario.

As an example, we choose a specific area of interest (e.g., a hot spot with higher phase evolution) to analyse in detail the arriving phases. As explained before, we use the PDP to estimate the arrival phase of the composite signal at any cuboid. We select the point (1.6m, 1m, 0.85m) to be consider the central position to locate two receive antennas separated a distance of 2λ , as it has been proved to be an optimal setting. The area of interest will be $3\lambda \times 3\lambda$ of dimension to estimate receiver antenna location.

A detailed *zoom in* of the zone under analysis is given in Figure 5.22, in which the phase evolution is presented.

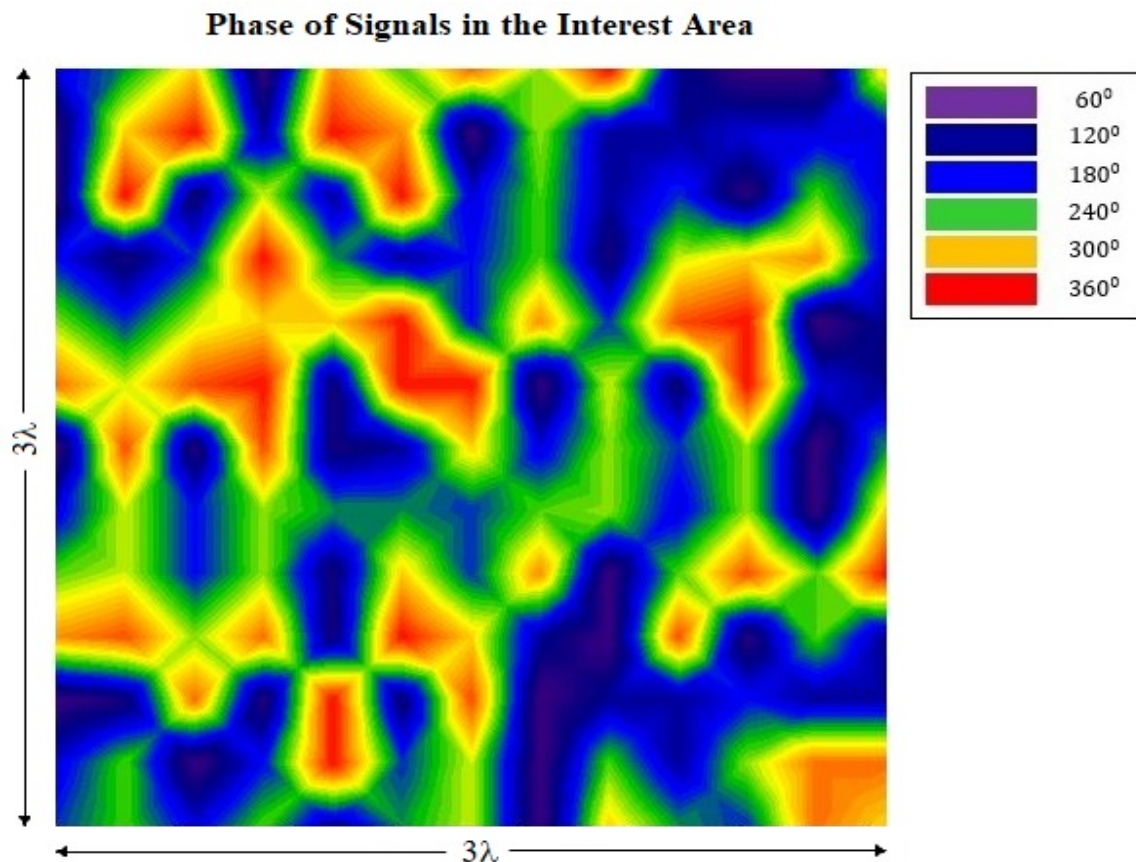


Figure 5.22 *Zoom In* at interest area of square 3λ located at the point (1.6m, 1m, 0.85m) showing the arrival phases of Composite Signals.

Additional, in Figure 5.23 a zoned diagram of average phase values is presented. Each one of the blocks corresponds to the 2D projection of the cuboids, of resolution 3cm (i.e., the delimited region is given by a tessellation of 13*13 average phase values).

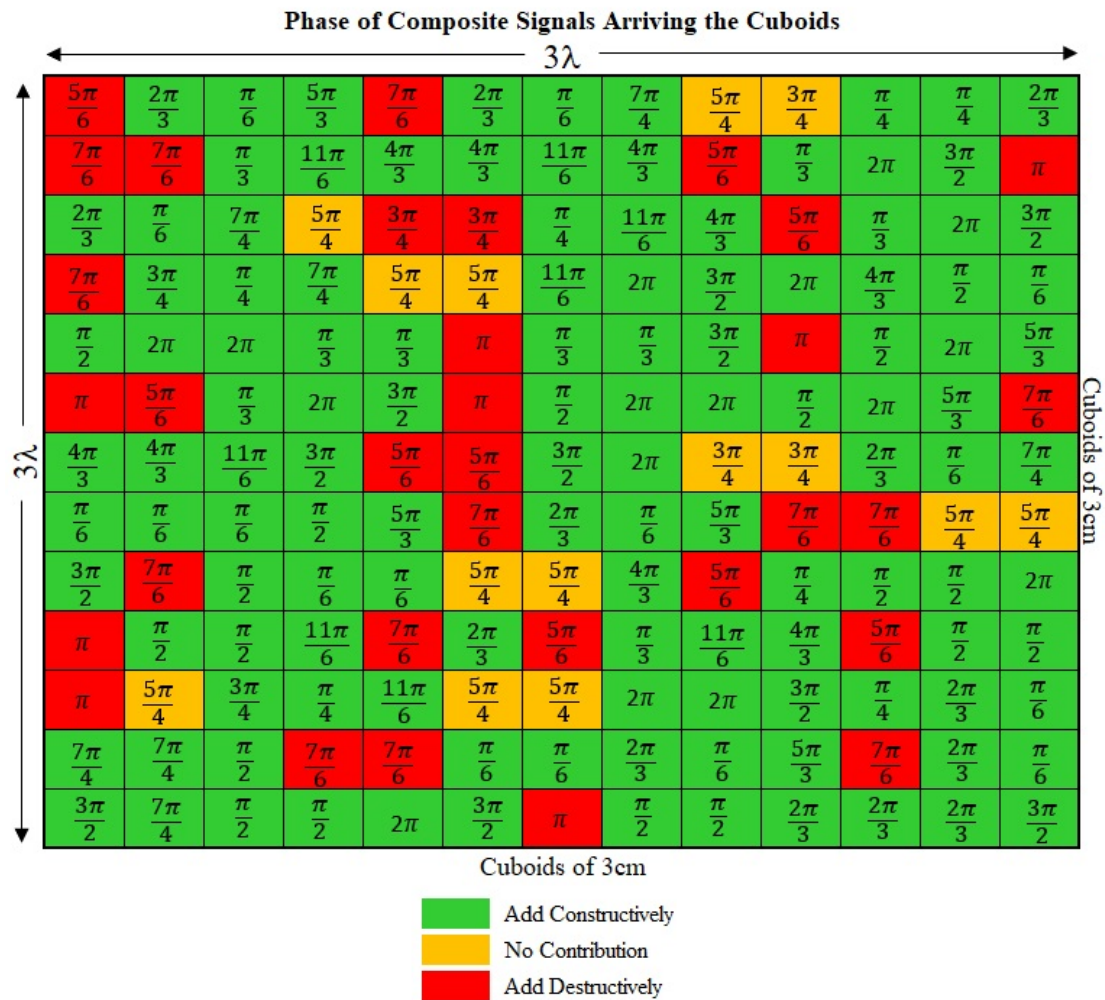


Figure 5.23 Zoom In at interest area of square 3λ located at the point (1.6m, 1m, 0.85m) showing average phase distribution per pixels.

As it can be seen, the samples taken in the area of interest exhibit a strong correlation between adjacent signals. We can differentiate a pattern where signals with pretty close phases are beside to each other in most cases.

This correlation is given by the use of 1 transmitter within the SIMO approach followed in the simulation scenario. Additive phase, counter phase and no-phase interaction are highlighted, in order to provide qualitative assessment in relation with phase distribution and the initial impact in received power levels, indicating zones with higher fading levels.

5.3.2.3 Spatial Receive Diversity Evaluation

In order to analyze spatial receive-diversity, we will evaluate the BER measurement between a configuration of 1 Tx – 1 Rx antenna (SISO channel), 1 Tx – 2 Rx and 1 Tx – 4 Rx antennas (SIMO channels).

The evaluation has been performed considering Additive White Gaussian Noise channel and assuming the channel being Narrowband Time-Invariant. As a potential case, the distributed RX configuration (RX1 at cuboid location (3,7) and RX2 at cuboid location (11,7) from the phase distribution depicted in Figure 5.23.

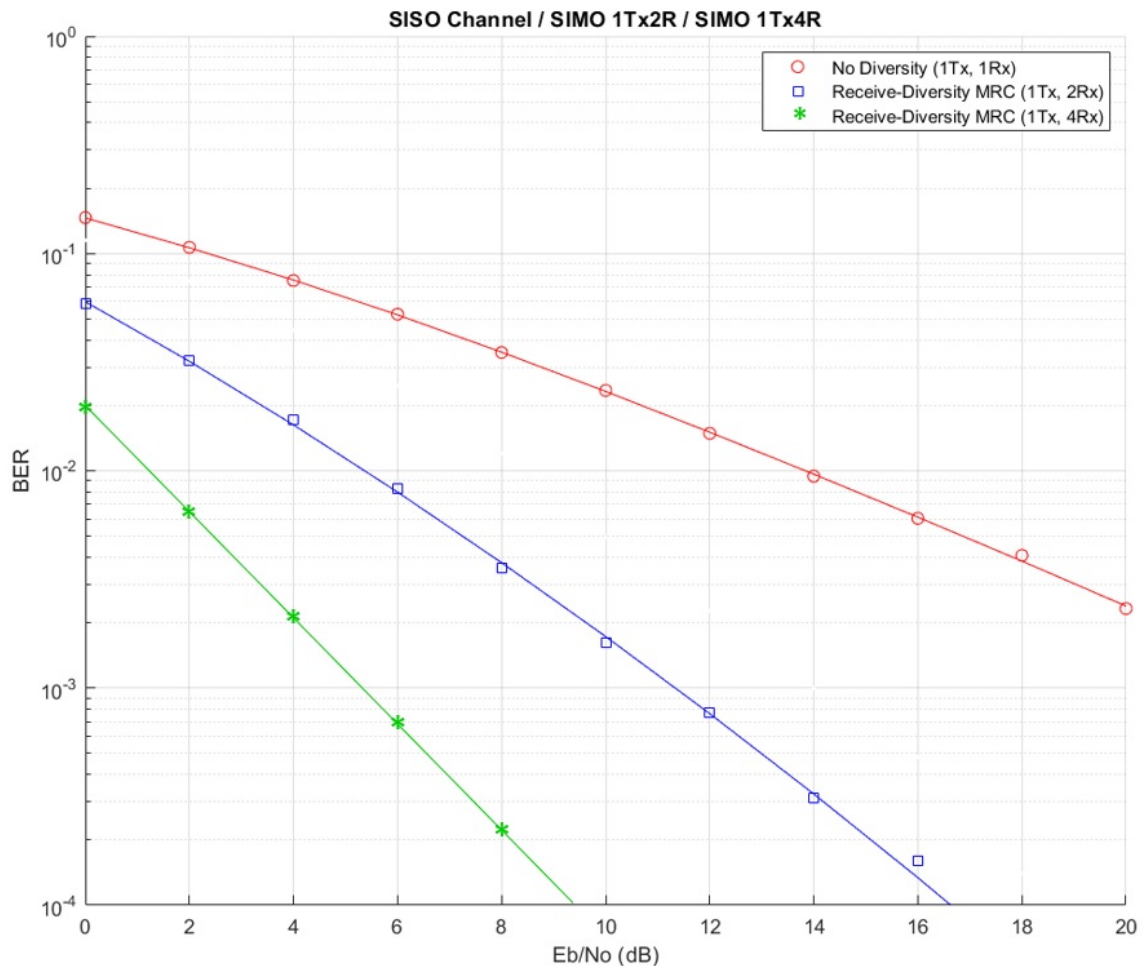


Figure 5.24 BER performance as a function of E_b/N_0 for Receive-Diversity and SISO/SIMO channels.

Figure 5.24 shows that receive-diversity (1 Tx – 2 Rx) exhibits improved performance in terms of quality of service. We can see that as the E_b/N_0 is increased, the BER measurement improves as expected in the SIMO channel, in direct relation with the phase excursion behavior. The analysis has been extended to the case of SIMO 1×4 , increasing the initial phase analysis area, providing an enhancement in the order of 7 dB in E_b/N_0 performance as compared with SIMO 1×2 .

5.3.3 Results and Application

In this work, deterministic 3D Ray Launching methodology has been employed in order to perform wireless channel estimation towards system level analysis of potential transceiver operating under a SIMO communication scheme.

Volumetric received power level estimations and time domain characterization from power delay profiles are processed in order to obtain phase variation profiles within the scenario under analysis.

These variations are employed in order to perform $1 \times N$ SIMO channel analysis, in order to assess in the impact on the location of potential receiver locations within the complete volume of the scenario.

The proposed methodology can assist in the network planning and design phases, given the inherent complexity in power and phase distributions, owing to relevant effects such as multipath propagation.

Future results will explore the integration of potential receiver configurations within different material elements and the extension of the employed models to consider different strategies for phase averaging and channel correlation.

Chapter 6

Conclusions and Future Work

WHIT the complete exploration of the wireless technologies accomplished during this whole doctoral thesis, and putting in evidence its importance in everyday life, after performing a series of analysis on the wireless channel and MIMO systems context, we finally arrived to the last chapter of the work. We present here the summarization of the most relevant results and conclusions found during the realization of this thesis. Firstly, in section 6.1 all the results and conclusions are listed, and then the verification of the fulfilment of the objectives delineated in Chapter 1 can be performed. Finally, section 6.2 lists future research lines derived and related to the thesis.

6.1 Conclusions

As stated in different chapters of the present document, this doctoral thesis was mainly motivated by the continuous growth of wireless networks technology and the inherent need for avant-garde techniques in this field. The most representative example is the appearance and development of 5G networks, for this reason the results of the research activity on this thesis was mostly focused in order to be applied in this standard. 5G is the result of the demand of more reliable, fast, and extended coverage mobile network. 5G is revolutionizing the way we communicate between people, between people and machines, and of course machine to machine. This is because 5G has capabilities that former technology does not have.

As already mentioned, 5G networks has three main application that are now possible: eMBB, uRLLC and mMTC. This thesis has three main study cases that can be useful in these three applications of 5G network.

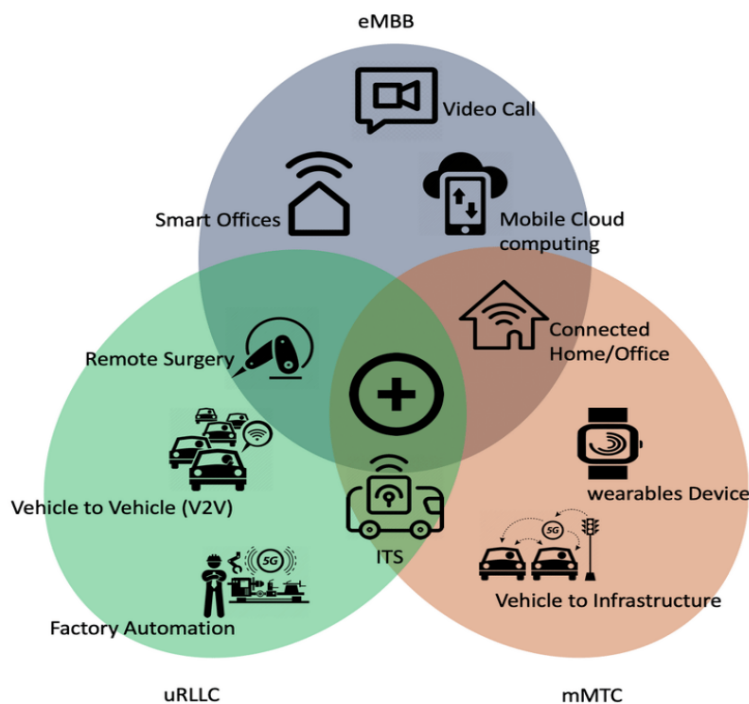


Figure 6.1 Three main use cases for 5G and examples of applications.

eMBB is the use of 5G as a progression from 4G LTE mobile broadband services, with faster connections, higher throughput, and more capacity. This will benefit areas of higher traffic such as stadiums, cities, and concert venues. Additional to the need of higher throughput and capacity for dense presence of people, the wireless channel will be greatly influenced by the effect of human bodies in the signal propagation, for this reason this effect was studied in this thesis.

uRLLC refer to using the network for mission critical applications that require uninterrupted and robust data exchange. The short-packet data transmission is used to meet both reliability and latency requirements of the wireless communication networks.

Finally, mMTC, would be used to connect to a large number of devices. 5G technology will connect some of the billion connected IoT devices, most will use the less expensive Wi-Fi. Drones, transmitting via 4G or 5G, will aid in disaster recovery efforts, providing real-time data for emergency responders, among other examples.

In the context of uRLLC and mMTC, key aspects such as antenna spacing, and phase evolution are relevant for the design and planning of communications systems to be deployed in these applications of 5G. For this reason, these aspects are also studied in this doctoral thesis.

All the applications depicted in Figures 6.1 has an evident importance in humankind, and all of them have the same in common, as implementations of wireless networks; the best RF planification is required, throughput and capacity prediction, and coverage estimation are also highly important parameters to achieve for the success of this deployments.

In this regard, wireless channel characterization and MIMO performance analysis of systems are of great importance and are the core objectives of this thesis. To achieve this work, the in-house developed 3D ray launching algorithm was employed in three specific complex indoor scenarios. Study cases of great relevance for different implementations such as 5G, WiFi 6, Zigbee, and so on.

The conclusions obtained from these three study cases after completing several simulation iterations and the corresponding analysis are now presented. Furthermore, the conclusion and results of this doctoral thesis, guided by the objectives defined in Chapter 1, are also listed in the following points:

- A complete assessment of wireless technologies currently in exploitation has been conducted, along with a study of state of the art about MIMO and space-time coding. After this: We conclude these activities validated the relevance of this kind of thesis and research activities.
- Another conclusion derives from the utilization of the in-house developed 3D ray launching tool for radio propagation analysis within three different environments, all of them being performed in complex indoor scenarios: The simulation methodology has been validated to be applicable to antenna spacing studies, human scattering influence analysis and evaluation of signal phase behaviour, providing a good trade-off between the accuracy of the data results (i.e. power level distribution, power delay profiles, etc.) and the computational time and resources needed.
- Complex indoor scenario, and more specifically a conference room, under test has been implemented and tested by means of an in-house developed 3D RL code. Different results have been obtained in terms of frequency dependent received power levels as well as time domain characteristics. Variations in the antenna spacing of a 2x2 MIMO system have been studied for a system operating at 5G NR FR1 compatible frequency of 3,7 GHz: We conclude that results show that as spacing is increased from 1λ to 3λ , there is an observable gain in the received power levels, which in turn are dependent on the specific configuration of the surrounding environment in terms of scattering distribution.

- Derived from the simulation results and analysis accomplished with varying antenna spacing. We validated this scenario and methodology by means of measurement campaign carried out with a VCO and a portable spectrum analyser: We can conclude that results obtained shows a similar trend compering to simulations in relation with observable gain as antenna spacing is increased from 1λ to 3λ .
- MIMO performance analysis has been accomplished by means of the implementation of a complex indoor scenario with the 3D RL tool, the scenario simulated is a conference room with a plenary layout. The wireless channel characterization was obtained in terms of power level distribution, power delay profiles and delay spread. In this context, a variety of human occupancy of 0%, 50% and 100% have been studied for a MIMO system operating at 3,7 GHz: We conclude that results show that 0% of human occupancy has 3 dB enhancement over 100% occupancy when analyzing BER values. Besides, it was also observed an important decrease in total power levels received; there is a loss of around 10 dBm when 50% occupancy, another 6 dBm lost when premise is complete compering with 50% and a total of 16 dBm of loss between 100% occupancy over empty place.
- Deterministic 3D Ray Launching methodology has been employed to perform wireless channel estimation towards system level analysis of potential transceiver operating under a SIMO communication scheme. Volumetric received power level estimations and time domain characterization from power delay profiles were processed in order to obtain phase variation profiles within the scenario under analysis. These variations were employed with the aim to perform $1\times N$ SIMO channel analysis, in order to assess the impact of potential receiver locations within the complete volume of the scenario. We conclude that the proposed methodology can assist in the network planning and design phases, given the inherent complexity in power and phase distributions, owing to relevant effects such as multipath propagation.

The complete analysis developed, the results, and conclusions obtained in this thesis with aid of the 3D RL algorithms, can be useful for the building of designing and planification tools that will improve the methods for wireless coverage planification, throughput and capacity forecast in bigger and complex indoor environments.

The summary of the process leaded to achieve this thesis is schematically depicted in Figure 6.2.

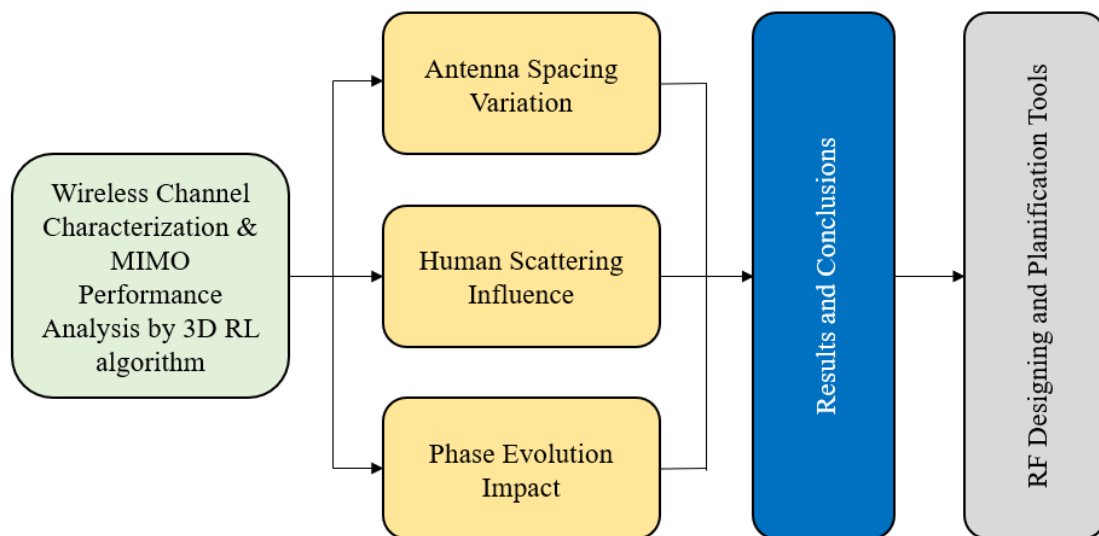


Figure 6.2 Summary of the work presented in this thesis.

Having into account the results and conclusions presented in this document, which are supported by its presentation and publication in international conferences such as EuCAP, where said works have been technically reviewed; We can state that the objectives of this doctoral thesis have been fulfilled satisfactorily.

6.2 Future Work

The thesis developed and the research activities accomplished leads to different lines. There are some potential lines of work to continue offering data and results for improving the radio planning task:

- Wireless channel characterization and MIMO performance analysis can be accomplished in different and bigger environments such as stadiums, cinemas, malls utilizing same RF parameters including 5G NR FR1 frequency band and same simulation characteristics. This can be helpful, for instance, in the definition of femtocell locations.
- With the help of the 3D ray launch algorithm, antenna spacing effect on the performance of wireless systems can be accomplished in others interesting frequency band such as 5 GHz. The results obtained in this specific operation frequency can be important for the evaluation and planification in IEEE 802.11ax (WiFi 6) standard.
- In the context of human scattering influence, in the form of RF signal power level distribution, a measurement campaign can be conducted to be used as input for MIMO analysis with electrical values and at the same time perform a general validation of the simulation results.
- Performing a batch of simulations using the 3D RL code, human scattering analysis can be achieved in a complex indoor scenario at 2,4 GHz. These results can be relevant for the deployment of Zigbee application in the context of IIoT where there will be possible dense human presence.
- In the context of distributed transceiver systems, future analysis can explore the integration of potential receiver configurations within different material elements and the extension of the employed models to consider different strategies for phase averaging and channel correlation.

Bibliography

- [1] Jose Maria Hernando R. Transmisión por Radio. 7ma Ed. Madrid, España. Ed. *Universidad Ramón Areces*, 2013.
- [2] ITU. "World Radiocommunication Seminar", Geneva, December 2016.
- [3] Warren L. Stutzman, Gary A. Thiele. Antenna Theory and Design. Third Ed. USA. *Wiley*, 2012.
- [4] William C. Y. Lee, "Mobile Communications. Design Fundamentals" 2nd Edition, *John Wiley & Sons*. 1993.
- [5] Roger L. Freeman. Radio System Design for Telecommunications. Third Edition. New York, USA. *Wiley*, 2007.
- [6] J. Walfisch and H. L. Bertoni, "A theoretical model of UHF propagation in urban environments," *IEEE Transaction on Antennas and Propagation*, vol. 36, nº 12, pp. 1788-1796, 1988.
- [7] J. D. Parsons and J. G. Gardiner, "Mobile communication systems," *Halsted Press*, 1989.
- [8] J. D. Parsons and P. J. D. Parsons, "The mobile radio propagation channel," vol. 81, *Wiley Online Library*, 2000.
- [9] Y. Okumura, E. Ohmori, T. Kawano and K. Fukuda, "Field strength and its variability in VHF and UHF land-mobile radio service," *Rev. Elec. Commun. Lab*, vol. 16, nº 9, pp. 825-873, 1968.
- [10] J. W. Schuster and R. J. Luebbers, "Comparison of GTD and FDTD predictions for UHF radio wave propagation in a simple outdoor urban environment", *IEEE Antennas and Propag. Society International Symposium*, vol. 3, pp. 2022-2025, 1997.

- [11] S. Y. Seidel, T. S. Rappaport, "Site-Specific Propagation Prediction for Wireless In-Building Personal Communication System Design", *IEEE Transactions on Vehicular Technology*, vol. 43, n° 4, pp. 879-891, 1994.
- [12] C. F. Yang, B. C. Wu and C. J. Ko, "A ray-tracing method for modeling indoor wave propagation and penetration," *IEEE Transactions on Antennas and Propagation*, vol. 46, n° 6, pp. 907-919, 1998.
- [13] A. Sibille, "Introduction," in *MIMO From Theory to Implementation*, 1st ed. Burlington, MA, USA: *Academic Press*, 2011, pp. xvii-xxiv.
- [14] J. H. Winters. "On the Capacity of Radio Communication Systems with Diversity in a Rayleigh Fading Environment". *IEEE J. Sel. Areas Comm*, Vol. SAC-5, No. 5, pp. 871-878, Jun. 1987.
- [15] G. J. Foschini. "Layered Space-Time Architecture for Wireless Communication in a Fading Environment When Using Multi-Element Antennas". *Bell Labs Technical Journal*, pp. 41-59, 1996.
- [16] V. Tarokh, N. Seshadri, A. R. Calderbank. "Space-Time Codes for High Data Rate Wireless Communication: Performance Criterion and Code Construction". *IEEE Trans. Inform. Theory*, Vol. 44, No. 2, pp. 744-765, Mar. 1998.
- [17] S. M. Alamouti. "A Simple Transmit Diversity Technique for Wireless Communications". *IEEE J. Sel. Areas Comm*, Vol. 16, No. 8, pp. 1451-1458, Oct. 1998.
- [18] V. Tarokh, H. Jafarkhani, A. R. Calderbank. "Space-Time Block Codes from Orthogonal Designs". *IEEE Trans. Inform. Theory*, Vol. 45, No. 5, pp. 1456-1467, Jul. 1999.
- [19] W. Su, Xi-Gen. Xia, K. J. Ray Liu. "A Systematic Design of High-Rate Complex Orthogonal Space-Time Block Codes". *IEEE Comm. Letters*, Vol. 8, No. 6, pp. 380-382, Jun. 2004.
- [20] J. Joung. "Space-Time Line Code". *IEEE Access*, Vol. 6, pp. 1023-1041, Nov. 2017.

-
- [21] Nelson Costa, Simon Haykin. "Multiple Antenna Channels and Correlation" in *Multiple-Input Multiple-Output Channel Models, Theory and Practice*, 1st ed. Hoboken, NJ, USA: *Wiley*, 2010, pp. 19-53.
- [22] L. Trigueros, P. Lopez-Iturri, L. Azpilicueta, Carlos Del-Río, F. Falcone. "Analysis of MIMO Performance in Complex Indoor Scenarios at 3.7 GHz Band for Future 5G Deployments". *16th EuCAP*, pp. xxx-xxx, 2022.
- [23] Horst J. Bessai. "MIMO Channel Problems and Solutions" in *MIMO Signals and Systems*, 1st ed. Siegen, DE: *Springer Science*, 2005, pp. 161-183.
- [24] Branka Vucetic, Jinhong Yuan. "Space-Time Block Codes" in *Space-Time Coding*, 1st ed. Chichester, SXW, ENG: *Wiley*, 2003, pp. 91-115.
- [25] B. Hochwald, T. L. Marzetta and C. B. Papadias. "A Transmitter Diversity Scheme for Wideband CDMA Systems Based on Space-Time Spreading". *IEEE J. Sel. Areas Comm*, Vol. 19, No. 1, pp. 48-60, Jan. 2001.
- [26] G. Ganesan, P. Stoica. "Space-Time Block Codes: A Maximum SNR Approach". *IEEE Trans. Inform. Theory*, Vol. 47, No. 4, pp. 1650-1656, May. 2001.
- [27] Branka Vucetic, Jinhong Yuan. "Space-Time Trellis Codes" in *Space-Time Coding*, 1st ed. Chichester, SXW, ENG: *Wiley*, 2003, pp. 117-143.
- [28] W. C. Jakes, *Microwave Mobile Communications*. New York, NY, USA: *Wiley*, 1994.
- [29] C. Chayawan and V. A. Aalo, "Average Error Probability of Digital Cellular Radio Systems using MRC Diversity in the Presence of Multiple Interferers", *IEEE Trans. Wireless Commun.*, vol.2, no. 5, pp. 860-864, Sep. 2003.
- [30] S. Roy and P. Fortier, "Maximal-Ratio Combining Architectures and Performance with Channel Estimation Based on a Training Sequence", *IEEE Trans. Wireless Commun.*, vol. 3, no. 4, pp. 1154-1164, Jul. 2004.

- [31] W. M. Gifford, M. Z. Win, and M. Chiani, "Diversity with Practical Channel Estimation", *IEEE Trans. Wireless Commun.*, vol. 4, no. 4, pp. 1935-1947, Jul. 2005.
- [32] K. S. Ahn and R. W. Heath, "Performance Analysis of Maximum Ratio Combining with Imperfect Channel Estimation in the Presence of Cochannel Interferences", *IEEE Trans. Wireless Commun.*, vol. 8, no. 3, pp. 1080-1085, Mar. 2009.
- [33] T. K. Y. Lo, "Maximum Ratio Transmission", *IEEE Int. Conf. Commun. (ICC)*, Vancouver, BC, Canada, Jun. 1999, pp. 1310-1314.
- [34] J. K. Cavers, "Single-User and Multiuser Adaptive Maximal Ratio Transmission for Rayleigh Channels", *IEEE Trans. Veh. Technol.*, vol. 49, no. 6, pp. 2043-2050, Nov. 2000.
- [35] Y. Chen and C. Tellambura, "Performance Analysis of Maximum Ratio Transmission with Imperfect Channel Estimation", *IEEE Commun. Lett.*, vol. 9, no. 4, pp. 3223-3224, Apr. 2005.
- [36] Ö. Yürür, C. H. Liu, C. Perera, M. Chen, X. Liu, and W. Moreno, "Energy-efficient and Context-aware Smartphone Sensor Employment", *IEEE Trans. Veh. Technol.*, vol. 64, no. 9, pp. 4230-4244, Sep. 2015.
- [37] P. Gao and C. Tepedelenlioglu, "SNR Estimation for Nonconstant Modulus Constellations", *IEEE Trans. Signal Process.*, vol. 53, no. 3, pp. 865-870, Mar. 2005.
- [38] J. Joung, "Space-Time Line Code for Massive MIMO and Multiuser Systems with Antenna Allocation", *IEEE Access*, Vol. 6, pp. 962-979, Nov. 2017.
- [39] J. Choi, J. Joung and Y. Cho, "Artificial-Noise-Aided Space-Time Line Code for Enhancing Physical Layer Security of Multiuser MIMO Downlink Transmission". *IEEE Systems Journal*, Vol. 16, pp. 1289-1300, May. 2021.

-
- [40] L. Azpilicueta, M. Rawat, K. Rawat, F. Ghannouchi, F. Falcone. "Convergence Analysis in Deterministic 3D Ray Launching Radio Channel Estimation in Complex Environments". *ACES Journal*, Vol.29, No.4, Apr. 2014.
- [41] P. Lopez-Iturri. "Analysis, Characterization and Modeling of Interference Sources on Wireless Communication Systems in Complex Indoor Scenarios". *Doctoral thesis*. February 2017.
- [42] M. Celaya-Echarri, L. Azpilicueta, J. Karpowicz, V. Ramos, P. Lopez-Iturri, F. Falcone. "From 2G to 5G Spatial Modeling of Personal RF-EMF Exposure Within Urban Public Trams". *IEEE Access*, Vol. 8, pp. 100930-100947, May. 2020.
- [43] S. Salous. *Radio Propagation Measurement and Channel Modelling*, 1st ed. London, U.K.: *Wiley*, 2013.
- [44] Hristov, H.D. *Fresnel Zones in Wireless Links, Zone Plate Lenses and Antennas*; *Artech House Inc.*: London, UK, 2000.
- [45] Recomendation UIT-R, p. 526-11, s. 1., "Propagación por difracción, serie p. propagación de las ondas radioeléctricas," Octubre 2009.
- [46] R. J. Luebbers, "A heuristic UTD slope diffraction coefficient for rough lossy wedges," *IEEE Transactions on Antennas and Propagation*, vol. 37, pp. 206-211, 1989.
- [47] R. J. Luebbers, "Comparison of lossy wedge diffraction coefficients with application to mixed path propagation loss prediction," *IEEE Transactions on Antennas and Propagation*, vol. 36, n°. 7, pp. 1031-1034, 1988.
- [48] L. Azpilicueta. "Characterization of Wireless Propagation in Complex Indoor Environments". *Doctoral thesis*. June 2015.
- [49] L. Trigueros, P. Lopez-Iturri, L. Azpilicueta, Carlos Del-Río, F. Falcone. "Analysis of Phase Evolution Impact in SIMO Operation in Distributed Transceiver Systems". *14th EuCAP*, pp. xxx-xxx, 2020.

- [50] L. Trigueros, L. Azpilicueta, Carlos Del-Río, F. Falcone. "Topological and Morphological Influence in the Performance of MIMO Techniques in Complex Indoor Scenarios". *6th EuCAP*, pp. 3134-3136, 2012.
- [51] Fermín Esparza Alfaro. "Algoritmo de Trazado de Rayos en Tres Dimensiones para la Caracterización de Entornos Interiores". *Dissertation*. 2009.
- [52] T. Otim, P. Lopez-Iturri, L. Azpilicueta, A. Bahillo, L. Díez, F. Falcone. "A 3D Ray Launching Time-Frequency Channel Modelling Approach for UWB Ranging Applications" *IEEE Access*, Vol. 4, pp. 97321-97334, May. 2020.
- [53] U. Karabulut, A. Awada, I. Viering, M. Simsek and G. P. Fettweis, "Spatial and Temporal Channel Characteristics of 5G 3D Channel Model with Beamforming for User Mobility Investigations," *IEEE Communications Magazine*, vol. 56, no. 12, pp. 38-45, 2018.
- [54] L. Azpilicueta, M. Rawat, K. Rawat, F. Ghannouchi and F. Falcone, "A Ray Launching-Neural Network Approach for Radio Wave Propagation Analysis in Complex Indoor Environments", *IEEE Transactions on Antennas and Propagation*, vol. 62, N. 5, pp. 2777-2785, May 2014.
- [55] L. Azpilicueta, F. Falcone, R. Janaswamy, "A Hybrid Ray Launching-Diffusion Equation Approach for Propagation Prediction in Complex Indoor Environments", *IEEE Antennas and Wireless Propagation Letters*, vol 16, pp. 214-217, 2017.
- [56] Ministry of Energy, Tourism and Digital Agend. Government of Spain." *Spain's 5G National Plan 2018-2020*".
- [57] Daniel E. Capano. "Wireless propagation fundamentals". *Industrial wireless tutorial*. August 2014.
- [58] K. S. Muttair, O. A. Al-Ani, M. F. Mosleh, "Outdoor to Indoor Wireless Propagation Simulation Model for 5G Band Frequencies", *IOP Conference Series Materials Science and Engineering*, March 2020.

- [59] Xiang-Chuan Gao, Jian-Kang Zhang, He Chen, Zheng Dong, Member, IEEE, and Branka Vucetic, “Energy-Efficient and Low-Latency Massive SIMO Using Noncoherent ML Detection for Industrial IoT Communications”, *IEEE Internet Of Things Journal*, Vol. 6, No. 4, August 2019.
- [60] L. Jing, E. De Carvalho, P. Popovski, and À. O. Martínez, “Design and performance analysis of noncoherent detection systems with massive receiver arrays,” *IEEE Trans. Signal Process*, vol. 64, no. 19, pp. 5000–5010, Oct. 2016.
- [61] A. Manolakos, M. Chowdhury, and A. Goldsmith, “Energy-based modulation for noncoherent massive SIMO systems,” *IEEE Trans. Wireless Commun.*, vol. 15, no. 11, pp. 7831–7846, Nov. 2016.
- [62] Khashayar Salehi Nobandegani, Paeiz Azmi, “A Study of the Extreme Effects of Fading Correlation and the Impact of Imperfect MMSE Channel Estimation on the Performance of SIMO Zero-Forcing Receivers and on the Capacity-Maximizing Strategy in SIMO Links”, *IEEE Transactions on Vehicular Technology*, Vol. 59, No. 3, March 2010.
- [63] Shengbo Xu, Weiyang Xu, Cunhua Pan, Maged ElKashlan, “Detection of Jamming Attack in Non-Coherent Massive SIMO Systems”, *IEEE Transactions on Information Forensics and Security*, Vol. 14, No. 9, September 2019.
- [64] B. S. Khan, S. Jangsher, A. Ahmed, A. Al-Dweik, "uRLLC and eMBB in 5G Industrial IoT: A Survey", *IEEE ComSoc*, July 2022.

Appendix A

Measurement Equipment Specification

Voltage Controlled Oscillator



Model: ZX95-3760-S+

Linear Tuning: 3200 to 3760 MHz

Features:

- Low phase noise
- Low pushing
- Low pulling

Applications:

- R & D
- Lab
- Instrumentation
- Wireless communications
- Satellite systems
- SAP/SAB

Electrical Specifications

| MODEL NO. | FREQ. (MHz) | | POWER OUTPUT (dBm) | PHASE NOISE dBc/Hz SSB at offset frequencies, kHz | | | | TUNING | | | | | NON HARMONIC SPURIOUS (dBc) | HARMONICS (dBc) | | PULLING pk-pk @ 12 dB (MHz) | PUSHING (MHz/V) | DC OPERATING POWER | |
|--------------|-------------|------|--------------------|---|-----|------|------|--------|-------------------|----------------------|---------------|---------------------------------|-----------------------------|-----------------|------|-----------------------------|-----------------|--------------------|------|
| | Min. | Max. | | Typ. | 1 | 10 | 100 | 1000 | VOLTAGE RANGE (V) | SENSI-TIVITY (MHz/V) | PORT CAP (pF) | 3 dB MODULATION BANDWIDTH (MHz) | | Typ. | Typ. | | | Max. | Typ. |
| ZX95-3760-S+ | 3200 | 3760 | +8 | -69 | -96 | -118 | -139 | 0.5 | 15 | 56-67 | 15 | 120 | -90 | -28 | -18 | 2.5 | 0.8 | 5 | 48 |

Omni-directional Broadband Antenna



Model: OmniLOG 30800

Frequency Range 300MHz - 8GHz, High Gain

Technical Data:

- Frequency range: 300MHz - 8GHz
- Design: Omni-directional
- Nominal impedance: 50 Ohm
- Polarisation: Linear
- VSWR (typ): < 3:1
- Max. Input Power: 5 Watts
- RF-connector: SMA (male)
- Temperature range: - 40°C to +85°C
- Dimensions (L/W/D): 173 x 62 x 9 mm
- Relative Humidity: 0% to 95%
- Weight: 54gr
- RoHs compliant
- Warranty: 10 years

Portable Spectrum Analyzer



Model: Agilent FieldFox N9912A

- Frequency: 2 MHz to 6 GHz
- Frequency resolution:
 - 2 MHz to 1.6 GHz 2.5 kHz
 - > 1.6 GHz to 3.2 GHz 5 kHz
 - > 3.2 GHz to 6 GHz 10 kHz
- Reflection (RF Out port):
 - 2 MHz to 4 GHz 60 dB (typical)
 - > 4 GHz to 6 GHz 55 dB (typical)
- Transmission measurement (Option 110):
 - 2 MHz to 2 GHz 72 dB (typical)
 - > 2 GHz to 3 GHz 67 dB (typical)
 - > 3 GHz to 5 GHz 58 dB (typical)
 - > 5 GHz to 6 GHz 49 dB (typical)
- Output power range:
 - High power
 - 2 MHz to 4 GHz < +8 dBm, +6 dBm (nominal)
 - > 4 GHz to 6 GHz < +7 dBm, +2 dBm (nominal)
 - Low power
 - 2 MHz to 4 GHz < -23 dBm, -25 dBm (nominal)
 - > 4 GHz to 6 GHz < -24 dBm, -25 dBm (nominal)
- Maximum input level (RF Out port): +23 dBm

Appendix B

STLC Encoding and Decoding Structures

Rate-One STLC Encoding and Decoding Structures for a System with Two Receive Antennas

| | | STLC encoding matrices | | Decoding function: $f(a, b) = a + b$ | |
|----------------------|--|--|----------------------------|--------------------------------------|--------------------------|
| | | | | for \tilde{x}_1 | for \tilde{x}_2 |
| $\mathbf{C}_{(1,2)}$ | $\mathbf{C}_{(1,2)}^a =$ | $\begin{bmatrix} h_1 & h_2 \\ h_2^* & -h_1^* \end{bmatrix}$ | | $f(r_{1,1}^*, r_{2,2})$ | $f(r_{2,1}^*, -r_{1,2})$ |
| | $\mathbf{C}_{(1,2)}^b =$ | $\begin{bmatrix} h_1 & h_2 \\ -h_2^* & h_1^* \end{bmatrix}$ | | $f(r_{1,1}^*, -r_{2,2})$ | $f(r_{2,1}^*, r_{1,2})$ |
| | $\mathbf{C}_{(1,2)}^c =$ | $\begin{bmatrix} h_1 & -h_2 \\ h_2^* & h_1^* \end{bmatrix}$ | | $f(r_{1,1}^*, r_{2,2})$ | $f(-r_{2,1}^*, r_{1,2})$ |
| | $\mathbf{C}_{(1,2)}^d =$ | $\begin{bmatrix} -h_1 & h_2 \\ h_2^* & h_1^* \end{bmatrix}$ | | $f(-r_{1,1}^*, r_{2,2})$ | $f(r_{2,1}^*, r_{1,2})$ |
| Type | Encoding s_1 and s_2 | | Decoding for \tilde{x}_1 | Decoding for \tilde{x}_2 | |
| 1 | $\begin{bmatrix} s_1^* \\ s_2 \end{bmatrix}$ | $= \mathbf{C}_{(1,2)} \begin{bmatrix} x_1 \\ x_2 \end{bmatrix}$ | $f(\cdot, \cdot)$ | $f(\cdot, \cdot)$ | |
| 2 | $\begin{bmatrix} s_1^* \\ s_2 \end{bmatrix}$ | $= \mathbf{C}_{(1,2)} \begin{bmatrix} x_1^* \\ x_2 \end{bmatrix}$ | $f^*(\cdot, \cdot)$ | $f(\cdot, \cdot)$ | |
| 3 | $\begin{bmatrix} s_1^* \\ s_2 \end{bmatrix}$ | $= \mathbf{C}_{(1,2)} \begin{bmatrix} x_1 \\ x_2^* \end{bmatrix}$ | $f(\cdot, \cdot)$ | $f^*(\cdot, \cdot)$ | |
| 4 | $\begin{bmatrix} s_1^* \\ s_2 \end{bmatrix}$ | $= \mathbf{C}_{(1,2)} \begin{bmatrix} x_1^* \\ x_2^* \end{bmatrix}$ | $f^*(\cdot, \cdot)$ | $f^*(\cdot, \cdot)$ | |
| 5 | $\begin{bmatrix} s_1 \\ s_2^* \end{bmatrix}$ | $= \mathbf{C}_{(1,2)}^* \begin{bmatrix} x_1 \\ x_2 \end{bmatrix}$ | $f^*(\cdot, \cdot)$ | $f^*(\cdot, \cdot)$ | |
| 6 | $\begin{bmatrix} s_1 \\ s_2^* \end{bmatrix}$ | $= \mathbf{C}_{(1,2)}^* \begin{bmatrix} x_1^* \\ x_2 \end{bmatrix}$ | $f(\cdot, \cdot)$ | $f^*(\cdot, \cdot)$ | |
| 7 | $\begin{bmatrix} s_1 \\ s_2^* \end{bmatrix}$ | $= \mathbf{C}_{(1,2)}^* \begin{bmatrix} x_1 \\ x_2^* \end{bmatrix}$ | $f^*(\cdot, \cdot)$ | $f(\cdot, \cdot)$ | |
| 8 | $\begin{bmatrix} s_1 \\ s_2^* \end{bmatrix}$ | $= \mathbf{C}_{(1,2)}^* \begin{bmatrix} x_1^* \\ x_2^* \end{bmatrix}$ | $f(\cdot, \cdot)$ | $f(\cdot, \cdot)$ | |
| 9 | $\begin{bmatrix} s_1^* \\ s_2 \end{bmatrix}$ | $= -\mathbf{C}_{(1,2)} \begin{bmatrix} x_1 \\ x_2 \end{bmatrix}$ | $-f(\cdot, \cdot)$ | $-f(\cdot, \cdot)$ | |
| 10 | $\begin{bmatrix} s_1^* \\ s_2 \end{bmatrix}$ | $= -\mathbf{C}_{(1,2)} \begin{bmatrix} x_1^* \\ x_2 \end{bmatrix}$ | $-f^*(\cdot, \cdot)$ | $-f(\cdot, \cdot)$ | |
| 11 | $\begin{bmatrix} s_1^* \\ s_2 \end{bmatrix}$ | $= -\mathbf{C}_{(1,2)} \begin{bmatrix} x_1 \\ x_2^* \end{bmatrix}$ | $-f(\cdot, \cdot)$ | $-f^*(\cdot, \cdot)$ | |
| 12 | $\begin{bmatrix} s_1^* \\ s_2 \end{bmatrix}$ | $= -\mathbf{C}_{(1,2)} \begin{bmatrix} x_1^* \\ x_2^* \end{bmatrix}$ | $-f^*(\cdot, \cdot)$ | $-f^*(\cdot, \cdot)$ | |
| 13 | $\begin{bmatrix} s_1 \\ s_2^* \end{bmatrix}$ | $= -\mathbf{C}_{(1,2)}^* \begin{bmatrix} x_1 \\ x_2 \end{bmatrix}$ | $-f^*(\cdot, \cdot)$ | $-f(\cdot, \cdot)^*$ | |
| 14 | $\begin{bmatrix} s_1 \\ s_2^* \end{bmatrix}$ | $= -\mathbf{C}_{(1,2)}^* \begin{bmatrix} x_1^* \\ x_2 \end{bmatrix}$ | $-f(\cdot, \cdot)$ | $-f^*(\cdot, \cdot)$ | |
| 15 | $\begin{bmatrix} s_1 \\ s_2^* \end{bmatrix}$ | $= -\mathbf{C}_{(1,2)}^* \begin{bmatrix} x_1 \\ x_2^* \end{bmatrix}$ | $-f^*(\cdot, \cdot)$ | $-f(\cdot, \cdot)$ | |
| 16 | $\begin{bmatrix} s_1 \\ s_2^* \end{bmatrix}$ | $= -\mathbf{C}_{(1,2)}^* \begin{bmatrix} x_1^* \\ x_2^* \end{bmatrix}$ | $-f(\cdot, \cdot)$ | $-f(\cdot, \cdot)$ | |

Here, $f(\cdot, \cdot)$ is a decoding function define as $f(a, b) = a + b$. Note that all the STLC encoding matrices fullfil an ortogonal property, i.e., $\mathbf{C}^H \mathbf{C} = \gamma_2 \mathbf{I}_2$, and their rank is two, which provides the full spatial-diversity order two. It is apparent that the decoding scheme is determined according to the encoding scheme.

List of Publications

L. Trigueros, P. Lopez-Iturri, L. Azpilicueta, Carlos Del-Río, F. Falcone.
“Analysis of Phase Evolution Impact in SIMO Operation in Distributed
Transceiver Systems”. 14th EuCAP, 2020.

L. Trigueros, P. Lopez-Iturri, L. Azpilicueta, Carlos Del-Río, F. Falcone.
“Analysis of MIMO Performance in Complex Indoor Scenarios at 3.7
GHz Band for Future 5G Deployments”. 16th EuCAP, 2022.

Scientific journal publication in submission process:

L. Trigueros, P. Lopez-Iturri, L. Azpilicueta, Carlos Del-Río, F. Falcone.
"Human Scattering Influence in the Performance of MIMO Techniques in
Complex Indoor Environments". IEEE Access.